Elsevier Editorial System(tm) for Toxicology in Vitro

Manuscript Draft

Manuscript Number:

Title: A systems toxicology approach for comparative assessment: Biological impact of an aerosol from a candidate modified-risk tobacco product and cigarette smoke on human organotypic bronchial epithelial cultures

Article Type: Research paper

Section/Category: Mechanisms

Keywords: Air-liquid interface; organotypic culture; cigarette smoke; modified-risk tobacco product; systems toxicology

Corresponding Author: Dr. Anita R Iskandar, Ph.D.

Corresponding Author's Institution: Philip Morris International R&D, Philip Morris Products S.A.

First Author: Anita R Iskandar, Ph.D.

Order of Authors: Anita R Iskandar, Ph.D.; Carole Mathis, Ph.D.; Walter K Schlage, Ph.D.; Stefan Frentzel, Ph.D.; Patrice Leroy, Ph.D.; Yang Xiang, Ph.D.; Alain Sewer, Ph.D.; Shoaib Majeed, MEng.; Laura Ortega-Torres, Dip.; Stephanie Johne, BSc.; Emmanuel Guedj, MSc.; Keyur Trivedi, MPhil.; Gilles Kratzer, MSc.; Celine Merg, MSc.; Ashraf Elamin, Ph.D.; Florian Martin, Ph.D.; Nikolai V Ivanov, Ph.D.; Manuel C Peitsch, Ph.D.; Julia Hoeng, Ph.D.

Abstract: This study reports a comparative assessment of the biological impact of a heated tobacco aerosol from the tobacco heating system (THS) 2.2 and smoke from a combustible 3R4F cigarette. Human organotypic bronchial epithelial cultures were exposed to an aerosol from THS2.2 (a candidate modified-risk tobacco product) or 3R4F smoke at similar nicotine concentrations. A systems toxicology approach was applied to enable a comprehensive exposure impact assessment. Culture histology, cytotoxicity, secreted pro-inflammatory mediators, ciliary beating, and genome-wide mRNA/miRNA profiles were assessed at various time points post-exposure. Series of experimental repetitions were conducted to increase the robustness of the assessment. At similar nicotine concentrations, THS2.2 aerosol elicited lower cytotoxicity compared with 3R4F smoke. No morphological change was observed following exposure to THS2.2 aerosol, even at nicotine concentration three times that of 3R4F smoke. Lower levels of secreted mediators and fewer miRNA alterations were observed following exposure to THS2.2 aerosol than following 3R4F smoke. Based on the computational analysis of the gene expression changes, 3R4F (0.13 mg nicotine/L) elicited the highest biological impact (100%) in the context of Cell Fate, Cell Proliferation, Cell Stress, and Inflammatory Network Models at 4 h post-exposure. Whereas, the corresponding impact of THS2.2 (0.14 mg nicotine/L) was 7.6%.

Suggested Reviewers: Christopher Coggins
Carson Watts Consulting (USA)

chris@carsonwattsconsulting.com

Erin H Hill
President of the Institute for In Vitro Sciences, Institute for In Vitro Sciences (USA)
ehill@iivs.org

Roman Kollar
Deutscher Tierschutzbund - the German Animal Welfare Federation
roman.kolar@tierschutzakademie.de

Tuula Heinonen
Finnish Centre for Alternative Methods
tuula.heinonen@uta.fi

PMI RESEARCH & DEVELOPMENT

27 Sep 2016

Daniel Acosta, Frank A. Barile, Bas J. Blaauboer
Editors Toxicology in Vitro

Dear Editors,

We are delighted to submit an original research manuscript entitled "**A systems toxicology approach for comparative assessment: Biological impact of an aerosol from a candidate modified-risk tobacco product and cigarette smoke on human organotypic bronchial epithelial cultures**" to be considered for a publication in Toxicology in Vitro journal. The advanced in vitro organotypic three-dimensional bronchial cultures offer new prospects in the field of human toxicology. The aim of this study was to conduct a comparative assessment of the biological impact of whole aerosol exposure from a heat-not-burn candidate modified-risk tobacco product—the tobacco heating system (THS) 2.2—relative to that of whole smoke from 3R4F reference cigarettes using human organotypic bronchial cultures.

Such a comparative assessment is in agreement with the recommendations of the Institute of Medicine and the Tobacco Product Assessment Consortium in that an assessment of modified-risk tobacco products should be evaluated in comparison with the impact of standard conventional products. Moreover, aligned with the 3R strategy and the Vision and Strategy of the Toxicity Testing in the 21st Century, the study was conducted using an in vitro human organotypic bronchial culture models and implemented a systems toxicological approach. Our systems toxicology assessment strategy combines computational biology analyses (i.e., a global analysis of mRNA and miRNA changes using a network-based approach) with various functional cell-based assays (i.e., cytotoxicity assay, secreted pro-inflammatory factor measurement, histological analysis, and cilia beating analysis). In this manuscript, we reported a collection of data based on a series of experimental repetitions that were performed within a 20-month period. The repetitions were aimed to increase the robustness of the toxicity assessment.

Our study not only reports a toxicity assessment of exposure but also further demonstrates the application of in vitro organotypic bronchial cultures. We believe that this work is highly aligned with Toxicology in Vitro journal that report original toxicological research involving the application or development of in vitro techniques. This manuscript has not been published and is not under consideration elsewhere[i]. All authors listed have contributed sufficiently to the project to be included as authors. We have included acknowledgements, competing interest, and funding resources. Thank you very much for your consideration.

Kind regards,

Anita R. Iskandar
On behalf of all authors

[i] The mRNA and miRNA datasets will be made publically available on ArrayExpress upon acceptance of the manuscript. If applicable, video microscopy recordings of the ciliary beat from the cultures are available and can be uploaded in the journal upon publication.

Manuscript
Click here to view linked References

Title Page

Title

A systems toxicology approach for comparative assessment: Biological impact of an aerosol from a candidate modified-risk tobacco product and cigarette smoke on human organotypic bronchial epithelial cultures

Author names and affiliations

Anita R. Iskandar, PhD.*
Philip Morris International R&D, Philip Morris Products S.A., Quai Jeanrenaud 5, 2000 Neuchâtel, Switzerland (part of Philip Morris International group of companies)
Anita.Iskandar@pmi.com

Carole Mathis, PhD.*
Philip Morris International R&D, Philip Morris Products S.A., Quai Jeanrenaud 5, 2000 Neuchâtel, Switzerland (part of Philip Morris International group of companies)
Carole.Mathis@pmi.com

Walter K. Schlage, PhD.
Biology Consultant, Max-Baermann-Str. 21, 51429 Bergisch Gladbach, Germany
WK.Schlage@t-online.de

Stefan Frentzel, PhD.
Philip Morris International R&D, Philip Morris Products S.A., Quai Jeanrenaud 5, 2000 Neuchâtel, Switzerland (part of Philip Morris International group of companies)
Stefan.Frentzel@pmi.com

Patrice Leroy, PhD.
Philip Morris International R&D, Philip Morris Products S.A., Quai Jeanrenaud 5, 2000 Neuchâtel, Switzerland (part of Philip Morris International group of companies)
Patrice.Leroy@pmi.com

Yang Xiang, PhD.
Philip Morris International R&D, Philip Morris Products S.A., Quai Jeanrenaud 5, 2000 Neuchâtel, Switzerland (part of Philip Morris International group of companies)
Yang.Xiang@pmi.com

Alain Sewer, PhD
Philip Morris International R&D, Philip Morris Products S.A., Quai Jeanrenaud 5, 2000 Neuchâtel, Switzerland (part of Philip Morris International group of companies)
Alain.Sewer@pmi.com

Shoaib Majeed, MEng.
Philip Morris International R&D, Philip Morris Products S.A., Quai Jeanrenaud 5, 2000 Neuchâtel, Switzerland (part of Philip Morris International group of companies)
Shoaib.Majeed@pmi.com

Laura Ortega-Torres, Dip.
Philip Morris International R&D, Philip Morris Products S.A., Quai Jeanrenaud 5, 2000 Neuchâtel, Switzerland (part of Philip Morris International group of companies)
Laura.OrtegaTorres@pmi.com

Stephanie Johne, BSc.
Philip Morris International R&D, Philip Morris Products S.A., Quai Jeanrenaud 5, 2000 Neuchâtel, Switzerland (part of Philip Morris International group of companies)
Stephanie.Johne@pmi.com

Emmanuel Guedj, MSc.
Philip Morris International R&D, Philip Morris Products S.A., Quai Jeanrenaud 5, 2000 Neuchâtel, Switzerland (part of Philip Morris International group of companies)
Emmanuel.Guedj@pmi.com

Keyur Trivedi, MPhil.
Philip Morris International R&D, Philip Morris Products S.A., Quai Jeanrenaud 5, 2000 Neuchâtel, Switzerland (part of Philip Morris International group of companies)
Keyur.Trivedi@pmi.com

Gilles Kratzer, MSc.
Philip Morris International R&D, Philip Morris Products S.A., Quai Jeanrenaud 5, 2000 Neuchâtel, Switzerland (part of Philip Morris International group of companies)
Gilles.Kratzer@gmail.com

Celine Merg, MSc.
Philip Morris International R&D, Philip Morris Products S.A., Quai Jeanrenaud 5, 2000 Neuchâtel, Switzerland (part of Philip Morris International group of companies)
Celine.Merg@pmi.com

Ashraf Elamin, PhD.
Philip Morris International R&D, Philip Morris Products S.A., Quai Jeanrenaud 5, 2000 Neuchâtel, Switzerland (part of Philip Morris International group of companies)
Ashraf.Elamin@pmi.com

Florian Martin, PhD.
Philip Morris International R&D, Philip Morris Products S.A., Quai Jeanrenaud 5, 2000 Neuchâtel, Switzerland (part of Philip Morris International group of companies)
Florian.Martin@pmi.com

Nikolai V. Ivanov, PhD.
Philip Morris International R&D, Philip Morris Products S.A., Quai Jeanrenaud 5, 2000 Neuchâtel, Switzerland (part of Philip Morris International group of companies)
Nikolai.Ivanov@pmi.com

Manuel C. Peitsch, PhD.
Philip Morris International R&D, Philip Morris Products S.A., Quai Jeanrenaud 5, 2000 Neuchâtel, Switzerland (part of Philip Morris International group of companies)
Manuel.Peitsch@pmi.com

Julia Hoeng, PhD.
Philip Morris International R&D, Philip Morris Products S.A., Quai Jeanrenaud 5, 2000 Neuchâtel, Switzerland (part of Philip Morris International group of companies)
Julia.Hoeng@pmi.com

*Contributed equally for the manuscript

Corresponding Author
Anita R. Iskandar, PhD.
Quai Jeanrenaud 5
CH-2000 Neuchâtel, Switzerland
Office phone: +41 58 242 2777
Email: anita.iskandar@pmi.com

Abstract

This study reports a comparative assessment of the biological impact of a heated tobacco aerosol from the tobacco heating system (THS) 2.2 and smoke from a combustible 3R4F cigarette. Human organotypic bronchial epithelial cultures were exposed to an aerosol from THS2.2 (a candidate modified-risk tobacco product) or 3R4F smoke at similar nicotine concentrations. A systems toxicology approach was applied to enable a comprehensive exposure impact assessment. Culture histology, cytotoxicity, secreted pro-inflammatory mediators, ciliary beating, and genome-wide mRNA/miRNA profiles were assessed at various time points post-exposure. Series of experimental repetitions were conducted to increase the robustness of the assessment. At similar nicotine concentrations, THS2.2 aerosol elicited lower cytotoxicity compared with 3R4F smoke. No morphological change was observed following exposure to THS2.2 aerosol, even at nicotine concentration three times that of 3R4F smoke. Lower levels of secreted mediators and fewer miRNA alterations were observed following exposure to THS2.2 aerosol than following 3R4F smoke. Based on the computational analysis of the gene expression changes, 3R4F (0.13 mg nicotine/L) elicited the highest biological impact (100%) in the context of Cell Fate, Cell Proliferation, Cell Stress, and Inflammatory Network Models at 4 h post-exposure. Whereas, the corresponding impact of THS2.2 (0.14 mg nicotine/L) was 7.6%.

Keywords

Reconstituted epithelium, air-liquid interface, transcriptomics, causal biological network modelling, product testing

Abbreviations

3D, Three-dimensional

AK, Adenylate kinase

BIF, Biological impact factor

CBF, Ciliary beating frequency

CCL, Chemokine (C-C motif) ligand

CFA, Cell fate

CPR, Cell proliferation

CS, Cigarette smoke

CST, Cell stress

CXCL, Chemokine (C-X-C motif) ligand

DEG, Differentially expressed gene

EGF, Epidermal growth factor

FDR, False discovery rate

FFT, Fast Fourier transformation

H&E, Hematoxylin and eosin

IL, Interleukin

IPN, Inflammatory process networks

MiRNA, microRNA

MMP, Matrix metalloproteinase

NPA, Network perturbation amplitude

PBS, Phosphate-buffered saline

QC, Quality control

REF, Reference

sICAM, Soluble intercellular adhesion molecule

THS, Tobacco heating system

TIMP, Tissue inhibitor of metalloproteinase

TSLP, Thymic stromal lymphopoietin

TNFA, Tumor necrosis factor alpha

VEGFA, Vascular endothelial growth factor alpha

Introduction

Growing concern over the toxicity of environmental pollutants and atmospheric aerosols has prompted research to investigate the mechanisms involved in lung injury and repair following exposure to toxicants (BeruBe et al., 2009). Exposure to cigarette smoke (CS) is associated with oxidative stress, inflammation, and genetic and epigenetic changes in the respiratory tract (Goldkorn et al., 2014). Although longitudinal clinical studies are valuable to assess potential human health risks associated with smoking, the adverse effects and disease manifestation often take decades to occur. Studies over such long observation periods are difficult or even impossible to conduct. Invasive procedures inherent to tissue sampling further contribute to the impracticality in studying the human respiratory pathophysiology. Alternatively, animal models can be used to investigate adverse effects following exposure and their underlying mechanisms. However, inhalation studies in animals pose ethical, physiological, and practical challenges (Paur et al., 2011). These challenges have prompted the search for alternative approaches. These approaches should be practical and cost-efficient, as well as provide more relevant insight to toxicity risk in humans (Committee on Toxicity Testing and Assessment of Environmental Agents, 2007).

Studies have demonstrated the relevance of *in vitro* organotypic human culture models to evaluate cellular and molecular changes at the tissue level. Organotypic cultures are now available for most tissues, and more accurately represent the physiological situation than monolayer cultures, whereby the three-dimensional (3D) organization of cells and extracellular matrix within tissues are maintained (Shamir and Ewald, 2014). These cell–cell and cell–matrix interactions are lacking in the traditional monolayer culture systems (Shamir and Ewald, 2014). To study the impact of exposure via inhalation, e.g., of cigarette smoke (CS), organotypic human culture models reconstituted from primary bronchial epithelial cells have been used in numerous studies to investigate the impact of CS (BeruBe et al., 2009; Iskandar et al., 2015; Mathis et al., 2013; Maunders et al., 2007; Talikka et al., 2014).

Unlike monolayer cultures, these organotypic bronchial cultures are grown at the air-liquid interface, allowing them to fully differentiate into a pseudostratified epithelium (BeruBe et al., 2009). The pseudostratified respiratory epithelium lines (almost entirely) the *in vivo* human

bronchi, trachea, and upper respiratory tract. The airway epithelium acts as a biological barrier restricting inhaled pathogens or chemicals from entering the tissue (Proud and Leigh, 2011). Similar to *in vivo* bronchial epithelium, *in vitro* bronchial cultures comprise basal cells, mucus-secreting (goblet) cells, and ciliated cells. These cells are held together by tight junctions, which control the permeability and maintain the polarity of the tissue. The polarized epithelium creates two distinct membrane-separated compartments: The apical (air-directed) and basolateral (medium-directed) side. The apical side of the culture mimics the characteristics of the *in vivo* mucociliary surface covered by a physiological mucus layer. Various studies using organotypic human bronchial cultures have reported that CS exposure altered normal cilia length and function (Åstrand et al., 2015; Aufderheide et al., 2015; Brekman et al., 2014) and ciliary beating frequency (Kuehn et al., 2015; Schmid et al., 2015). Various pro-inflammatory mediators have also been detected in the basolateral media of organotypic bronchial cultures to assess the inflammatory responses following exposure (Azzopardi et al., 2015; Iskandar et al., 2015).

In addition to the similar morphological and functional features shared by *in vitro* organotypic bronchial cultures and *in vivo* epithelium, the global gene expression profiles of *in vitro* organotypic bronchial cultures share similarities with those of *in vivo* bronchial epithelial cells collected by brushing (Mathis et al., 2013; Pezzulo et al., 2011). It should be acknowledged that some differences have been reported; for example, organotypic cultures express higher levels of basal cell-related genes, whereas brushed cells express higher levels of cilia-related genes (Dvorak et al., 2011). This is attributed to the higher proportion of basal cells present in organotypic bronchial cultures, but a higher proportion of ciliated cells present in *in vivo* brushed bronchial cells (Dvorak et al., 2011). Nevertheless, following CS exposure (compared with the air exposure control), the gene expression profiles of *in vitro* organotypic bronchial cultures closely resemble those of *in vivo* brushed airway epithelial cells obtained from smokers (compared with non-smokers' brushed cells) (Iskandar et al., 2013; Mathis et al., 2013; Pezzulo et al., 2011). The CS-induced alterations in the gene expression profiles suggested that CS exposure affected normal xenobiotic metabolism, oxidant/antioxidant balance, and elicited DNA damage and repair mechanism (Iskandar et al., 2015; Mathis et al., 2015; Maunders et al., 2007). Altogether, the air-liquid interface bronchial epithelial cultures can reflect more appropriately the anatomical,

physiological, and molecular alterations of *in vivo* human bronchial epithelium than the submerged monolayer cultures.

Aligned with the 3Rs strategy—animal-use should be reduced, refined, and replaced—*in vitro* studies using relevant test systems and systems biology approaches offer new prospects in the field of human toxicology (Daneshian et al., 2011). The aim of this study was to conduct a comparative assessment of the biological impact of whole aerosol exposure from a heat-not-burn candidate modified-risk tobacco product—the tobacco heating system (THS) 2.2—relative to that of whole smoke from 3R4F reference cigarettes using human organotypic bronchial cultures. Such a comparative assessment would be aligned with the recommendations of the Institute of Medicine and the Tobacco Product Assessment Consortium in that an assessment of modified-risk tobacco products should be evaluated in comparison with the impact of standard conventional products (Berman et al., 2015; Institute of Medicine, 2012).

For a more comprehensive assessment of the biological impact, a systems toxicological approach (Sauer et al., 2016; Sturla et al., 2014) was applied in this study, in which cytotoxicity, secreted pro-inflammatory mediators, ciliary beating, culture histology, and genome-wide mRNA/miRNA profiles were analyzed at various time points post-exposure. Cytotoxicity associated with the exposure was determined by measuring the levels of adenylate kinase (AK) released into the basolateral media. Such assays are commonly used to determine cell death based on the leakage of cellular components, e.g., lactate dehydrogenase or AK enzyme (Blaauboer, 2008). Moreover, upon stimuli, cells can activate an inflammatory response leading to the secretion of various pro-inflammatory mediators (e.g. cytokines, chemokines, and growth factors) (Lambrecht and Hammad, 2012). Therefore, in this study, the inflammatory responses of the cultures following exposure were assessed by measuring the concentration of various mediators in the basolateral media. Furthermore, ciliary beating frequency was measured because of the known association between CS exposure and reduced mucociliary clearance, which is dependent upon normal ciliary beating frequency (CBF) (Kreindler et al., 2005; Stanley et al., 1986). In addition, a histological assessment of the cultures was conducted to evaluate the anatomical complexity of the culture models following exposure. Histological analyses allow a visualization of the microscopic features of the cells in their 3D structures (Cormack, 2001), thus enabling a morphological

comparison with the *in vivo* human bronchial epithelium (Uraih and Maronpot, 1990). Finally, the global gene alterations were used to detect specific molecular targets or pathway mechanisms linked to the exposure. A network-based analysis (i.e., the network perturbation amplitude algorithm (Martin et al., 2014) leveraging causal biological network models (Boue et al., 2015) and transcriptome profiles), was performed to obtain a more meaningful biological insight relevant for human respiratory biology. To obtain a robust assessment, a series of six experimental phases were conducted where different batches of bronchial cultures were obtained. The cultures were exposed to whole 3R4F smoke or whole THS2.2 aerosol at similar nicotine concentrations. In addition, a dose range assessment was conducted to detect the likelihood of adverse toxicity effects of THS2.2 aerosol on the organotypic bronchial cultures.

Materials and Methods

Organotypic culture models

Two organotypic bronchial epithelial culture models were used in this study (**Table 1**):

- EpiAirway™ (MatTek Corporation, Ashland, MA, USA) reconstituted from primary bronchial epithelial cells of a 23-year old male, non-smoker, no pathology reported, and
- MucilAir™ Bronchial (Epithelix Sàrl, Geneva, Switzerland) reconstituted from primary bronchial epithelial cells of a 28-year old male, non-smoker, no pathology reported.

Table 1. Culture models and endpoint measurements

	Phase of the Experimental Study					
	Exp 1	**Exp 2**	**Exp 3**	**Exp 4**	**Exp 5**	**Exp 6**
	Dec 2013	**Feb 2014**	**Mar 2015**	**Jun 2015**	**Jul 2015**	**Sep 2015**
Culture Model	EpiAirway™	EpiAirway™	MucilAir™	MucilAir™	MucilAir™	MucilAir™
Insert Material	Translucent (opaque) polycarbonate	Translucent (opaque) polycarbonate	Transparent polyethylene terephthalate	Transparent polyethylene terephthalate	Transparent polyethylene terephthalate	Transparent polyethylene terephthalate
Donor Information	23 y old male, non-smoker	23 y old male, non-smoker	28 y old male, non-smoker	28 y old male, non-smoker	28 y old male, non-smoker	28 y old male, non-smoker
Endpoints						
Cytotoxicity	Yes	Yes	Yes	Yes	Yes	Yes
IHC	No	No	Yes	Yes	Yes	Yes
CBF	No*	No*	Yes	Yes	Yes	Yes
Secretion of mediators	Yes	Yes	Yes	Yes	Yes	Yes
mRNA/miRNA profiles	Yes	Yes	Yes	Yes	Yes	Yes
Exposure Run	1–2	1–2	3	3	3	3
Replicate per Run	3	3	1	1	1	1

*Because of the transluscent insert materials, ciliary beating frequency assessment could not be conducted. Abbreviation: Exp, experiment; CBF, ciliary beating frequency; IHC, immunohistochemistry.

The cultures were grown in 6.5 mm Transwell® inserts; the dimension of the insert was chosen based on its fitting for the Cultivation Base Module of the Vitrocell® 24/48 exposure system. Upon arrival, the EpiAirway™ bronchial cultures were placed in their fresh culture media (5.5 mL/well) provided by the supplier, pre-warmed to 37°C, in 12-well culture plates. Similarly, upon arrival, the MucilAir™ bronchial cultures were placed in their fresh culture media (0.7 mL/well) provided by the supplier, pre-warmed to 37°C, in 24-well culture plates. All cultures were maintained at the air-liquid interface at 37°C (5% CO_2, 90% humidity) with medium change every 2–3 days according to the supplier's instructions. The cultures were regularly inspected

microscopically to check for potential morphological changes, as well as for bacterial or fungal contamination.

Three days before exposure (referred to as an exposure run), the apical sides of the cultures were washed gently by a dropwise addition of a total of 200 µL culture media (pre-warmed to 37°C) that was subsequently aspirated slowly. After exposure, the cultures were maintained without medium change until sample collections (according to the experimental design).

Aerosol/smoke generation and exposure at the air-liquid interface

3R4F reference cigarettes were purchased from the University of Kentucky (Kentucky Tobacco Research & Development Center). The candidate modified-risk tobacco product, termed tobacco heating system (THS) 2.2, was obtained from Philip Morris International R&D, Neuchâtel, Switzerland. THS2.2 uses a "heat-not-burn" based technology that heats tobacco instead of burning it. The specification and comparative analyses of THS2.2 aerosol and 3R4F smoke have been reported before in a previous publication (Phillips et al., 2016). The 3R4F cigarettes and THS2.2 sticks were conditioned for at least 48 h and up to 21 d at 22 ± 1°C with a relative humidity of 60 ± 3%, according to ISO standard 3402 (International Organization for Standardization).

The smoke and aerosol were generated according to the Health Canada smoking protocol (55 mL puff over two sec, twice per min with an 8 sec pump exhaust time) (Health Canada, 1999). Each 3R4F cigarette was smoked to a standard butt length (approximately 35 mm), and each THS2.2 was aerosolized for a total of 12 puffs per stick. For an exposure run, 3R4F reference cigarettes were smoked using a 30-port carousel smoking machine (SM) (SM2000; Philip Morris, International) connected to a Vitrocell® 24/48 exposure system (Vitrocell Systems GmbH, Waldkirch, Germany), **Figure 1**A. Another dedicated 30-port carousel smoking machine was used to generate the aerosol from THS2.2 that was connected to another Vitrocell® 24/48 exposure system, **Figure 1**B. For a 28-min exposure run, 10 3R4F cigarettes were smoked and 10 THS2.2 sticks were aerosolized. The duration of exposure (28 min) was chosen according to a previous report (Mathis et al., 2013), in which a 28-min exposure compared with 7, 14, and 21 min exposure of 3R4F exposure induced the highest concentration of secreted matrix

metalloproteinase (MMP)-1 in bronchial organotypic cultures. The secretion of MMP-1 was considered as a control to demonstrate the responsiveness of organotypic airway cultures following CS exposure (Mathis et al., 2013).

The Vitrocell® 24/48 exposure system is equipped with a Dilution/Distribution Module where the smoke/aerosol stream can be mixed with fresh air (Majeed et al., 2014). The set-up allows adjustment of the smoke/aerosol concentrations applied to the organotypic bronchial cultures, which are located in the Cultivation Base Module of the Vitrocell® 24/48 exposure system (**Figure 1**). In this study, for the exposure run, two different concentrations of smoke from 3R4F cigarettes were applied: 0.13 mg nicotine/L and 0.25 mg nicotine/L, corresponding to smoke concentrations in the Dilution/Distribution Module of approximately 8% and 15% (v/v) 3R4F smoke in filtered air, respectively (**Figure 1**A). These concentrations were chosen based on previous observations from which measurable effects were observed without overt tissue destruction (Iskandar et al., 2015). For the assessment of THS2.2, three different concentrations of THS2.2 aerosol were applied: 0.14 mg nicotine/L, 0.25 mg nicotine /L, and 0.42 mg nicotine/L, corresponding to aerosol concentrations in the Dilution/Distribution Module of 13%, 24%, and 31% aerosol in air (v/v), respectively (**Figure 1**B). Two of the concentrations were matched to the nicotine concentrations in the diluted 3R4F smoke. Nicotine was used as the internal reference compound to compare the impact of 3R4F smoke and THS2.2 aerosol (the nicotine yield from one 3R4F cigarette is roughly 1.4-fold greater than from one THS2.2 stick, (Gonzalez-Suarez et al., 2016)).

A similar exposure set-up was applied for the dose range assessment of THS2.2, in which seven different concentrations of THS2.2 aerosol were tested: 0.14 mg; 0.22 mg; 0.37 mg; 0.55 mg; 0.77 mg; 1.02 mg; and 1.79 mg nicotine/L aerosol. For all exposure runs, a paired design was implemented in which air-exposed samples for each of the endpoints and post-exposure collection time points were included (in every exposure run).

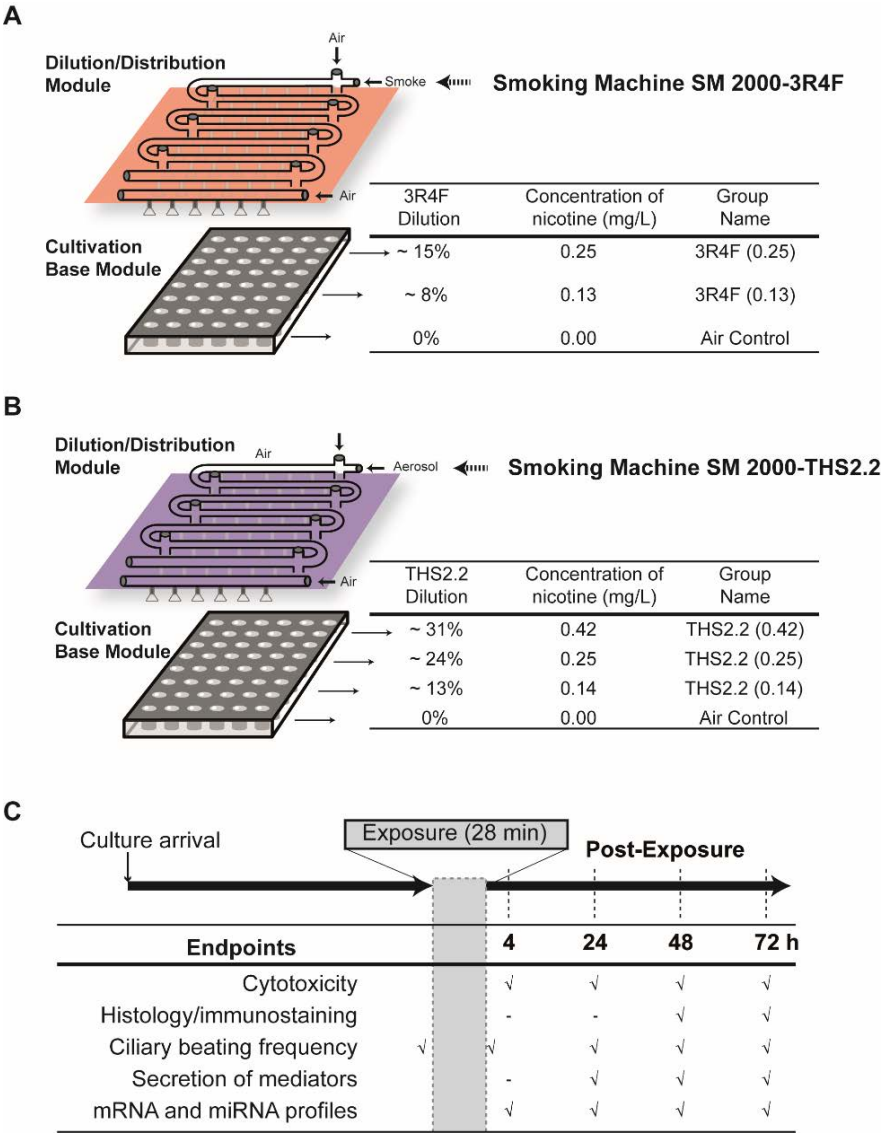


Figure 1. Experimental design

The study comprised six experimental phases. In experimental phase 1 and 2, one to two independent exposure runs were conducted; in experimental phase 3 – 6, at least three independent exposure runs were conducted. During a given exposure run, the cultures were exposed to 3R4F smoke or THS2.2 aerosols using two independent Vitrocell® 24/48 exposure systems. Smoke and aerosols were diluted with air to achieve specific target nicotine concentrations (mg nicotine/L smoke or mg nicotine/L aerosol) at the particular row within the exposure chamber (A, B). For each exposure condition, the cultures were exposed continuously for 28 min to the smoke or aerosol. Endpoints were measured at different time points before and after exposure (C). The total number of samples per endpoint is given in **Supplementary Table 2**.

To characterize the applied smoke/aerosol, the concentrations of nicotine in the whole smoke and aerosol, and the concentrations of representative carbonyls deposited in the Cultivation Base Module of the Vitrocell® 24/48 exposure system were measured (the data reported in **Supplementary Table 1** and **Supplementary Figure 1**). For the nicotine measurement, 3R4F smoke or THS2.2 aerosol (at the applied concentrations) was trapped in EXtrelut® 3NT columns (Merck Millipore, Billerica, MA, USA). Following extraction, the samples were subjected to gas chromatography-flame ionization detection as previously reported (Majeed et al., 2014). For the carbonyl measurement, each row of the Cultivation Base Module was filled with phosphate-buffered saline (PBS) and exposed to the targeted concentrations of 3R4F smoke or THS2.2 aerosol for 28 min. Representative carbonyls were measured using the high performance liquid chromatography-tandem mass spectrometry method, described previously (Majeed et al., 2014).

Tissue processing, embedding, sectioning and staining

The cultures were washed three times with PBS, fixed for 2 h in freshly prepared 4% paraformaldehyde, and washed again three times with PBS. The fixed cultures were separated from the inserts and bisected at the mid-point prior to processing (ASP300 S tissue processor; Leica Biosystem Nussloch GmbH, Nussloch, Germany). The two bisected pieces per culture sample were embedded in paraffin. Five µm-thick cross-sections were cut using a microtome, mounted on glass slides, and stained with hematoxylin (Merck Millipore) and eosin (Sigma-Aldrich, St. Louis, MO, USA) (H&E)/Alcian blue (Sigma-Aldrich) using an ST5020 automated slide stainer (Leica Biosystem Nussloch GmbH). Digital images of each slide (comprising of the two cross-sections per culture sample) were generated using a slide scanner (NanoZoomer 2.0, Hamamatsu Photonics, K.K., Tsukuba, Japan).

Immunohistochemistry (IHC) analysis

IHC was performed to (quantitatively) evaluate whether the proportions of different cell types were impacted by the exposure. The expression of p63, Ki67, and FoxJ1 in the culture sections were examined to detect basal cells, proliferating cells, and columnar ciliated cells, respectively. Automated immunostaining was performed using a Leica BOND-MAX autostainer (Leica Biosystem Nussloch GmbH) with the following primary antibodies: anti-Ki67 (ready to use (RTU), Leica Biosystem-PA0230); anti-p63 (1:100µL, Abcam-ab735, Abcam, Cambridge, UK),

and anti-FoxJ1 (1:2000µL, Abcam-ab40869, Abcam). Digital images of the slides were generated upon scanning using the Hamamatsu NanoZoomer slide scanner (Hamamatsu Photonics, K.K.) Evaluation of the p63, Ki67, and FoxJ1 immunostaining was performed using Tissue Studio 2.0 and Image Miner software (Definiens AG, Munich, Germany). The software was developed with the capability to classify, identify, and discriminate between cellular compartments (nucleus, cilia, and cytoplasm) and the insert membrane. Subsequently, the software, which is equipped with a built-in algorithm, segments the digital pictures and subsequently classifies the objects based on their staining intensity (weak, moderate, and strong staining). The total count of strong staining was considered positive for Ki67; the total count of strong and moderate staining was considered positive for p63; the total count of strong, moderate, and weak staining was considered positive for FoxJ1. The relative proportion of positively stained cells (relative to the total cell number) for each specific marker was calculated.

Adenylate kinase (AK) cytotoxicity assay

AK activity was measured from the basolateral medium, using either a Bioluminescence Cytotoxicity Assay Kit (BioVision, Inc. Milpitas, CA, USA) or a ToxiLight™ bioassay kit (Lonza, Rockland, MA, USA), following the manufacturers' instructions. AK activity was measured using luminescence-compatible 96-well microtiter-plates and a FluoStar Omega reader (BMG Labtech GmbH, Ortenberg, Germany). For a given experimental repetition, only one specific kit was used. The cytotoxicity levels were derived following a normalization to the positive and negative controls for each of the experimental repetitions. The positive control values (i.e., considered as 100% cytotoxicity) were obtained from cultures treated with 1% Triton X-100 to induce a complete lysis of the cells. The negative control values were obtained from untreated or PBS-treated cultures. The normalization formula is given in the **Supplementary Materials and Methods**.

Measurement of secreted pro-inflammatory mediators

Multi-analyte profiling (MAP) of pro-inflammatory mediators secreted in the basolateral media was carried out according to the manufacturer's instructions. Briefly, 25-µL samples of basolateral medium were collected at different post-exposure times (24, 48, and 72 h post-exposure as cross-sectional samples). Luminex® xMAP® Technology (Luminex, Austin, TX,

USA)-based analysis was employed using commercially available Milliplex panels (EMD Millipore Corp., Schwalbach, Germany) to measure the following analytes: Chemokine (C-C motif) ligand (CCL) -1, -2, -5, 20; colony-stimulating factor (CSF)-2, -3; chemokine (C-X-C motif) ligand (CXCL)-1, -8, -10; epidermal growth factor (EGF); interleukin (IL)-1α, IL-1β, IL-6, IL-13; vascular endothelial growth factor alpha (VEGFA); tumor necrosis factor alpha (TNFA); soluble intercellular adhesion molecule (sICAM); matrix metalloproteinase (MMP)-1, MMP-9; tissue inhibitor of metalloproteinase (TIMP)-1; and thymic stromal lymphopoietin (TSLP). Samples were analyzed on a Luminex®, 200™ or FLEXMAP 3D®, equipped with the xPONENT software v.4.2 (Luminex). If the measured concentrations were below the limit of detection, a constant value was used (i.e., half of the lower limit of detection). To demonstrate the capacity of the culture to respond against known pro-inflammatory stimuli, for each of the experimental phases, as positive controls, three cultures were treated with a combination of TNFA and IL-1β added to the basolateral medium at 10 ng/mL each (for a 24 h incubation); whereas, the basal levels of secreted mediators were assessed by measuring a set of triplicate samples following a PBS treatment (added in to the basolateral media).

Ciliary beating frequency (CBF) measurements

Ciliary beating frequencies were measured before and after exposure to 3R4F smoke or THS2.2 aerosol at various time points. Using the Leica DMIL light microscope (Leica, Wetzlar, Germany) and CiliaMetrix high-speed camera (La Haute École de Gestion, Geneva, Switzerland), video recordings of the cultures were generated (2 microscopic fields per culture, each for 512 frames). The measurement was done by placing the cultures at 37°C on a stage-top incubator system (CU-501, Live Cell Instrument, Seoul, South Korea). Automated image analysis software from either CiliaMetrix or CiliaFA was used, the latter running on open-source software (ImageJ) (Smith et al., 2012) . The CiliaFA software extracts the pixel intensities of the region of interest (ROI) over time from previously recorded video sequences, generating a total of 1,600 ROI and converting the pixel intensity into ciliary beating frequency (between 3–52 Hz) based on a fast Fourier transformation (FFT) signal processing.

All 1,600 FFT power magnitudes detected were summed up to obtain a single power spectrum. For one sample, one spectrum was obtained by determining the mean of all spectra obtained from

the two different visual fields. The spectrum was smoothed by using a moving mean value on 10 points (the delta, Δ, between points was approximately 0.18 Hz). Finally, the cilia beating frequency of a given sample was derived from the highest magnitude of the FFT (2.5 Hz was considered the lowest limit of the detected frequency). In a given spectrum, a frequency less than 1.25-times the lowest magnitude was considered noise and not included in the calculation. The FFT power magnitudes were normalized to the ambient noise (the formula is given in the **Supplementary Materials and Methods**). The FFT power magnitudes were subsequently integrated (sum) to those corresponding to the measured frequency described before. Finally, the summed FFT power magnitudes were normalized to the ambient noise, and to their corresponding air control (within a given exposure run, the paired sample).

RNA/microRNA isolation and array analyses

Total RNA including microRNA (miRNA) was isolated after washing the culture inserts twice with cold (4°C) PBS at both the basal and apical sides. The cells were then disrupted in 700 µL QIAzol™ lysis buffer (Qiagen, Hilden, Germany) followed by RNA extraction using a Qiagen miRNeasy Mini Kit and a QIAcube robot (Qiagen). The quantity of the purified RNA was determined using a NanoDrop™ ND8000 spectrophotometer (Thermo Fisher Scientific, Waltham, MA, USA). The quality of the RNA was analyzed using an Agilent 2100 Bioanalyzer (Agilent Technologies, Santa Clara, CA, USA). Samples with an RNA integrity number (RIN) below 6 were not processed.

For the mRNA array, 100 ng of total RNA were reverse-transcribed to cDNA using an Affymetrix® HT 3' IVT PLUS kit (Affymetrix, Santa Clara, CA, USA). The cDNA was labeled and amplified to complementary RNA (cRNA). The fragmented and labeled cRNA was hybridized to a GeneChip® Human Genome U133 Plus 2.0 Array (Affymetrix) in a GeneChip® Hybridization Oven 645 (Affymetrix) according to the manufacturer's instructions. Arrays were washed and stained on a GeneChip® Fluidics Station FS450 DX (Affymetrix) using the Affymetrix® GeneChip® Command Console® Software (AGCC software v-3.2, protocol FS450_0001).

For the miRNA array, a FlashTag™ Biotin HSR kit (Affymetrix) was used to label the miRNA. 200 ng of total RNA containing low molecular weight RNA were biotinylated and hybridized to miRNA arrays version 4.0 (Affymetrix) in a GeneChip® Hybridization Oven 645 (Affymetrix) according to the manufacturer's instructions. Arrays were washed and stained on a GeneChip® Fluidics Station FS450 DX (Affymetrix) using the Affymetrix® GeneChip® Command Console® Software (AGCC software v-3.2, protocol FS450_0002).

Finally, the arrays were scanned using a GeneChip® Scanner 3000 7G (Affymetrix). Raw images from the scanner were saved as DAT files. The AGCC software automatically gridded the DAT file image and extracted probe cell intensities into a CEL file.

Processing raw CEL files of the mRNA microarray

The raw CEL files were background-corrected, normalized, and summarized using frozen-robust multiarray analysis (McCall et al., 2010). Background correction and quantile normalization were used to generate microarray expression values from all arrays passing quality control checks, and were performed using the custom CDF environment HGU133Plus2_Hs_ENTREZG v16.0 (Dai et al., 2005), as previously described in a greater detail (Iskandar et al., 2016).

For each experimental factor combination item, concentration and post-exposure, a model to estimate the treatment effect was fitted with *limma* (Smyth, 2004), by including the covariate exposure run as a blocking variable to account for the pairing during an exposure run (exposed vs. air control). The *p*-values for each computed effect were adjusted across genes using the Benjamini-Hochberg false discovery rate (FDR) method. Differentially expressed genes were defined as a set of genes whose FDR was < 0.05. The mRNA array dataset is available in the Arrays Express repository (ID: *available upon acceptance*).

Network perturbation amplitude analysis on the transcriptomic data

The network perturbation amplitude (NPA) methodology is described in a greater detailed in a previous publication (Martin et al., 2014). Briefly, the methodology aims to contextualize transcriptome profiles (treatment vs. control, or exposed vs. air control) by combining the alterations in gene expression into differentiated node values i.e., one value for each node of a

causal network model (Boue et al., 2015). Relevant network models used for the analysis in this study are listed (**Supplementary Table 3**). The differential node values are determined by fitting procedures inferring the values that best satisfy the directionality of the causal relationships contained in the network model (e.g., positive or negative signs). NPA scores carry a confidence interval accounting for experimental variation, and the associated *p*-values are computed. In addition, companion statistics, derived to inform the specificity of the NPA score to the biology described in the network models, are reported as *O and K* if their *p*-values fall below the threshold of significance (0.05). A network is considered to be significantly impacted by exposure if the three values (the *p*-value for experimental variation, *O, and K*) are below 0.05. The methodology has been described in a greater detail previously (Martin et al., 2014).

In addition to the impact/perturbation scores at the levels of network and subnetwork, the effects of exposure were further quantified as a systems-wide metric for biological impact—the biological impact factor (BIF) (Hoeng et al., 2012; Thomson et al., 2013). This positive value of BIF summarizes the impacts of the exposure on the cellular system into a single number, thus enabling a simple and high-level evaluation of the treatment effects across various time points. Calculating the BIF required the collection of all applicable hierarchically structured network models (**Supplementary Table 3**) and involved aggregating the NPA values of the individual networks.

Processing of the raw CEL files of the miRNA microarray

The CEL files were read using the *oligo* package in the Bioconductor suite of microarray analysis tools for the *R* statistical software environment (Carvalho and Irizarry, 2010; Huber et al., 2015; R Core Team, 2013). Quality control (QC) of the miRNA raw data was performed as previously described (Iskandar et al., 2016), using the *arrayQualityMetrics* package (Kauffmann et al., 2009). Normalized probe-level data were obtained by applying robust multi-array normalization and summarized at the probeset-level using the median polish method (Bolstad et al., 2003). Using the annotation provided by Affymetrix and the latest miRNA nomenclature according to miRBase v21 (Kozomara and Griffiths-Jones, 2013), only the probesets pertaining to human miRNA were kept in the expression matrix. Additionally, the probesets that are not available on Affymetrix GeneChip® miRNA 3.0 arrays were not considered (to maintain the compatabiluty

with other studies using organotypic cultures published before (Iskandar et al., 2016; Zanetti et al., 2016)). Only the miRNA probesets with significantly higher intensity values than their matched background probes must be considered as "detected" (Affymetrix miRNA QCT Tool, 2011). A *p*-value threshold of 0.01 was chosen to determine the detection calls based on Wilcoxon tests. If a miRNA probeset was detected in more than 50% of the samples in at least one sample group, then it was kept for the further analysis; otherwise, it was discarded.

For each comparison (exposed vs air control, at a given stimulus, dose, and post-exposure time point), a submatrix was extracted from the global expression matrix by keeping only those samples belonging to the corresponding treatment or control groups, as well as the miRNA probesets that were detected in more than 50% of the samples in at least one of the two sample groups. A linear model for differential expression was applied to the resulting submatrices using the moderated t statistic implemented in the *limma* package (Ritchie et al., 2015). The models included an additional variable to take into account the exposure runs. Subsequently, adjusted *p*-values were obtained following multiple testing corrections using the Benjamini-Hochberg FDR (Benjamini and Hochberg, 1995). miRNAs below the FDR threshold of 0.05 were considered to be differentially expressed.

Correlation analysis

The repeatability/reproducibility of the experimental repetitions was explored using correlation analyses on the following groups of endpoints: 1) Functional cell-based assays, which include the AK assay, Luminex-based measurement of secreted analytes and (when applicable) immunostaining quantification, and 2) mRNA profiles. Pearson and Spearman correlations were computed for each of these endpoint groups by correlating the means of the endpoint values (normalized to their corresponding controls) obtained from the specific aggregation of the experimental repetition as described in the text.

Before correlating the endpoint values of the functional cell-based assays, the difference (Δ) between the exposed samples and air controls was calculated for each of the concentrations tested, endpoints, and post-exposure time points. To compute the difference (Δ) for the AK assay, normalized levels were used (the normalization procedures are described in the Materials and

Methods: AK cytotoxicity assay). For the immunostaining quantification, the proportion of positive stained cells was used. For the secreted pro-inflammatory mediators, the logarithmic base 10 of the measured concentrations was used to compute the difference (Δ). Subsequently, for each of these endpoints (for a given concentration and post-exposure time point), the mean values of the differences obtained from specific aggregations of experimental repetitions were correlated as specified in the text.

To obtain the correlations of the mRNA profiles, the $\log_2$(fold-changes) in mRNA between the exposed samples and air controls were calculated (for a given concentration and post-exposure time point). The mean fold-changes in each mRNA obtained from a specific aggregation of experimental repetitions were correlated to the other aggregation as specified in the text. For example, we first combined the gene expression data from experiments 1 and 2 and obtained the average fold-change for each gene in the dataset. Similarly, the combined gene expression data from experiments 3 and 4 were combined, and the average fold-changes were obtained. Finally, correlation plots for the fold changes between experiments 1–2 and 3–4 were produced.

Results

Morphology and cytotoxicity of the bronchial organotypic cultures following exposure

Figure 2 shows representative pictures of the cultures examined 72 h post-exposure to air (controls), 3R4F smoke, or THS2.2 aerosol. The H&E- and Alcian blue-stained culture sections of the air-exposed cultures showed the typical pseudostratified structure of airway epithelium, comprising basal cells, ciliated cells, and mucus-secreting goblet cells. Similar morphological structures were observed across the air-exposed samples assessed at different post-exposure time points (72 h post-exposure **(Figure 2)** and at 48 h post-exposure **(Supplementary Figure 2)**).

Following 3R4F smoke applied at 0.13 mg nicotine/L (also referred to as group "3R4F (0.13)"), fewer cilia and goblet cells were observed as compared with the air control at 72 h post-exposure **(Figure 2)**. Pyknotic (condensed) and karyorrhexic (fragmented) nuclei were observed in the 3R4F (0.13)-exposed cultures, indicating the presence of apoptotic cells. Following 3R4F smoke exposure applied at 0.25 mg nicotine/L (also referred to as group "3R4F (0.25)"), a complete detachment of the epithelial cells from the membrane was observed in the majority of the samples **(Figure 2)**, which precluded further histological evaluation (e.g. immunohistochemistry) in this group. Analogous effects were observed at 48 h post-exposure **(Supplementary Figure 2)**.

When THS2.2 aerosol was applied at nicotine concentrations comparable to those of 3R4F smoke, the morphology of the cultures 72 h after exposure to THS2.2 aerosol at 0.14 mg nicotine/L (referred to as "THS2.2 (0.14)" and at 0.25 mg nicotine/L (referred to as "THS2.2 (0.25)") resembled that of the air control **(Figure 2)**. Moreover, following THS2.2 aerosol applied at a higher concentration (0.42 mg nicotine/L, group "THS2.2 (0.42)"), the culture morphology was not different from that of the air-exposed control. Similar effects were observed at 48 h post-exposure **(Supplementary Figure 2)**.

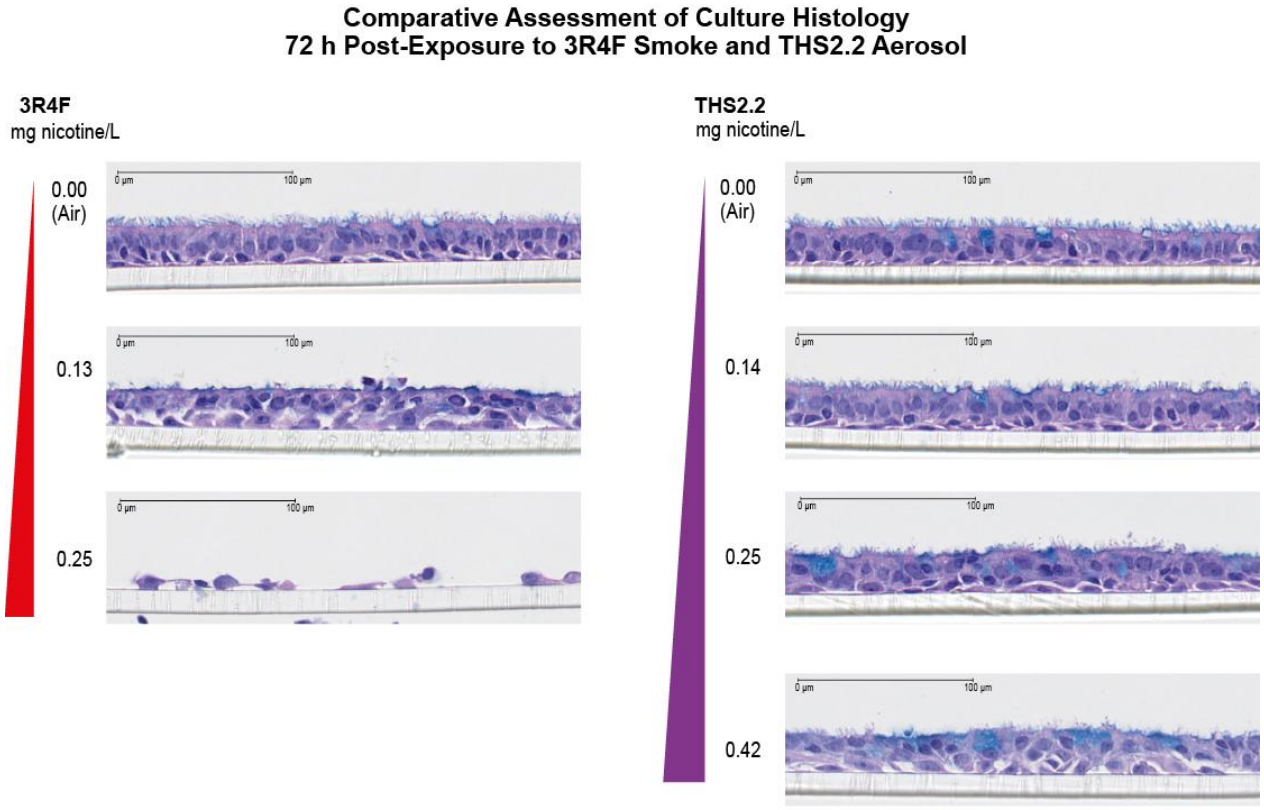


Figure 2. Histology 72 h post-exposure

Representative pictures (taken from experimental repetition 3) of the haematoxylin and eosin (H&E) and Alcian blue-stained culture sections at 72 h post-exposure to 3R4F smoke (left) and THS2.2 aerosol (right) applied at (at least) two comparable nicotine concentrations. Representative pictures for the assessment at 48 h post-exposure are given in **Supplementary Figure 2**.

To detect possible adverse toxic effects of the whole THS2.2 aerosol exposure, a dose range assessment of THS2.2 aerosol exposure was conducted (applied at concentrations ranging from 0.14 to 1.79 mg nicotine/L aerosol). **Figure 3** shows that at 72 h post-exposure, alteration in the culture morphology was only observed in the cultures exposed to THS2.2 aerosol concentrations above 1 mg nicotine/L.

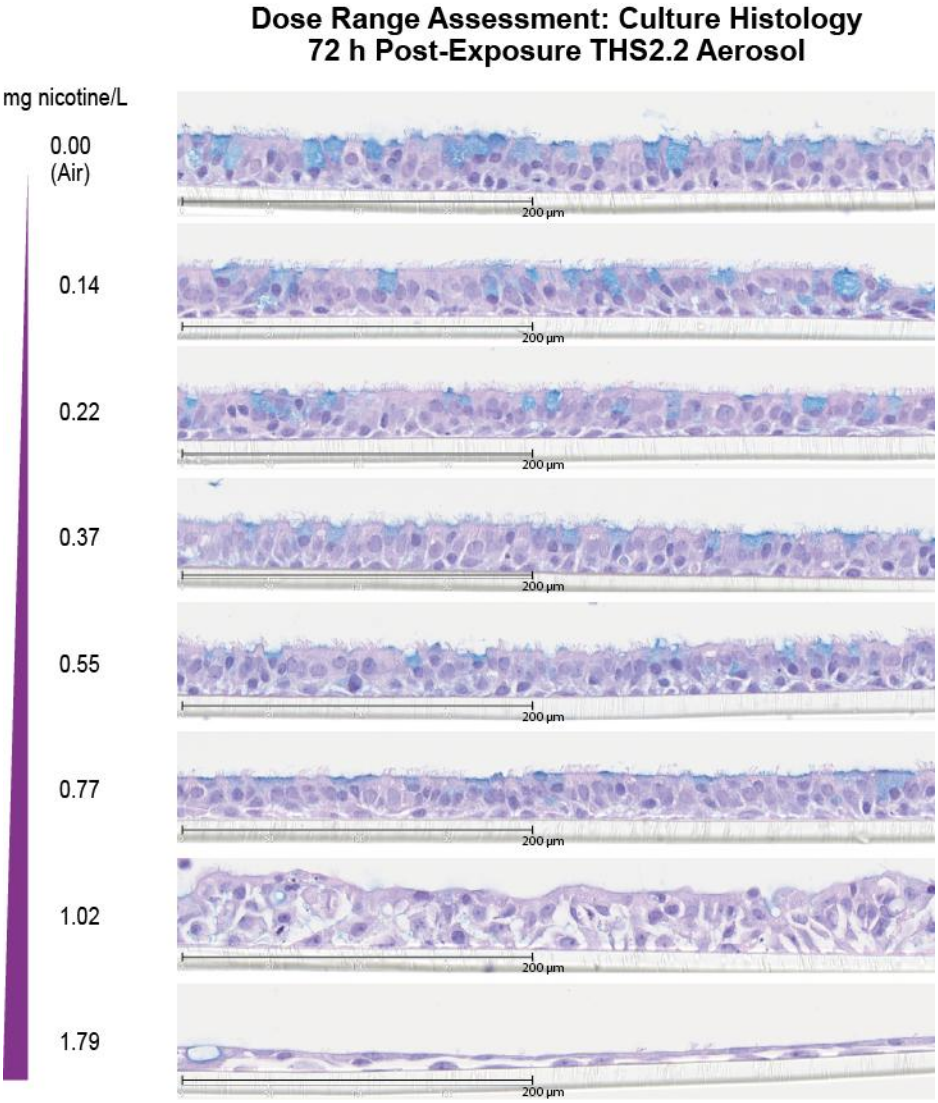


Figure 3. Histology after exposure to a broad range of THS2.2 aerosol concentrations
Representative pictures of the hematoxylin and eosin (H&E)-and Alcian blue-stained MucilAir™ culture sections at 72 h post-exposure to THS2.2 aerosol applied at various nicotine concentrations.

Furthermore, cytotoxicity associated with the exposure was determined by measuring the activity of AK released into the basolateral media following exposure. Damage to cells results in an increased level of AK in the basolateral media, the activity of which can thus infer the degree of cytotoxicity.

At 4 h post-exposure, the cytotoxicity levels across all groups were not significantly different (**Figure 4**). At the later post-exposure time points, greater cytotoxicity levels were detected predominantly for 3R4F (0.25)-exposed cultures (about 24% increased cytotoxicity at 24 h post-exposure, and about 53% increased cytotoxicity at both 48 and 72 h post-exposure). In contrast, the cytotoxicity levels of all THS2.2-exposed groups were comparable to those of the air controls at all post-exposure time points.

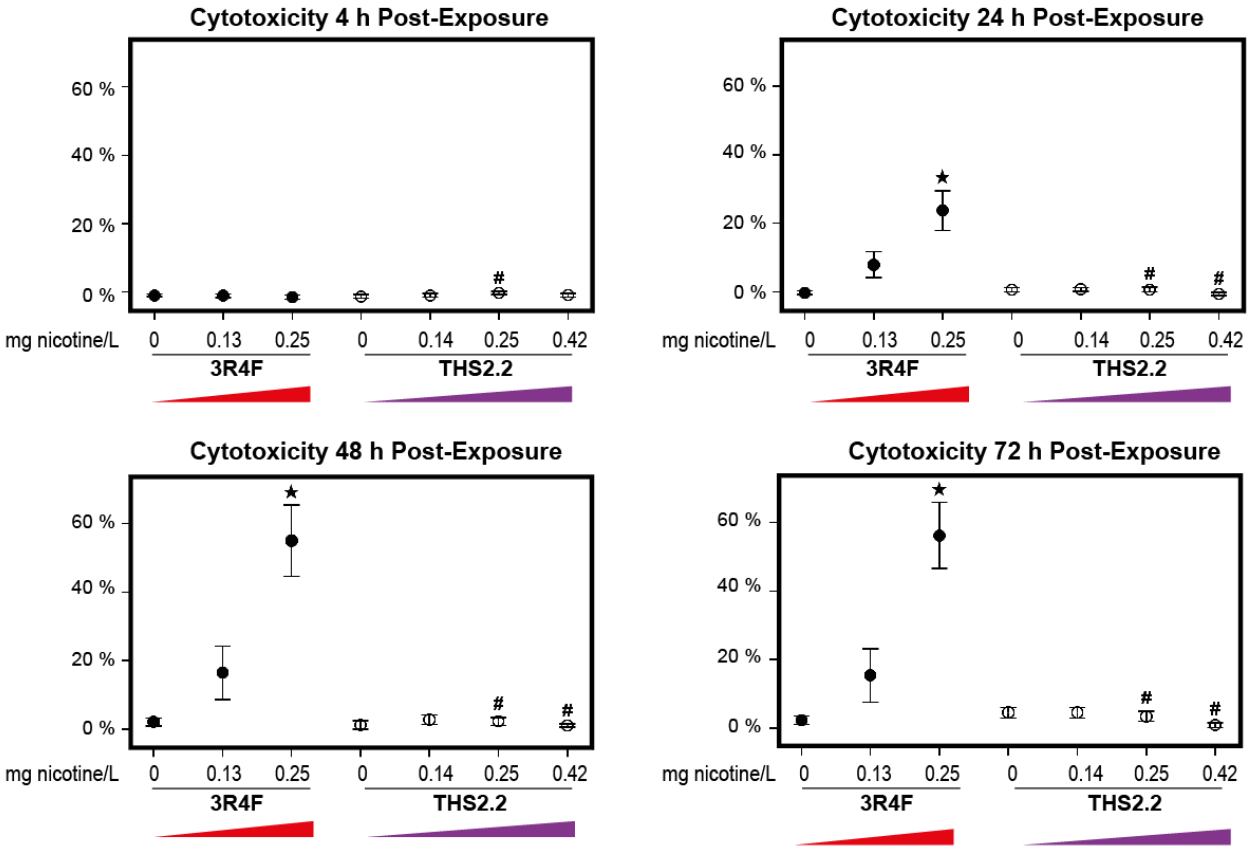


Figure 4. Cytotoxicity levels after exposure

Mean cytotoxicity levels were assessed using an adenylate kinase (AK) assay at various time points of post-exposure following 3R4F smoke and THS2.2 aerosol exposures applied at (at least) two comparable nicotine concentrations. AK levels were normalized relative to the positive and negative control (taken as 100% and 0% cytotoxicity, respectively, as described in Materials and Methods). ★*p*-value < 0.05 vs. its corresponding air control. # p-value < 0.05 vs. 3R4F (0.25).

FoxJ1, p63, and Ki67 immunostaining following exposure

Immunohistochemical staining of FoxJ1, p63, and Ki67 was conducted to evaluate the proportions of ciliated cells, basal cells, and proliferating cells, respectively. The staining was performed in the culture sections collected at 48 and 72 h post-exposure. **Figure 5** shows representative images of the stained cultures.

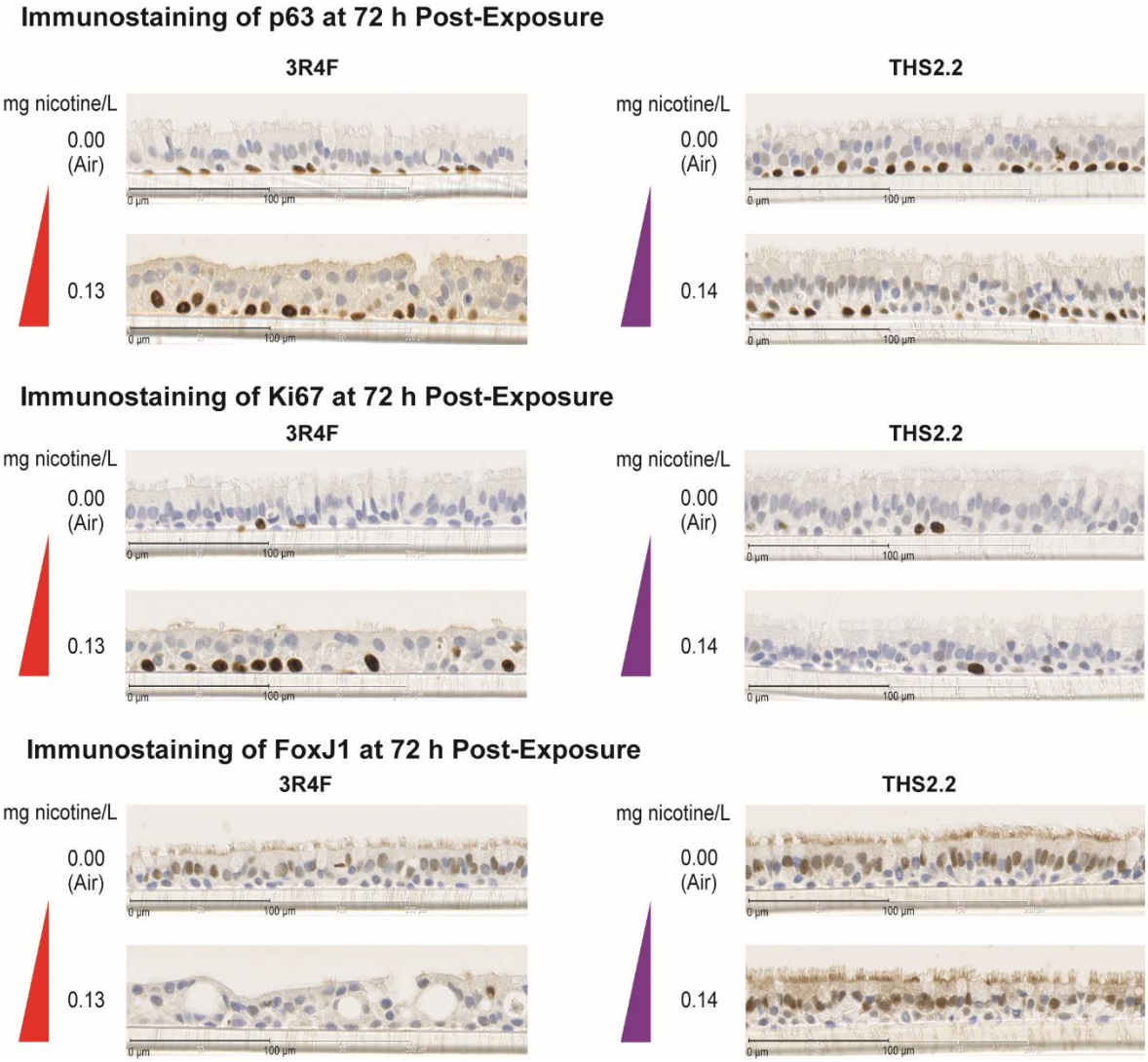


Figure 5. Immunostained bronchial culture sections following exposure
Representative pictures of the p63-, Ki67-, and FoxJ1-positive stained culture sections examined at 72 h post-exposure (part of the experimental repetition 3). 3R4F smoke and THS2.2 aerosol were applied at comparable nicotine concentrations (i.e., 3R4F (0.13) and THS2.2 (0.14)).

Exposure to 3R4F (0.13) smoke was linked to increased proportions of p63-positive basal cells at both 48 and 72 h post-exposure (**Table 2**), while the increased at 72 h post-exposure did not reach statistical significance (*p*-value = 0.09). The proportions of Ki67-positive proliferating cells in the 3R4F (0.13)-exposed samples were almost twice of the air-exposed at 72 h post-exposure, although the difference was not statistically significant (*p*-value = 0.18). The proportions of FoxJ1-positive ciliated cells following 3R4F (0.13) exposure were only 50% of the air control (*p*-value = 0.06 at 48 h post-exposure; *p*-value = 0.19 at 72 h post-exposure).

At all concentrations tested, THS2.2 aerosol exposure did not remarkably alter the proportion of p63, ki67, and FoxJ1 at 48 and 72 h post-exposure, despite decreases in Ki67 proportion at 72 h following THS2.2 (0.14) and THS2.2 (0.25) and an increase in FoxJ1-positive staining at 48 h post-exposure to THS2.2 (0.14). However, dose-dependent effects of THS2.2 aerosol on the proportion of these markers were not observed (**Table 2**).

Table 2. Quantification of p63, Ki67, and FoxJ1-positive stained cells

	P63		**Ki67**		**FoxJ1**	
	Post-Exposure		**Post-Exposure**		**Post-Exposure**	
	48 h	**72 h**	**48 h**	**72 h**	**48 h**	**72 h**
3R4F (Air)	20.99 ± 1.52 (N = 11)	24.11 ± 1.50 (N = 9)	4.58 ± 0.59 (N = 11)	5.81 ± 0.44 (N = 9)	19.90 ± 4.17 (N = 11)	17.34 ± 5.69 (N = 9)
3R4F (0.13)	28.79± 2.19* (N = 9)	29.98 ± 1.99 (N = 8)	6.73 ± 1.24 (N = 9)	11.14 ± 3.63 (N = 8)	10.64 ± 4.13 (N = 9)	8.67 ± 1.82 (N = 8)
THS2.2 (Air)	21.47± 2.72 (N = 6)	19.64 ± 2.95 (N = 6)	3.96 ± 0.94 (N = 6)	4.71 ± 0.72 (N = 6)	23.09 ± 2.21 (N = 6)	25.56 ± 5.64 (N = 6)
THS2.2 (0.14)	19.99 ± 2.13 (N = 6)	20.94 ± 1.55 (N = 6)	5.20 ± 0.91 (N= 6)	3.24 ± 0.57* (N = 6)	31.61 ± 5.08* (N = 6)	26.63 ± 6.98 (N = 6)
THS2.2 (0.25)	19.91 ± 2.30 (N = 6)	18.68 ± 0.53 (N = 6)	2.14 ± 0.37 (N= 6)	1.96 ± 0.45* (N = 6)	25.72 ± 4.90 (N = 6)	28.56 ± 7.45 (N = 6)
THS2.2 (0.42)	18.14 ± 1.21 (N = 6)	22.86 ± 4.17 (N = 6)	2.90 ± 0.44 (N = 6)	2.28 ± 0.93 (N = 6)	29.32 ± 3.70 (N = 6)	28.25 ± 6.14 (N = 6)

Mean proportions of the positive-stained cells were reported (± standard error of the mean). *p-value < 0.05 vs. its corresponding air control. The proportion of positively-stained cells was digitally quantified relative to the total cell number in a given culture section. Numbers in parentheses indicate the total samples per group.

Alterations in ciliary beating frequency

Following 3R4F (0.13) exposure, reduced ciliary beating frequency (CBF) levels were observed at 48 and 72 h post-exposure, but not at the earlier post-exposure time points **(Table 3)**. An almost complete reduction in CBF was observed at 72 h post-exposure to 3R4F (0.13). Following 3R4F (0.25) smoke exposure, the CBF values were very low (below or around the 2.5 Hz detection threshold) at all post-exposure time points.

At the comparable concentration (0.13 or 0.25 mg nicotine /L), THS2.2 aerosol exposure did not pronouncedly alter the beating frequency. There was no immediate impact on the CBF levels following THS2.2 aerosol at all concentrations tested. Even at 72 h post-exposure, the CBF levels were reduced only by approximately 20–28% (relative to those before exposure to THS2.2 aerosol).

Table 3. Ciliary beating frequency (Hz) before and after exposure

	3R4F (Air Control)	**3R4F (0.13)**	**3R4F (0.25)**	
	0 mg nicotine/L	**0.13 mg nicotine/L**	**0.25 mg nicotine/L**	
Time of Measurement				
Before Exposure	7.03 ± 0.67 (N = 3/3)	7.79 ± 0.16 (N = 3/3)	7.91 ± 0.35 (N = 3/3)	
0 h Post-Exposure	10.14 ± 0.75 (N = 3/3)	11.78 ± 2.81 (N = 3/3)	< Threshold (N = 3/3)	
24 h Post-Exposure	5.68 ± 0.26 (N = 3/3)	10.02 ± 1.41 (N = 2/3)	< Threshold (N = 3/3)	
48 h Post-Exposure	11.25 ± 2.78 (N = 3/3)	4.80 ± 2.17 (N = 3/3)	2.64 ± 0.00 (N = 2/3)	
72 h Post-Exposure	5.92 ± 0.16 (N = 3/3)	6.33*; < Threshold (N = 3/3)	< Threshold (N = 3/3)	
	THS2.2 (Air Control)	**THS2.2 (0.14)**	**THS2.2 (0.25)**	**THS2.2 (0.42)**
	0 mg nicotine/L	**0.14 mg nicotine /L**	**0.25 mg nicotine /L**	**0.42 mg nicotine /L**
Time of Measurement				
Before Exposure	9.79 ± 0.72 (N = 9/9)	9.63 ± 0.64 (N = 9/9)	10.16 ± 0.54 (N = 9/9)	10.35 ± 0.70 (N = 9/9)
0 h Post-Exposure	10.02 ± 0.89 (N = 9/9)	10.14 ± 0.62 (N = 9/9)	10.27 ± 0.57 (N = 9/9)	9.82 ± 0.55 (N = 9/9)
24 h Post-Exposure	7.03 ± 0.70 (N = 6/6)	6.59 ± 0.49 (N = 6/6)	6.24 ± 0.27 (N = 6/6)	6.09 ± 0.27 (N = 6/6)
48 h Post-Exposure	8.67 ± 0.46 (N = 9/9)	8.65 ± 0.58 (N = 9/9)	8.91 ± 0.69 (N = 9/9)	8.22 ± 0.53 (N = 9/9)
72 h Post-Exposure	9.38 ± 1.02 (N = 9/9)	6.95 ± 1.12 (N = 9/9)	8.14 ± 1.17 (N = 7/9)	7.89 ± 1.24 (N = 7/9)

Mean ± SEM is shown. Numbers in parentheses indicate the number of samples from which frequency signals were detected, out of the total number of samples where ciliary beating measurement was done. *Only one replicate (out of the three samples) had a ciliary beating frequency (CBF) value above the threshold.

Moreover, a power analysis was conducted to measure the beating signals that were detected by the software (the FFT power magnitudes reflect the beating signals within the measurement area). The power of the detected signal, depending on the proportion of beating cells in the measurement area, was calculated for each group relative to the respective air control (taken as 100 %). A complete reduction in the beating signal was detected immediately after exposure (0 h post-exposure) to 3R4F (0.13) and 3R4F (0.25) **(Table 4)**. At 24 and 48 h post-exposure to 3R4F (0.13), a slight recovery of the signal was observed. However, at 72 h post-exposure, the power of the beating signals remained low (less than 10% of the level before exposure). At all post-exposure time points following 3R4F (0.25) exposure, the beating signals were very low (less than 1 % of the level before exposure).

When THS2.2 aerosol was applied at nicotine concentrations comparable to those of 3R4F smoke (i.e. THS2.2 (0.14) and THS2.2 (0.25)), approximately a 30–40% reduction in the beating signal was observed immediately after exposure (0 h post-exposure). No further reduction of the beating signal was observed at the later time points post-exposure to THS2.2 (0.14) and THS2.2 (0.25) **(Table 4)**. When THS2.2 aerosol was administered at 0.42 mg nicotine/L, the detected signals were comparable to those following THS2.2 (0.14) or THS2.2 (0.25) at the various post-exposure time points. Furthermore, a dose-dependent effect of THS2.2 aerosol on the beating signals was not observed.

Table 4 Power (%) of the detected beating signal before and after exposure

	3R4F (Air Control) 0 mg nicotine/L	3R4F (0.13) 0.13 mg nicotine/L	3R4F (0.25) 0.25 mg nicotine/L	
Time of Measurement				
Before Exposure	100.00 ± 75.81 (N = 3)	74.87 ± 39.28 (N = 3)	84.26 ± 41.67 (N = 3)	
0 h Post-Exposure	100.00 ± 55.54 (N = 3)	0.40 ± 0.13 (N = 3)	0.04 ± 0.02 (N = 3)	
24 h Post-Exposure	100.00 ± 84.80 (N = 3)	33.77 ± 32.46 (N = 3)	0.10 ± 0.02 (N = 3)	
48 h Post-Exposure	100.00 ± 44.67 (N = 3)	23.81 ± 22.21 (N = 3)	0.55 ± 0.15 (N = 3)	
72 h Post-Exposure	100.00 ± 69.17 (N = 3)	6.53 ± 6.26 (N = 3)	0.39 ± 0.13 (N = 3)	
	THS2.2 (Air Control) 0 mg nicotine/L	**THS2.2 (0.14) 0.14 mg nicotine /L**	**THS2.2 (0.25) 0.25 mg nicotine /L**	**THS2.2 (0.42) 0.42 mg nicotine /L**
Time of Measurement				
Before Exposure	100.00 ± 21.48 (N = 9)	99.35 ± 22.43 (N = 9)	130.08 ± 24.63 (N = 9)	140.13 ± 30.20 (N = 9)
0 h Post-Exposure	100.00 ± 23.70 (N = 9)	68.17 ± 20.14 (N = 9)	77.87 ± 18.31 (N = 9)	78.83 ± 25.94 (N = 9)
24 h Post-Exposure	100.00 ± 31.89 (N = 6)	62.29 ± 13.67 (N = 6)	77.91 ± 10.99 (N = 6)	62.94 ± 17.17 (N = 6)
48 h Post-Exposure	100.00 ± 32.88 (N =9)	56.85 ± 14.20 (N =9)	87.11 ± 19.60 (N =9)	62.99 ± 16.74 (N =9)
72 h Post-Exposure	100.00 ± 17.39 (N = 9)	64.34 ± 10.57 (N = 9)	62.32 ± 13.70 (N = 9)	42.96 ± 10.62 (N = 9)

The power of the detected signal was calculated relative to that of the air control (taken as 100 %). Mean ± SEM is shown. Numbers in parentheses indicate the number of samples.

Secretion of pro-inflammatory mediators following exposure

The inflammatory response of the bronchial cultures following exposure was assessed by measuring the concentrations of secreted mediators in the basolateral media at 24, 48 and 72 h post-exposure (they were sampled cross-sectionally). The concentration of various pro-inflammatory mediators were measured using Luminex-based technology.

Figure 6 shows the individual concentrations of representative pro-inflammatory mediators per sample for each group. The data illustrate that for most mediators, the greater the concentration of 3R4F smoke, the higher the concentrations of the mediators (an exception is observed for VEGFA). Following THS2.2 aerosol exposure, in most cases, no alteration of the mediator concentration was observed. In only few cases where significant differences were found following THS2.2 exposure, the changes were minimal as compared with those following 3R4F smoke (at all nicotine concentrations tested). For the few cases in which significantly different mediator concentrations following THS2.2 exposure were observed, THS2.2 aerosol was applied at nicotine concentration of 0.44 mg nicotine/L, which was almost twice than the nicotine concentration in the highest dose of 3R4F (0.25 mg nicotine/L). Also, the significant differences following THS2.2 aerosol were observe predominantly at the earlier post-exposure time point, which were in contrast with those following 3R4F smoke exposure—the differences remained significant at 72 h post-exposure.

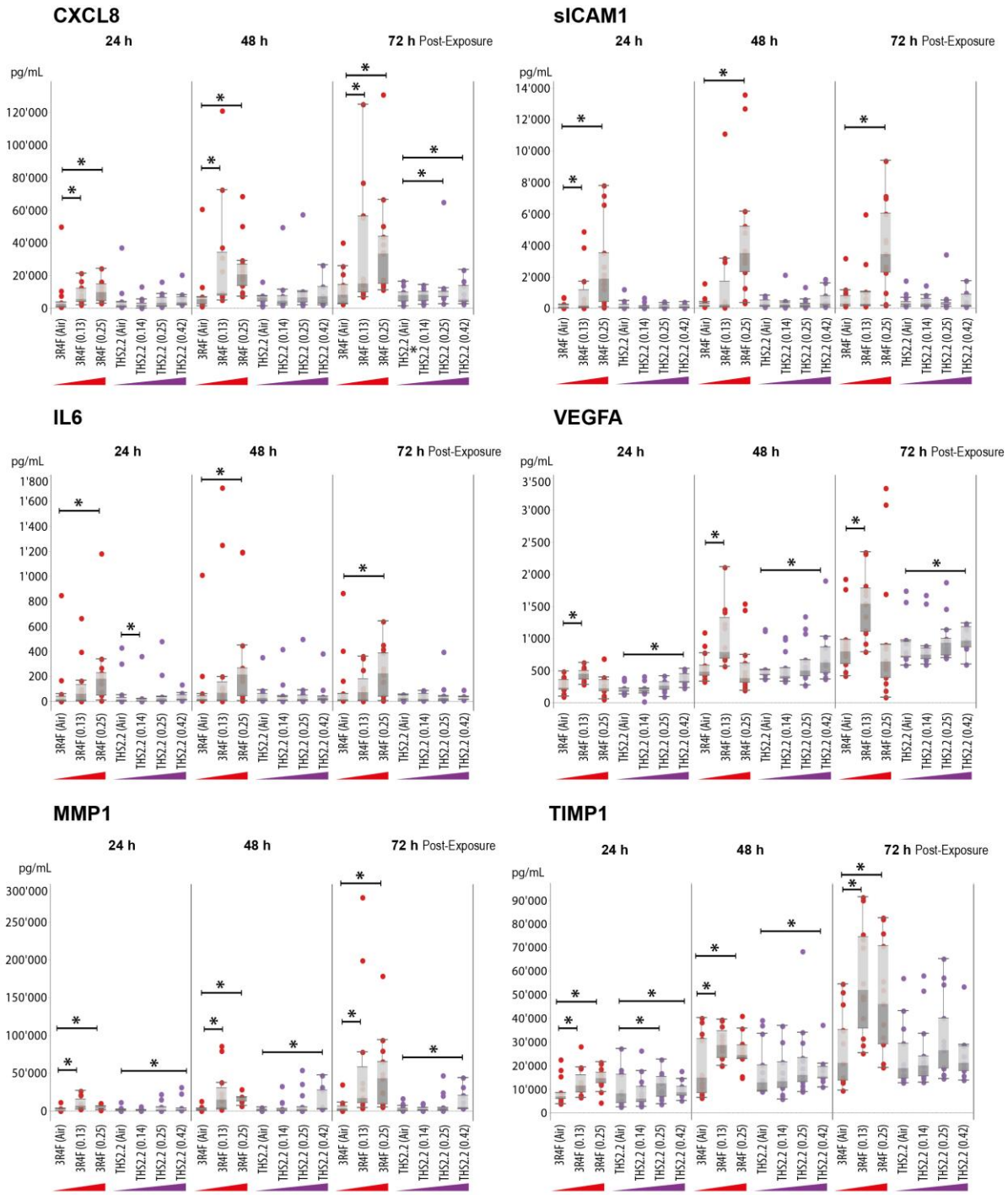


Figure 6. Concentration of pro-inflammatory mediators released in the basolateral media after exposure

Concentrations of representative pro-inflammatory mediators are shown. Each dot indicates the concentrations detected in each sample measured in a total of six experimental repetitions. The box plots shows the upper whisker (1.5 times the interquartile range), upper quartile, median, lower quartile, and lower whisker (1.5 times the interquartile range). *indicates *p*-value < 0.05 vs. its corresponding air control. For all mediators measured following exposure, their fold-changes (exposed vs. their respective air controls) are reported in **Supplementary Figure 3**.

Network-based differential gene expression analysis

Possible exposure-specific alterations at the cellular and molecular level associated with THS2.2 aerosol and 3R4F smoke exposure were examined in cultures that were not substantially damaged. This choice was made because molecular alterations associated with severely damaged tissue only reflect the damaged that has already occurred (Davis et al., 2013). Therefore, because substantial tissue damage (**Figure 2**) was observed in 3R4F (0.25)-exposed cultures, the gene expression analysis was conducted only in the cultures exposed to 3R4F (0.13), THS2.2 (0.14), THS2.2 (0.25), and THS2.2 (0.42).

Expression of many genes was found to be significantly altered following 3R4F (0.13) smoke exposure (compared with air-exposed cultures), even at 72 h post-exposure (**Table 5**). In contrast, the gene expression following THS2.2 exposure was mainly altered at 4 h post-exposure, but was considerably less perturbed at 24, 48, and 72 h post-exposure (for all concentrations tested). Volcano plots of the microarray data showing the relative expression of mRNA following exposure are shown in **Supplementary Figure 4**.

Table 5. Number of significantly differentially expressed genes

Post-Exposure	Group (mg nicotine/L)	3R4F (0.13)	THS2.2 (0.14)	THS2.2 (0.25)	THS2.2 (0.42)
4 h	Upregulated	2049	171	1517	1981
	Downregulated	2533	97	1620	2430
24 h	Upregulated	3871	2	71	733
	Downregulated	3724	0	20	530
48 h	Upregulated	3374	0	0	57
	Downregulated	2537	0	0	42
72 h	Upregulated	2624	0	1	61
	Downregulated	2112	0	0	23

Numbers indicate those that are significantly different at FDR < 0.05.

The impact of exposure on various biological processes was quantitatively evaluated from the transcriptomic data leveraging a network-based systems biology approach (Martin et al., 2014). The Network Perturbation Amplitude (NPA) algorithm was used to translate gene fold-changes into the magnitude of changes in cellular signaling (Martin et al., 2014). The NPA score can thus reflect an exposure-induced alteration of certain biological processes, captured in causal network models (Boue et al., 2015). Moreover, the overall systems impact—i.e., the aggregation of the network perturbations—referred to as the Biological Impact Factor (BIF) was also computed (see

Materials and Methods). This approach uses biological network models composed of interrelated cause-and-effect relationships. These causal network models can be grouped into various families modelling biological processes involved in Cell Proliferation (CPR), Cell Fate (CFA), Cell Stress (CST), and inflammatory response (IPN, Inflammatory Process Networks) (Boue et al., 2015). The edges of the networks carry a causal directionality between two nodes (increase or decrease) based on information extracted from scientific literature (Martin et al., 2014). The nodes correspond to biological entities (e.g., protein abundances, protein activities, chemical compounds, or biological processes described as molecular entities); thus, they can be considered as the functional layer of the network models (often referred to as "backbone nodes"). Because many of the backbone nodes are supported by literature-derived knowledge regarding their ability to regulate the expression of particular genes, each network model has a "measurable layer" consisting of mRNA nodes. As a result, a transcriptome profile (exposed vs. control samples) can be used to predict the activity of the functional layer of the network. To quantify the perturbation of various biological network models (i.e., the biological impact) following exposure to 3R4F smoke and THS2.2 aerosol, the transcriptome profiles—collected at 4 h, 24 h, 48 h, and 72 h after exposure (exposed vs. control samples)—were used.

Figure 7 shows the overall biological impact (in the context of the biology covered in the network models) for each exposure condition compared with the corresponding air control. At the 4 h post-exposure time point, 3R4F at 0.13 mg nicotine/L smoke exposure produced the highest impact on the tissues; thus, the relative BIF was set to 100 % (the reference, REF). The impact of 3R4F (0.13) exposure decreased with increasing duration of the post-exposure period. A 40 % reduction in the impact factor was found at 24 h post-exposure to 3R4F (0.13) (relative BIF = 59.6 %), as compared with that at 4 h post-exposure (relative BIF = 100 %). At 48 h and 72 h post-exposure time-points, the relative BIFs of 3R4F (0.13) were 30.2% and 23.4%, respectively.

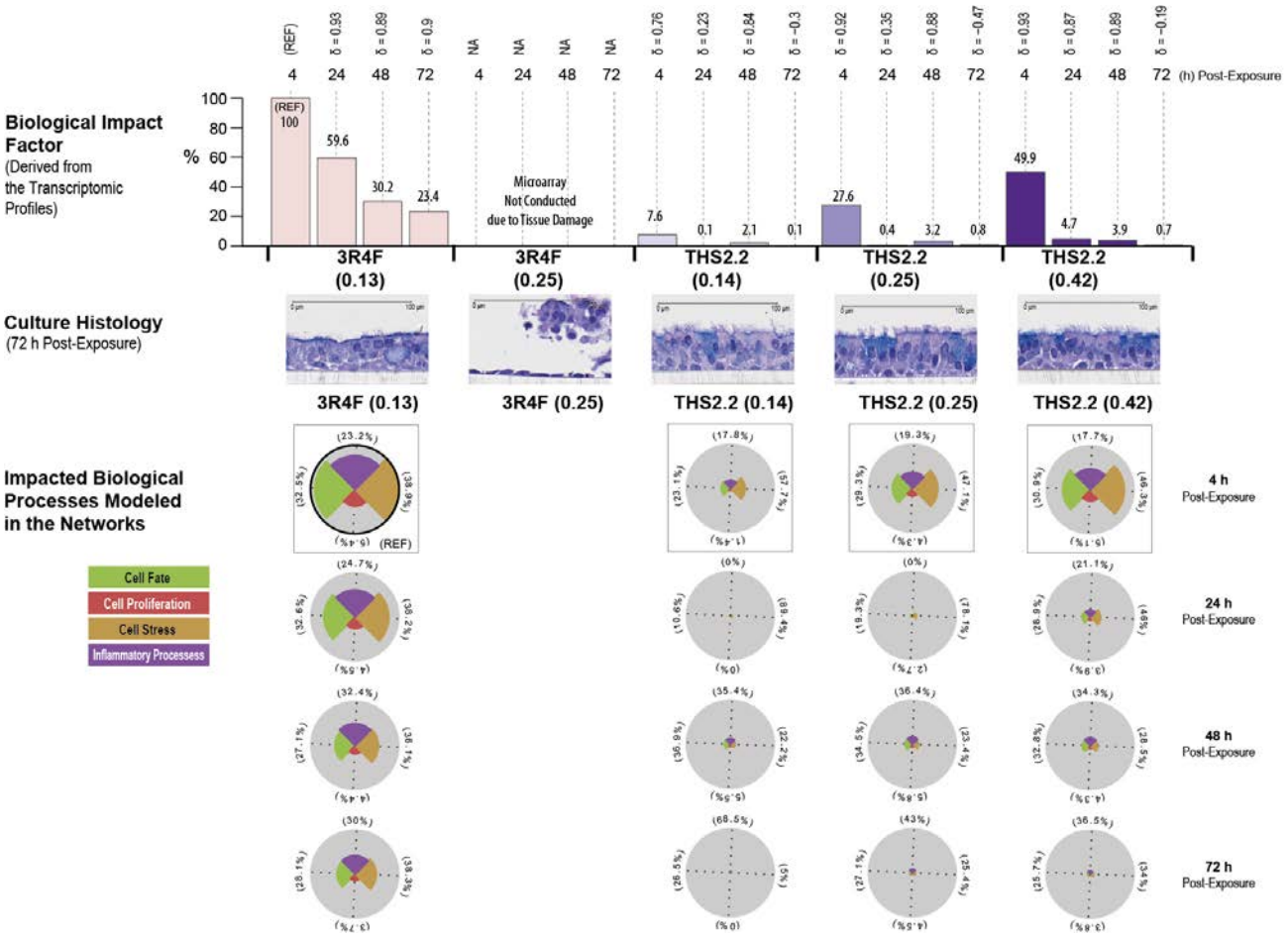


Figure 7. Relative Biological Impact Factor (BIF) derived from cumulated network perturbations impacted by 3R4F and THS2.2 exposure compared with the air controls

Upper panel: Percentage Relative BIF is plotted on the y-axis (upper panel). The highest BIF value, marked as the reference (REF) is taken as 100%. The δ values (δ in [−1, 1]) given above the bars indicate how similar the underlying networks perturbed following a particular exposure relative to those of the REF. δ = 0 indicates no similarity of the perturbed networks; δ = 1 indicates identical underlying networks being perturbed; δ = −1 indicates that completely opposite underlying networks were perturbed. Middle panel: Representative histological section of the cultures at 72 h post-exposure. Lower panel: Each starplot represents the corresponding bar in the BIF plot. A slice of the starplot indicates one of the Cell Fate, Cell Stress, Cell Proliferation, and Inflammatory Network families. The area of each slice of the starplot refers to its relative contribution to the relative BIF (expressed as % in brackets). The starplot of the REF is outlined with a thick black line.

When THS2.2 aerosol was applied at nicotine concentrations comparable to those of 3R4F smoke, the relative BIF of THS2.2 (0.14) at 4 h post-exposure was only 7.6%. A sharp decline of the biological impact (a 98 % reduction as compared with the 4 h post-exposure time point) was observed at 24 h post-exposure to THS2.2 (0.14), which continued to decline thereafter. The relative BIF values following exposure to the higher concentrations of THS2.2 aerosol (THS2.2 (0.25) and THS2.2 (0.42)) at 4 h post-exposure were 27.6% and 49.9%, respectively. Almost complete reductions in the biological impact (> 90% reductions as compared with the 4 h post-exposure time point) were observed at 72 h post-exposure to THS2.2 (0.25) and THS2.2 (0.42); with relative BIFs of 0.8% and 0.7%, respectively.

An overview of the different biological processes that contributed to the overall BIF for each exposure is illustrated as starplots below the bars (**Figure 7**). The starplots are used to represent the contribution of each perturbed network family to the overall BIF. Among the network families, the patterns of the perturbed networks were similar between 3R4F smoke and THS2.2 aerosol: highest for the Cell Stress (CST) network family, followed by the Cell Fate (CFA), Inflammatory Processes network (IPN), and Cell Proliferation (CPR).

Because each network family consists of a set of network models, the BIF can be decomposed down to the network level. **Figure 8** displays a heatmap of the perturbation amplitude score (NPA score) of each network. Reflecting the overall BIF, the highest NPA scores were observed at the 4 h post-exposure time point and gradually decreased with increasing post-exposure duration.

At a concentration of 0.13 mg nicotine/L, 3R4F smoke had a significant impact on almost all networks within the Cell Fate, Cell Stress, and Inflammatory Processes families. Within the Cell Proliferation network family, Wnt, PGE2, Nuclear Receptor, Mapk, Jak Stat, Growth Factor, and Cell Cycle networks were markedly perturbed following 3R4F (0.13) exposure. At a comparable nicotine concentration (i.e., THS2.2 (0.14)), the degree of network perturbations (NPA scores) was much lower than the NPA score following 3R4F (0.13) exposure.

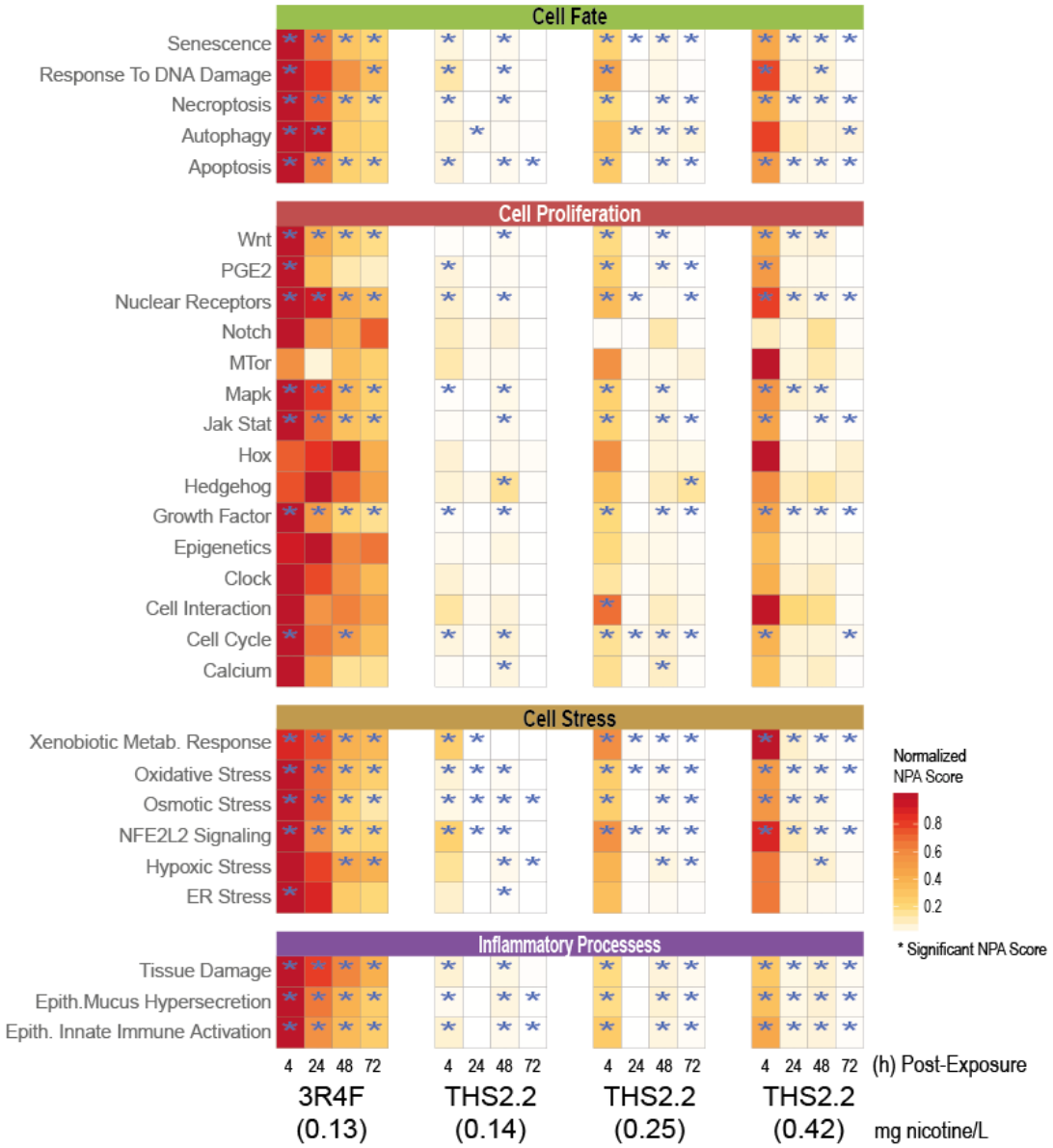


Figure 8. Heatmap of Network Perturbation Amplitude (NPA) scores of biological networks impacted by 3R4F and THS2.2 exposure

The network names are listed on the left side of the heatmap with the corresponding network family at the top of each cluster. The color gradient represents the NPA scores, which were normalized to the maximum NPA score per network. The star symbols (*) in the heatmap indicate that the network is considered to be significantly impacted by exposure (i.e., the three values—the confidence interval, *O*, and *K** statistics—are below 0.05, as described in the Materials and Methods). Abbreviations: Epith., epithelial; Metab., metabolism.

A gene-set analysis was also conducted as a complementary method. The results are reported as a heatmap of the enrichment scores **(Supplementary Figure 5)**. The gene-set analysis shows that the gene expression data from the tissues exposed to 3R4F (0.13) were greatly associated with far more KEGG pathway annotations than the annotations associated with THS2.2 (0.14) aerosol.

Differential Expression of Selected Genes Regulating Cell Stress and Inflammation

In addition to the network and gene-set analysis, the differentially expressed genes that regulate cell stress and inflammatory processes are displayed in **Figure 9** and **Figure 10**, respectively.

Exposure to 3R4F (0.13) smoke was associated with pronounced expression changes of genes regulating oxidative stress and xenobiotic stress. The majority of these genes were significantly altered at all post-exposure time points tested. The expression levels of *SLC7A11*, *MAFF*, *HMOX1*, *CYP1A1*, and *CYP1B1* were strongly increased at all post-exposure time points after 3R4F (0.13) exposure. At a comparable nicotine concentration, THS2.2 (0.14) aerosol was associated with significant expression changes of these genes only at 4 h post-exposure. Higher concentrations of THS2.2 aerosol applied to the bronchial cultures were associated with greater fold-changes of these genes relative to the air control.

Expression of genes involved in DNA damage response (e.g., *DDIT3*), endoplasmic reticulum stress (e.g., *SLC3A2, ATF6*), heat shock (e.g., *DNAJB9*) or hypoxic stress (e.g., *VEGFA, CA12*), were significantly altered after 3R4F (0.13) smoke exposure at all post-exposure time points. However, THS2.2 aerosol at a comparable nicotine concentration (i.e. THS2.2 (0.14)) did not impact the expression levels of the majority of these genes. When THS2.2 aerosols were applied at 0.25 and 0.42 mg nicotine/L, the expression levels of these genes were only altered at the earlier post-exposure time points.

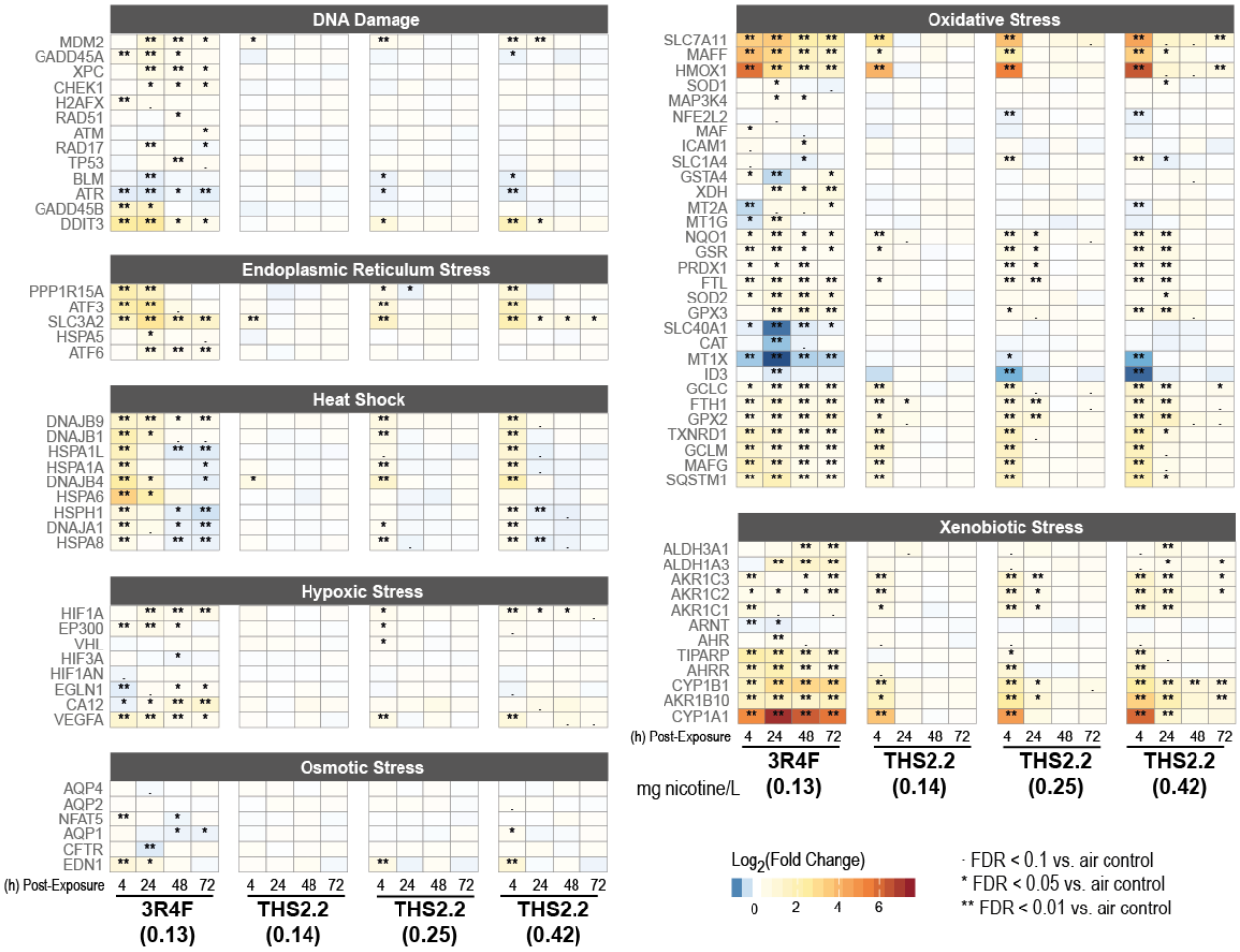


Figure 9. Differential expression changes of genes regulating cellular stress following 3R4F and THS2.2 exposure

Gene symbols are listed on the left side of the heatmap. Specific stress-related processes are marked at the top of each cluster. The color gradient reflects the alterations in gene expression as compared with the respective air controls.

As shown in **Figure 10**, the expression level of various genes involved in inflammatory processes was altered following 3R4F (0.13) smoke exposure at all post-exposure time points tested. At the comparable nicotine concentration, THS2.2 (0.14) did not elicit a significant alteration the expression of these genes. Following exposure to THS2.2 aerosol at higher concentrations (i.e. 0.25 and 0.42 mg nicotine/L), significant alterations of the expression of the genes were found predominantly at 4 h post-exposure time point.

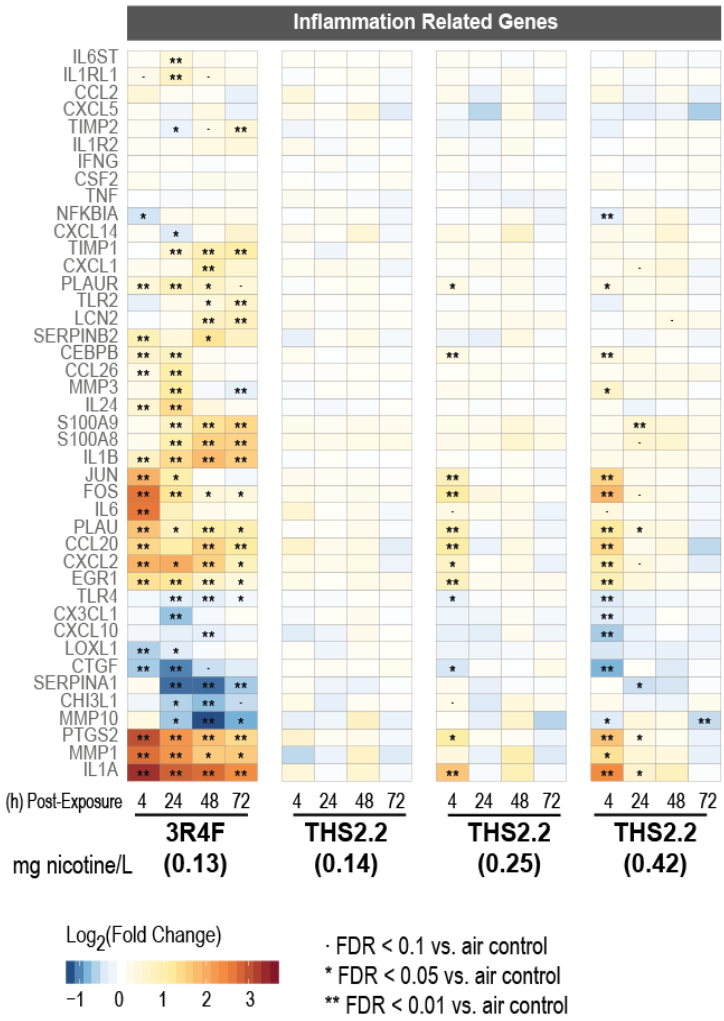


Figure 10. Differential expression changes in genes related to inflammatory processes following 3R4F and THS2.2 exposure

Gene symbols are listed on the left side of the heatmap. The color gradient reflects the alterations in gene expression as compared with their respective air control.

Alterations in miRNA profiles of the bronchial epithelial cultures following exposure

MiRNA expression profiles of the cultures following exposure to 3R4F (0.13) and THS2.2 (0.14), THS2.2 (0.25), and THS2.2 (0.42) were obtained to further assess the toxicity-related molecular mechanisms associated with the exposure. Among all exposure groups, 3R4F (0.13) exposure elicited the largest number of altered miRNAs at a given post-exposure time point tested **(Figure 11)**. The greatest number of altered miRNAs was observed at the 72 h post-exposure time point. None of the miRNAs were significantly changed following THS2.2 aerosol at the comparable nicotine concentration (i.e., the THS2.2 (0.14)).

Only two miRNAs were found to be significantly altered following THS2.2 (0.25) exposure. Decreased levels of miR-4669 and miR-4701 were detected at the 48 h post-exposure time point following THS (0.25) exposure; there was no dose-dependent impact of THS2.2 exposure on either miRNAs **(Figure 11)**. Following exposure to the highest concentration of THS2.2 (i.e., THS2.2 (0.42)), increased miR-378 and miR-320 levels were detected at 72 h post-exposure exposure; both were also increased at 72 h post-exposure to 3R4F (0.13).

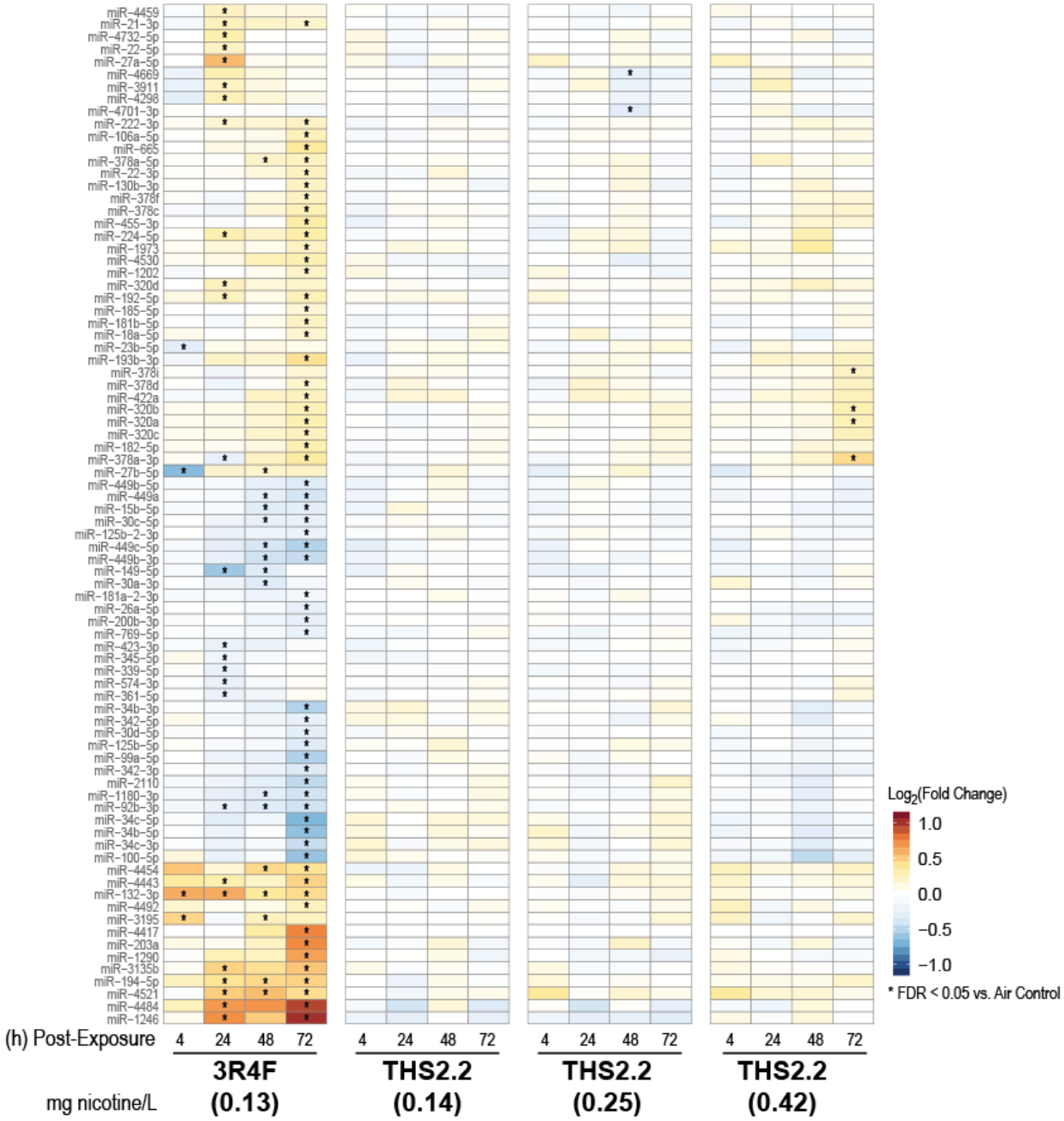


Figure 11 Alteration of miRNAs in bronchial epithelial tissue cultures following exposure
MiRNAs are listed on the left side of the heatmap. The color gradient reflects the alterations in miRNA expression as compared with the respective air controls.

Correlations of endpoint measurements across the different experimental repetitions

The present study reports a collection of data aggregated from six experimental repetitions. For each of the repetitions, a different batch of cultures was obtained from the supplier specified in **Table 1**. To explore the variability and reproducibility of the outcomes across the six experimental repetitions, correlations of the endpoint values following 3R4F smoke and THS2.2 aerosol exposure (normalized to their corresponding air controls) were computed.

First, to explore the robustness of the study design, correlations of the endpoint values were generated from experimental repetitions 3, 4, 5, and 6, in which MucilAir™ bronchial cultures were used for all of the exposure experiments (thus, the experimental design can be fairly compared across the repetitions independent of the test system variability). **Figure 12**A shows correlations of the endpoint values from the functional assays (i.e. AK assay, pro-inflammatory mediator measurement, and IHC quantification) between those obtained in experimental repetitions 3–4 and those obtained in experimental repetitions 5–6. Similarly, for the gene expression, correlation plots of the $\log_2$(fold-changes) were generated (representative plots of endpoint values at4 h post-exposure for 3R4F (0.13) and THS2.2 (0.14) are shown in **Figure 12**B). The plots show positive correlations between the measured values across experimental repetitions 3, 4, 5, and 6 following 3R4F exposure. Moreover, the analysis showed that the Pearson and Spearman correlation coefficients associated with THS2.2 exposure were smaller than those of 3R4F exposure. This finding was expected, because of the reduced impact of THS2.2 aerosol compared with 3R4F smoke. The correlation plots of the gene expression fold-changes of all groups and post-exposure time points are given in **Supplementary Figure 7**, which demonstrates a similar finding.

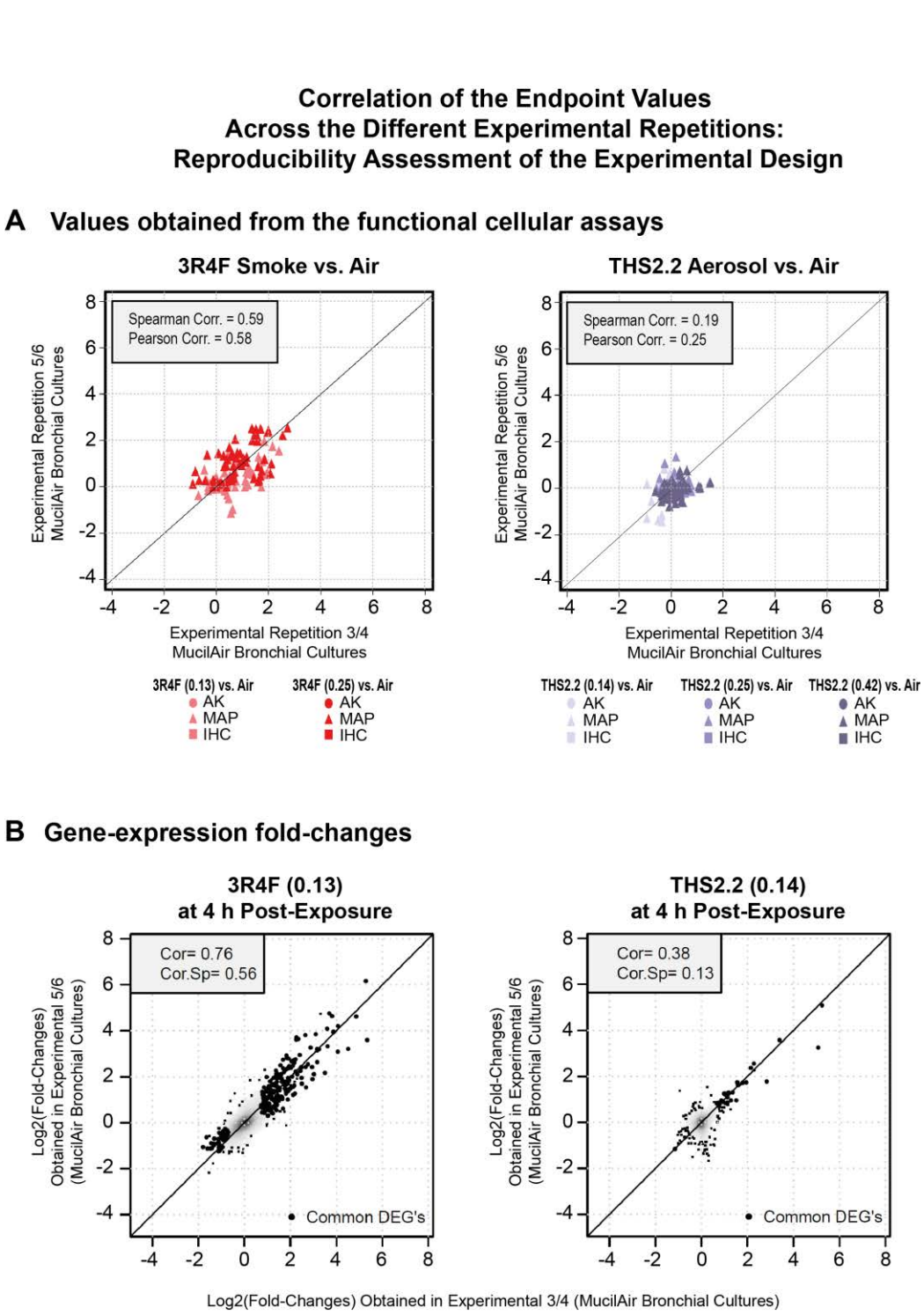


Figure 12. Correlation of endpoint values to explore the reproducibility of the experimental design

The mean of the endpoint values (the difference between exposed vs. air controls) from the various functional assays (A) obtained from the experimental repetitions 3 and 4, were correlated to those obtained from experimental repetitions 5 and 6. The $\log_2$(fold-changes) in gene expression in cultures at 4 h post-exposure to 3R4F (0.13) and THS2.2 (0.14), compared with their air controls, obtained from experimental repetitions 3 and 4 were correlated to those obtained from experimental repetitions 5 and 6 (B). Each dot represents a gene. DEG, differentially expressed genes.

Second, to explore the comparability of the observations obtained using two different organotypic human bronchial culture models, correlations of the endpoint values were computed between those obtained from experimental repetitions 1–2 (EpiAirway™ bronchial cultures) and those obtained from experimental repetitions 3–4 (MucilAir™ bronchial cultures) **(Figure 13)**. The figure shows that the Pearson and Spearman correlations remained positive for 3R4F exposure, but relatively weaker than those reported in **Figure 12**, wherein one culture model was used. Weak correlations for THS2.2-induced changes were expected because of the reduced biological impact associated with THS2.2 aerosol exposure. The correlations of the gene expression fold-changes in all groups and post-exposure time points are reported in **Supplementary Figure 8**. Furthermore, a side-by-side comparison of the cell-type specific gene expression changes from the two models was done. The alteration of cell-type specific gene expressions from experimental repetitions 1–2 (EpiAirway™ bronchial cultures) and those obtained from experimental repetitions 3–4 (MucilAir™ bronchial cultures) were highly comparable as illustrated in **Figure 14**.

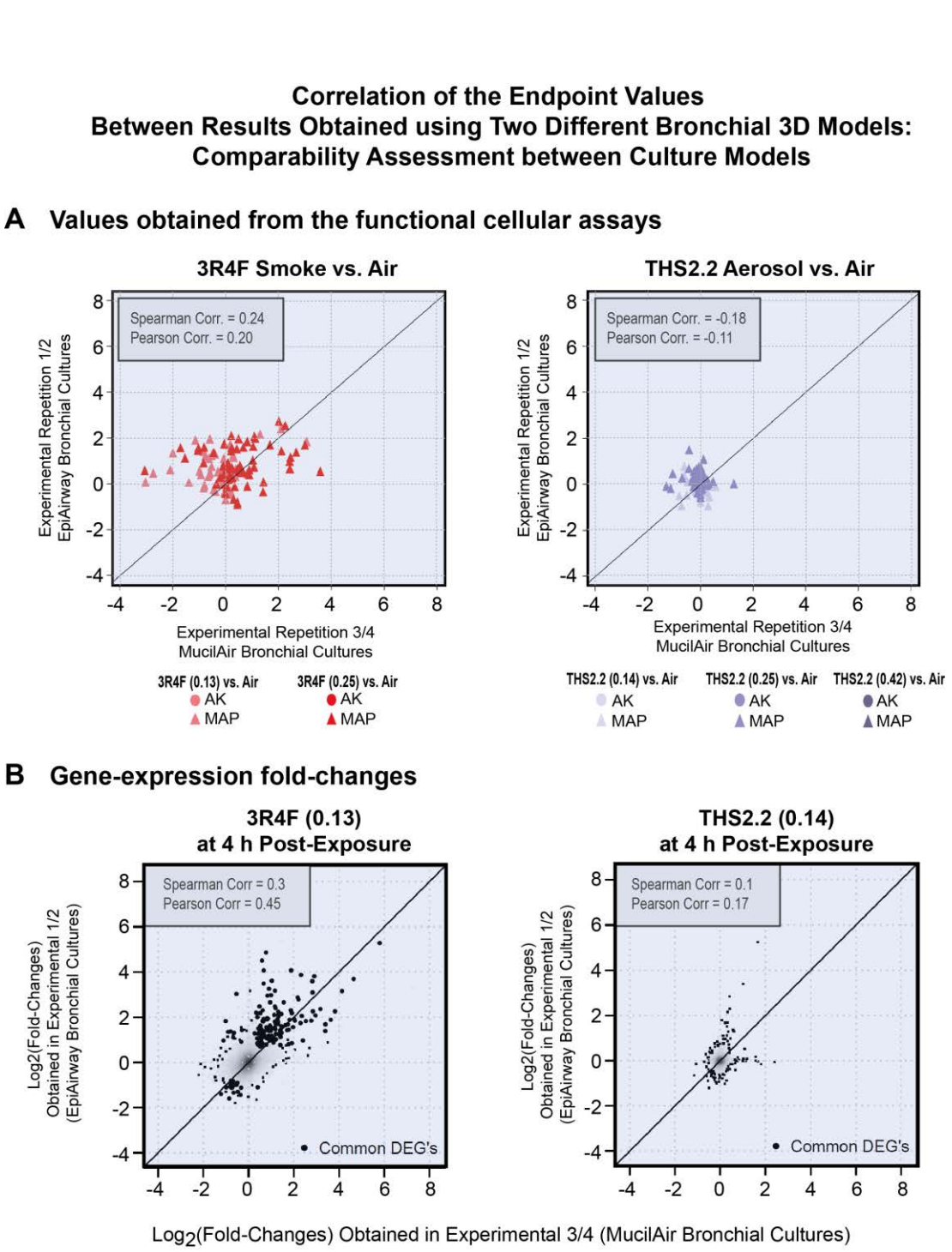


Figure 13. Correlation of endpoint values to compare the response of the two different bronchial culture models following exposure

The mean of the endpoint values (the difference between exposed vs. air control) from the various functional assays (A) obtained from MucilAir™ bronchial cultures (*x-axis*) were correlated to those obtained from EpiAirway™ bronchial cultures (*y-axis*). The $\log_2$(fold-changes) in gene expression in cultures at 4 h post-exposure to 3R4F (0.13) and THS2.2 (0.14), as compared with their air controls, from MucilAir™ bronchial cultures (*x-axis*) were correlated to those obtained from EpiAirway™ bronchial cultures (*y-axis*) (B). Each dot represents a gene. DEG, differentially expressed genes.

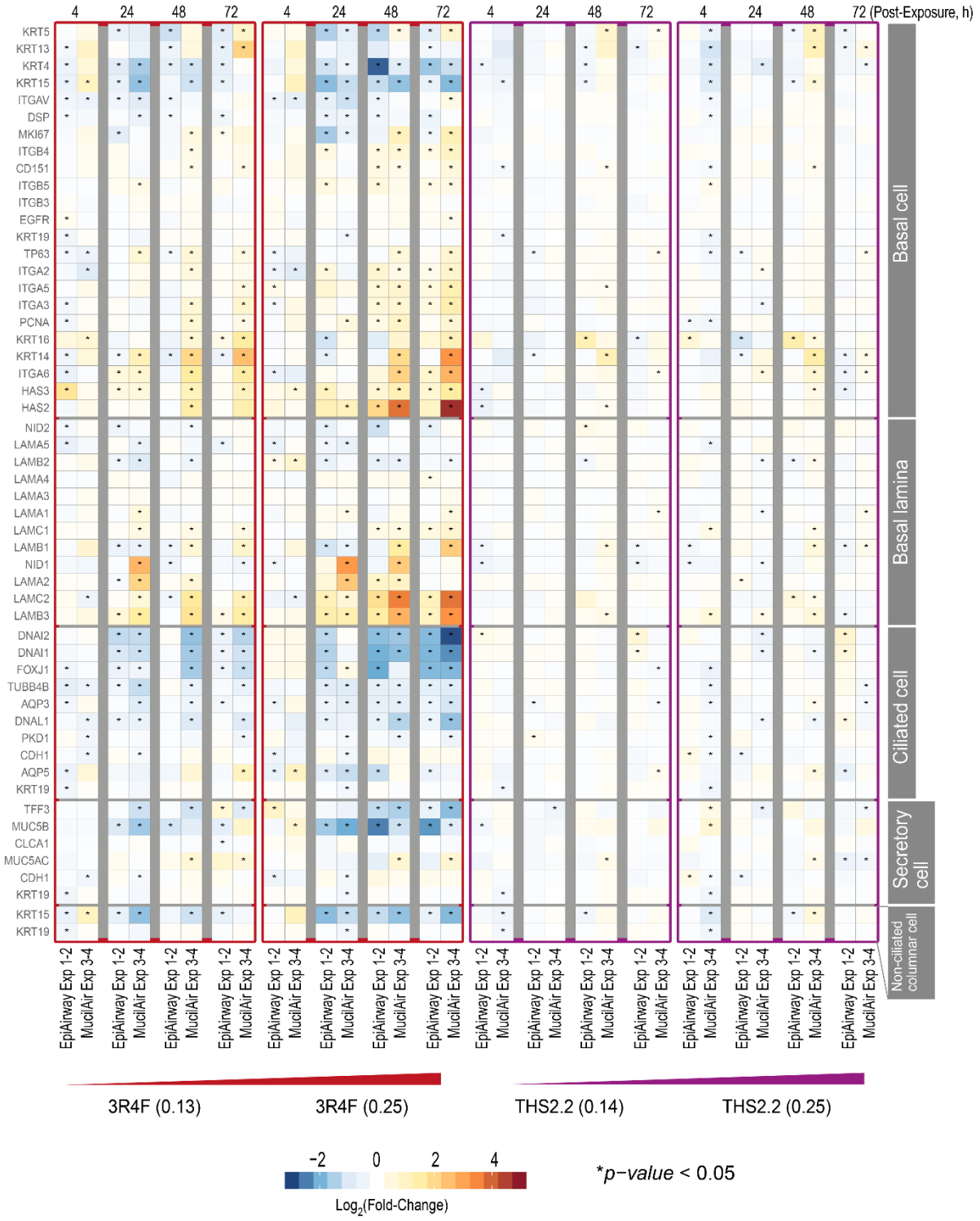


Figure 14. Heatmap of cell-type specific gene expression profiles of the two different bronchial culture models.

Gene symbols are listed on the left side of the heatmap. Specific cell types are marked at the right side. The color gradient reflects the alterations in gene expression as compared with the respective air controls.

Discussion

Alternative to animal models, the air-liquid interface organotypic *in vitro* models can be developed from primary human airway epithelial cells. Thus, the human organotypic airway culture models provide a more relevant scenario for a human toxicological assessment of ambient inhalable particles (e.g., aerosols, cigarette smoke, and nanoparticles). The study aims to conduct a comparative assessment of the biological impact of whole aerosol from a heat-not-burn product, THS2.2 (a candidate modified-risk tobacco product) relative to that of whole smoke from the combustible reference cigarette 3R4F. The THS2.2 aerosol and 3R4F smoke were applied at matched concentrations of nicotine. A total of six experimental repetitions were conducted within an approximately 20-month period, using human organotypic bronchial tissue cultures (EpiAirway™ and MucilAir™ models). Various biological endpoints (e.g., cytotoxicity, tissue histology, ciliary beating function, inflammatory marker release, and mRNA and miRNA expression changes) were assessed at different time points (4, 24, 48, and 72 h) after a single 28-min exposure. The combination of various functional assays with a high-throughput omics approach offers an integrative way for the systems toxicological assessment of THS2.2 aerosol.

The suitability of the Vitrocell® 24/48 exposure system for the assessment of smoke exposure has been reported previously (Adamson et al., 2013; Majeed et al., 2014). The Dilution/Distribution Module of Vitrocell® 24/48 exposure system allows a simultaneous administration of various dilutions of smoke/aerosol to the biological test system (located in the Cultivation Base Module of the system). Multiple samplings of smoke and aerosol were conducted throughout the study period, from which we confirmed that the target nicotine concentrations (in 3R4F smoke and THS2.2 aerosol) were effectively applied in each of the experimental repetitions (**Supplementary Table 1**). Moreover, the concentrations of representative carbonyls deposited in the PBS-filled Cultivation Base Module (**Supplementary Figure 1**) were analyzed to further characterize the diluted smoke and aerosol at the sites of exposure. These activities were conducted to ensure the appropriate generation of the smoke/aerosol throughout the study.

Readouts based on the release of cellular components following a toxic impact are commonly used to assess cytotoxicity *in vitro*. A commercially available assay kit, which measures the activity of AK released into the basolateral medium of the cultures (referred to as the AK assay),

was used in this study to evaluate the toxicity associated with the 3R4F smoke and THS2.2 aerosol. The results indicated that overt cytotoxicity was elicited mainly following exposure to the highest concentration of 3R4F smoke (0.25 mg nicotine/L). Increased cytotoxicity levels were detected at 24 h post-exposure, which reached a level of 53% at both 48 and 72 h (relative to the Triton X-induced 100% cytotoxicity). The histological evaluation revealed a similar depiction, in which tissue damage detected after exposure to 3R4F (0.25) at 72 h post-exposure; the pseudostratified epithelial cultures were extremely thin and lifted entirely from the membrane (in most cases). Thus, a histological evaluation and immunostaining analysis were not performed for this group. The smoke-induced damage following a 28-min exposure to 3R4F concentration of 0.25 mg nicotine/L (equivalent to approximately 15% 3R4F smoke dilution) was observed previously in organotypic bronchial epithelial cultures (Iskandar et al., 2015), organotypic bronchial epithelial co-cultured with fibroblasts (Iskandar et al., 2015), and organotypic nasal cultures (Iskandar et al., 2016). The lower concentration of 3R4F smoke (0.13 mg nicotine/L) elicited only a transient cytotoxicity, which was correlated with visible damage to the pseudostratified epithelial cells (i.e., signs for cell death, cell detachment, and larger intercellular spaces). This minor cytotoxicity impact and morphological alteration following 3R4F smoke at 0.13 mg nicotine/L (equivalent to approximately 8% 3R4F smoke dilution) was consistently observed in our previous studies in both organotypic bronchial and nasal cultures (Iskandar et al., 2015; Iskandar et al., 2016). Exposure to THS2.2 aerosol at comparable nicotine concentrations (i.e., THS2.2 (0.14) and THS2.2 (0.25)) did not notably induce cytotoxicity. Only when THS2.2 aerosol was applied at concentrations above 1 mg nicotine/L, was noticeable tissue damage observed. Overall, we found that the alterations in the culture morphology (a loss of pseudostratified epithelial integrity and tissue damage) were only observed when THS2.2 aerosol was applied at a nicotine concentration at least four times that of 3R4F smoke.

Immunostaining analyses at 72 h post-exposure revealed increased proportions of proliferating Ki67- and p63-positive basal cells following 3R4F (0.13) exposure. This suggests the occurrence of minor basal cell hyperplasia, which is known to be an adaptive response in *in vivo* respiratory epithelia upon stimuli (Musah et al., 2012; Schlage et al., 1998). Moreover, FoxJ1-positive ciliated cell numbers were reduced in the cultures following exposure to 3R4F (0.13). Brekman and colleagues reported that during a differentiation phase, overexpression of FoxJ1 reversed the

CS extract-induced inhibition of ciliated cell differentiation in bronchial epithelial cells (Brekman et al., 2014). Moreover, treatment with CS extract resulted in reduced ciliary beat frequency in organotypic bronchial epithelial cells that were linked with reduced expression of FoxJ1 and Dnai2 (Milara et al., 2012). In line with this report, we observed in the present study that the reduced proportions of FoxJ1-positive stained cells following 3R4F (0.13) exposure were accompanied by a diminishing signal of the ciliary beating (power analysis) immediately after exposure (0 h), and at 24, 48, and 72 h post-exposure. However, the beating frequency was not strikingly altered following 3R4F (0.13) exposure, suggesting that the few remaining ciliated cells were capable of eliciting a normal beating. When tissue damage was observed, i.e., in 3R4F (0.25)-exposed cultures, cilia beating signal and CBF were not detected (if at all, the CBF was only detected at a marginal level nearing the threshold of a detectable frequency, 2.5 Hz). This finding is consistent with a previous observation in organotypic bronchial cultures within 3 h after exposure to CS (Åstrand et al., 2015; Schmid et al., 2015). In contrast, THS2.2 aerosol at the comparable concentration (i.e., THS2.2 (0.14)), or even at higher concentrations, did not substantially alter the proportion of Ki-67, p63, and FoxJ1 markers. Although in few instances, statistically significant differences were obtained, dose-dependent effefcts of THS2.2 aerosol on any of these markers were not observed. Similarly, a dose-response impact of THS2.2 aerosol (and time-dependent impact) on CBF was not observed, despite a slight reduction in the cilia beating signal that could be observed following exposure to THS2.2 (0.25) and THS2.2 (0.42). One limitation of the present study is that the impact of 3R4F smoke and THS2.2 aerosol on the apical surface liquid (ASL) was not investigated. Proper ciliary beating and the properties of ASL are known to influence mucociliary clearance in the airway (Cohen et al., 2009). Therefore, future studies should assess whether the alterations in cilia beating frequency were accompanied by a depletion and/or viscosity change of ASL or solely attributable to the loss of cilia activity.

The concentrations of various mediators in the basolateral media were measured to assess the inflammatory response following exposure. Among the mediators, at given post-exposure time points, the highest fold-increase (**Supplementary Figure 3**) was prominently observed for MMP-1 (range, 5.2-fold – 9.8-fold, following 3R4F smoke exposure). MMP-1 expression is known to be upregulated following CS exposure (Mercer et al., 2009). The link between smoking and emphysema has been attributed to the alteration of MMP-1 expression in lung epithelial cells

(Mercer et al., 2009). Thus, the increased MMP-1 concentrations following 3R4F (0.15) and 3R4F (0.25) exposure could be linked to the overt morphological changes (damage to the pseudostratified epithelium) observed in these groups (discussed in the previous paragraph). In contrast, MMP-1 concentrations were not altered following exposure to THS2.2 aerosol applied at the comparable nicotine concentrations (i.e. THS2.2 (0.14) and THS2.2 (0.25)), and even at the higher concentration of nicotine (THS2.2 (0.42)). Furthermore, the results suggested a dose-dependent increase in mediator concentrations following 3R4F smoke exposure, with the exception of VEGFA. The concentration of VEGFA in the basolateral media following exposure to 3R4F (0.25) was comparable to the concentration following air exposure. The lack of increased concentrations of VEGFA following 3R4F exposure at 0.25 mg nicotine/L (equivalent to 15% 3R4F smoke) was previously observed in organotypic bronchial epithelial cultures (Iskandar et al., 2015), organotypic bronchial epithelial co-cultured with fibroblasts (Iskandar et al., 2015), and organotypic nasal cultures (Iskandar et al., 2016). This finding suggests that when the damage was substantial (evidenced by the culture histology of the 3R4F (0.25)-exposed cultures), a repair mechanism did not occur likely because of unrepairable damage. In 3R4F (0.13)-exposed cultures, a significant increase in VEGFA concentrations (1.7-fold increase, **Supplementary Figure 3**) was detected, supporting the initiation of a repair mechanism following exposure to 3R4F at 0.13 mg nicotine/L—this finding was observed before in our previous studies (Iskandar et al., 2015; Iskandar et al., 2016). The role of VEGF in tissue repair and proliferation (Roberts et al., 2007) has been linked to increased compensatory growth during repair processes (Marwick et al., 2006). In contrast, THS2.2 aerosol exposure at all concentrations did not substantially alter the concentrations of secreted mediators, including VEGFA. In few cases, statistically significant differences between the mediator concentrations in the THS2.2-exposed groups and the air controls were found. However, the significant differences were predominantly observed for the changes following THS2.2 aerosol exposure applied at the highest concentration (0.44 mg nicotine/L) and/or at the early post-exposure time points. This is in contrast with those changes following 3R4F smoke exposure, where the differences remained to be significant at the 72 h post-exposure time point. Moreover, even following the highest nicotine concentration in the THS2.2 aerosol, the altered concentrations of the pro-inflammatory mediators were minimal as compared to those following 3R4F smoke exposure at any concentrations tested (relative to their corresponding air-exposed controls).

To obtain further insights into the associated molecular perturbations elicited by the exposures, we conducted a systems toxicology-based risk assessment. The systems approach leverages a computational analysis of genome-wide gene expression changes using biological network models. This methodology has been useful to gain insights into the mechanistic impact of CS exposure on various organotypic epithelial culture models (Hoeng et al., 2014; Iskandar et al., 2015; Iskandar et al., 2016; Mathis et al., 2015; Schlage et al., 2014; Talikka et al., 2014; Zanetti et al., 2016). Because molecular changes in already-damaged tissue can only serve as a confirmation "rather than being predictive or mechanistic" (Davis et al., 2013), the cellular and molecular investigation in the present study was done only in cultures with minimal damage—those exposed to 3R4F (0.13), and THS2.2 (0.14), (0.25), and (0.42). One readout of the network-based approach is the quantification of the biological impact factor (BIF) that utilizes transcriptome profiles. The BIF metric allows a systems-wide measure of the exposure impact by aggregating all of the quantified perturbations in various network models (Hoeng et al., 2012; Thomson et al., 2013). Based on the BIF analysis, as compared with THS2.2 exposure at all concentrations tested for given post-exposure time points, 3R4F (0.13) elicited the strongest biological impact on the agglomeration of various processes modelled in the networks (taken as 100% relative BIF). This BIF comprised four perturbed biological-network-families (i.e. Cell Stress, Cell Proliferation, Cell Fate, and Inflammatory Response) that reached peak perturbation at 4 h post-exposure and declined thereafter. The decreasing perturbation scores of various biological network models with post-exposure duration was consistent with our previous observations in organotypic bronchial and nasal cultures (Iskandar et al., 2015; Iskandar et al., 2016; Talikka et al., 2014). Furthermore, in the present study, we observed that the same network models were perturbed following THS2.2 aerosol exposure but at a substantially lower level than those upon 3R4F exposure: The relative BIF of THS2.2 (0.14) was only 7.5%, as compared with the 100% BIF following 3R4F (0.13) exposure.

To support the interpretations of the network-based transcriptome analysis, different panels showing the differential expression of genes involved in the cellular stress response and inflammation were provided. Consistent observations were found between the network analysis and the gene panel-analysis. Perturbation of Xenobiotic Metabolism Response network model

following exposure was reflected by significant expression changes of genes listed in the Xenobiotic Stress panel (*CYP*s, *AKR*s, *AHR*, *AHRR*, *ALDH*s). Moreover, the perturbed Oxidative Stress network model was consistent with significant expression changes of genes within the Oxidative Stress gene panels. Finally, the gene expression profile listed in the inflammation-related gene panel mirrors the perturbation of networks within the Inflammatory Process Network. A striking difference in the expression patterns of these genes following 3R4F and THS2.2 exposure was observed: These genes were significantly differently expressed at all time points following exposure to 3R4F (0.13), whereas THS2.2 aerosol at 0.14; 0.25; or 0.42 mg nicotine/L elicited only transient alterations at 4 h post-exposure. This observation suggests that the THS2.2 aerosol elicited reversible effects that were managed by rapid cellular compensation; however, 3R4F smoke provoked more severe effects that overwhelmed the fast cellular stress response and repair mechanisms, resulting in a slower and less pronounced recovery during the observation period (up to 72 h post-exposure).

The current study further explored the interplay between mRNA and miRNA changes because the same RNA extract was used to performed both mRNA and miRNA arrays. In contrast with the mRNA response profiles (where the number of significantly altered mRNAs decreased with increasing duration of the post-exposure period), the miRNA response profiles—predominantly altered following 3R4F (0.13) exposure—showed an increasing number of differentially expressed miRNA species with increasing post-exposure duration. Thus, the results presented here provided additional insights into the dynamic behavior of miRNAs following CS exposure. The delayed occurrence of the miRNA expression changes relative to the mRNA expression changes suggests a secondary rather than a direct response to the exposures. This is consistent with our previous observation in 3R4F-exposed organotypic bronchial epithelial cultures (Mathis et al., 2015) and a a previous study using melanoma cells stimulated with interferon-γ (Nazarov et al., 2013). Nazarov and colleagues reasoned that the "delayed" response of miRNA may reflect a cellular attempt to mitigate an earlier perturbation of the gene expression following stimuli (Nazarov et al., 2013).

The greatest differential expression changes were observed for miR-4484 and miR-1246 following 3R4F (0.13) exposure at 72 h post-exposure. Although their specific function is

unknown, both miRNAs have been reported to be mitochondrial miRNAs (Borralho et al., 2014). Compared with a previous 3R4F exposure study in organotypic bronchial cultures (Mathis et al., 2015), we observed the consistent downregulation of miR-30, miR-342, and miR-449 expression. The 3R4F-induced upregulation of miR-4521, miR-193, miR-224, and miR-203; and the 3R4F-induced downregulation of miR-2110, miR-1180, miR-149, and miR-27b were observed also in nasal organotypic epithelial cultures following 3R4F exposure (Iskandar et al., 2016). The downregulation of miR-4521 expression and upregulation of miR-27b following 3R4F exposure could be linked to smoking-induced hypoxia as previously reported (Camps et al., 2014). Because many of the biological functions of the identified miRNAs were unknown, we used the DIANA-TarBase tool (Vlachos et al., 2015) to interpret the miRNA profile (reported in **Supplementary Figure 6**). This analysis showed various KEGG pathways that were linked to the miRNA alterations. However, in many cases, the same miRNA target genes were associated with several KEGG pathways. Therefore, we consider that these pathway annotations are less specific and cannot be used to identify the mechanism associated with the exposure-induced impact. MiRNA expression was not altered following THS2.2 (0.14) exposure. Only two miRNAs were significantly downregulated following THS2.2 (0.25) exposure: miR-4669 and miR-4701, function unknown. Moreover, miR-320a/b and miR-378a/i were significantly upregulated at 72 h post-exposure following THS2.2 (0.42); they were similarly found to be upregulated following 3R4F (0.13) exposure. The altered miR-320 levels following exposure could be related to the observed alterations in genes regulating oxidative stress (shown in the Oxidative Stress gene panel, **Figure 9**); studies have demonstrated that miR-320 is induced upon oxidative stress (Schrottmaier et al., 2014; Tang et al., 2012). Furthermore, both miR-378a and miR-378i belong to a large family of evolutionary conserved miRNAs (among miR-378a/b/c/d/e/f/h/i) (Megiorni et al., 2014). MiR-378 recognizes the 3′-UTR of aryl hydrocarbon receptor (AHR) and suppresses its expression (Nakano et al., 2016). Because AHR is known to mediate the expression of CYP1A1 (Ma, 2001), it is likely that the upregulation of miR-378 contributed to the exposure-induced CYP1A1 mRNA levels observed in this study (shown in the xenobiotic stress gene panel, **Figure 9**).

Furthermore, the results described here are the aggregated data of six experimental repetitions. The first two experimental repetitions used EpiAirway™ bronchial cultures reconstituted from

the epithelial cells of a 23-year old non-smoker male. The last four experimental repetitions used MucilAir™ bronchial cultures reconstituted from the epithelial cells of a 28-year old non-smoker male. To explore the repeatability/reproducibility of the experimental design, correlations were computed between the endpoint values generated from experimental repetitions 3–4 and those from repetitions 5–6, all of which were conducted using MucilAir™ cultures. Positive correlations were observed from this analysis, suggesting that the experimental design was fairly robust, and resulting in reproducible observations. In addition, to explore the responses of the different culture models, the endpoint values generated from repetitions 1–2 (where EpiAirway™ cultures were used) were correlated to those from repetitions 3–4 (where MucilAir™ cultures were used). The results showed that positive correlations remained detectable for the 3R4F-induced changes, even though the correlations were weaker. The reduced correlations were expected because of the inherent variation regarding the donors and processing methodology for the reconstitution of the organotypic culture models by the two providers. Nevertheless, when the alterations in cell-type specific genes were compared side-by-side, the changes were greatly comparable between the two models. Future studies should also explore the use of various donor profiles (e.g., male, female) for such assessment. Culture models reconstituted from smoker donors could be leveraged for *in vitro* switching studies (from a conventional cigarette smoking to a modified-risk tobacco product). Nevertheless, the correlations remained positive. Moreover, because of the overall reduced impact of THS2.2 aerosol on the various endpoints, we did anticipate that the Pearson and Spearman correlations of the endpoint values following THS2.2 exposure would be weaker than those following 3R4F exposure.

Conclusions and Outlook

In summary, we have shown that at similar nicotine concentrations, aerosol of the heat-not-burn product THS2.2 elicited a reduced biological impact in organotypic bronchial cultures, as compared with 3R4F smoke exposure across all measured endpoints. This study further demonstrated that combining functional analyses (based on cellular-based assays) with various omics and high-throughput technologies provides a holistic approach of an assessment to study the biological impact of exposure. Utilization of causal biological network models relevant to the bronchial tissue could advance a mechanism-based assessment; for example, inflammatory processes and cellular stress response were elicited at a lower degree following THS2.2 aerosol than 3R4F smoke. Furthermore, the network-based computational analysis on the gene transcription changes allowed a quantification of the a relative impact of the exposure. The data showed that 3R4F (0.13) elicicted the highest biological impact (RBIF = 100%) in the context of Cell Fate, Cell Proliferation, Cell Stress, and Inflammatory Network Models at 4 h post-exposure. In contrast, the corresponding RBIF of THS2.2 (0.14) at 4 h post-exposure was 7.6%. Even at the 1.7-fold and 3-fold higher e concentrations, THS2.2 aerosol exposure only elicited 27.6% and 49.9% RBIF, respectively, at 4 h post-exposure time point. The present datasets could be further leveraged to explore potential biomarkers of exposure in clinical studies (e.g., pro-inflammatory mediators, specific gene markers). The work reported here demonstrates that a systems toxicology approach (Sauer et al., 2016; Sturla et al., 2014), which is aligned with the new toxicity-testing paradigm proposed by the 21st Century Toxicology framework (Berg et al., 2011; Sheldon and Cohen Hubal, 2009), can be implemented under the 3Rs principle to refine, reduce, and eventually replace animal studies (Doke and Dhawale, 2015).

Supplementary Materials

Supplementary Table 1. Target and actual nicotine concentrations in the smoke and aerosol

Group	Experiment	Exp. 1	Exp. 2	Exp. 3	Exp. 4	Exp. 5	Exp. 6
	Month	Dec 2013	Feb 2014	Mar 2015	Jun 2015	Jul 2015	Sep 2015
3R4F Concentration Level 1	Target Nicotine (mg/L)	0.13	0.13	0.13	0.13	0.13	0.13
	Vitrocell Dilution (%)	8	8	7	7	7	7
	Actual Nicotine (mg/L)	0.148 ± 0.007 (N = 3)	0.103 ± 0.009 (N = 8)	0.151 ± 0.006 (N = 3)	0.137 ± 0.006 (N = 3)	0.144 ± 0.001 (N = 3)	NA
3R4F Concentration Level 2	Target Nicotine (mg/L)	0.25	0.25	0.25	0.25	0.25	0.25
	Vitrocell Dilution (%)	15	15	13	13	13	13
	Actual Nicotine (mg/L)	0.275 ± 0.007 (N = 3)	0.254 ± 0.034 (N = 8)	0.268 ± 0.012 (N = 4)	0.235 ± 0.005 (N = 3)	0.253 ± 0.007 (N = 3)	NA
THS2.2 Concentration Level 1	Target Nicotine (mg/L)	0.15	0.15	0.15	0.15	0.15	NA
	Vitrocell Dilution (%)	12	12	13	13	13	NA
	Actual Nicotine (mg/L)	0.140 ± 0.003 (N = 4)	0.139 ± 0.011 (N = 5)	0.144 ± 0.007 (N = 4)	0.137 ± 0.006 (N = 4)	0.137 ± 0.009 (N = 3)	NA
THS2.2 Concentration Level 2	Target Nicotine (mg/L)	0.25	0.25	0.25	0.25	0.25	NA
	Vitrocell Dilution (%)	23	22	24	24	24	NA
	Actual Nicotine (mg/L)	0.271 ± 0.010 (N = 4)	0.227 ± 0.010 (N = 5)	0.263 ± 0.008 (N = 4)	0.283 ± 0.020 (N = 4)	0.223 ± 0.007 (N = 3)	NA
THS2.2 Concentration Level 3	Target Nicotine (mg/L)	NA	NA	0.42	0.42	0.42	NA
	Vitrocell Dilution (%)	NA	NA	31	31	31	NA
	Actual Nicotine (mg/L)	NA	NA	0.495 ± 0.006 (N = 4)	0.393 ± 0.019 (N = 4)	0.369 ± 0.035 (N = 3)	NA

Actual nicotine concentrations in the smoke/aerosol were measured following trapping of smoke/aerosol in EXtrelut® 3NT columns; at least three independent samplings were done per experimental repetition. Nicotine concentrations are expressed as mean ± SEM. Abbreviation: N, number of samples (trapped in the EXtrelut® 3NT columns); NA, Not available (the concentrations were not tested in the corresponding experimental repetition); SEM, standard error of the mean; THS, tobacco heating system.

Supplementary Table 2. Sample numbers for each endpoints

		Endpoint					
	Group	**AK**	**MAP**	**IHC**	**CBF**	**mRNA Array**	**miRNA Array**
Before Exposure	**3R4F (0.13)**	NA	NA	NA	3	NA	NA
	3R4F (0.25)	NA	NA	NA	3	NA	NA
	3R4F (Air)	NA	NA	NA	3	NA	NA
	THS2.2 (0.14)	NA	NA	NA	9	NA	NA
	THS2.2 (0.25)	NA	NA	NA	9	NA	NA
	THS2.2 (0.42)	NA	NA	NA	9	NA	NA
	THS2.2 (Air)	NA	NA	NA	9	NA	NA
0 h Post-Exposure	**3R4F (0.13)**	NA	NA	NA	3	NA	NA
	3R4F (0.25)	NA	NA	NA	3	NA	NA
	3R4F (Air)	NA	NA	NA	3	NA	NA
	THS2.2 (0.14)	NA	NA	NA	9	NA	NA
	THS2.2 (0.25)	NA	NA	NA	9	NA	NA
	THS2.2 (0.42)	NA	NA	NA	9	NA	NA
	THS2.2 (Air)	NA	NA	NA	9	NA	NA
4 h Post-Exposure	**3R4F (0.13)**	11	NA	NA	NA	12	12
	3R4F (0.25)	12	NA	NA	NA	12	12
	3R4F (Air)	12	NA	NA	NA	13	13
	THS2.2 (0.14)	12	NA	NA	NA	13	13
	THS2.2 (0.25)	12	NA	NA	NA	13	13
	THS2.2 (0.42)	9	NA	NA	NA	9	8
	THS2.2 (Air)	12	NA	NA	NA	13	12
24 h Post-Exposure	**3R4F (0.13)**	14	12	NA	3	14	14
	3R4F (0.25)	15	13	NA	3	15	15
	3R4F (Air)	15	13	NA	3	16	15
	THS2.2 (0.14)	12	13	NA	6	13	13
	THS2.2 (0.25)	12	13	NA	6	13	13
	THS2.2 (0.42)	9	9	NA	6	9	9
	THS2.2 (Air)	12	13	NA	6	13	12
48 h Post-Exposure	**3R4F (0.13)**	14	12	9	3	15	13
	3R4F (0.25)	15	13	NA	3	13	8
	3R4F (Air)	15	13	11	3	16	16
	THS2.2 (0.14)	12	13	6	9	13	13
	THS2.2 (0.25)	12	13	6	9	13	13
	THS2.2 (0.42)	9	9	6	9	9	9
	THS2.2 (Air)	12	13	6	9	13	12
72 h Post-Exposure	**3R4F (0.13)**	16	12	8	3	15	15
	3R4F (0.25)	17	13	NA	3	14	9
	3R4F (Air)	17	13	9	3	16	15
	THS2.2 (0.14)	12	13	6	9	13	12
	THS2.2 (0.25)	12	13	6	9	13	13
	THS2.2 (0.42)	9	9	6	9	9	9
	THS2.2 (Air)	12	13	6	9	13	13

*Only conducted in experimental repetition 3, 4, 5 and 6 using the MucilAir™ bronchial 3D culture model.
** Only conducted in experimental repetition 3, 4, and 5 using the MucilAir™ bronchial 3D culture model.

Supplementary Table 3. List of network models considered in the study

Number	Abbreviated network family name	Network name
1	CFA	Apoptosis
2	CFA	Autophagy
3	CFA	Necroptosis
4	CFA	Response to DNA Damage
5	CFA	Senescence
6	CPR	Calcium
7	CPR	Cell Cycle
8	CPR	Cell Interaction
9	CPR	Clock
10	CPR	Epigenetics
11	CPR	Growth Factor
12	CPR	Hedgehog
13	CPR	Hox
14	CPR	Jak Stat
15	CPR	Mapk
16	CPR	mTor
17	CPR	Notch
18	CPR	Nuclear Receptors
19	CPR	PGE2
20	CPR	Wnt
21	CST	Endoplasmic Reticulum Stress
22	CST	Hypoxic Stress
23	CST	NFE2L2 Signaling
24	CST	Osmotic Stress
25	CST	Oxidative Stress
26	CST	Xenobiotic Metabolism Response
27	IPN	Epithelial Innate Immune Activation
28	IPN	Epithelial Mucus Hypersecretion
29	IPN	Tissue Damage

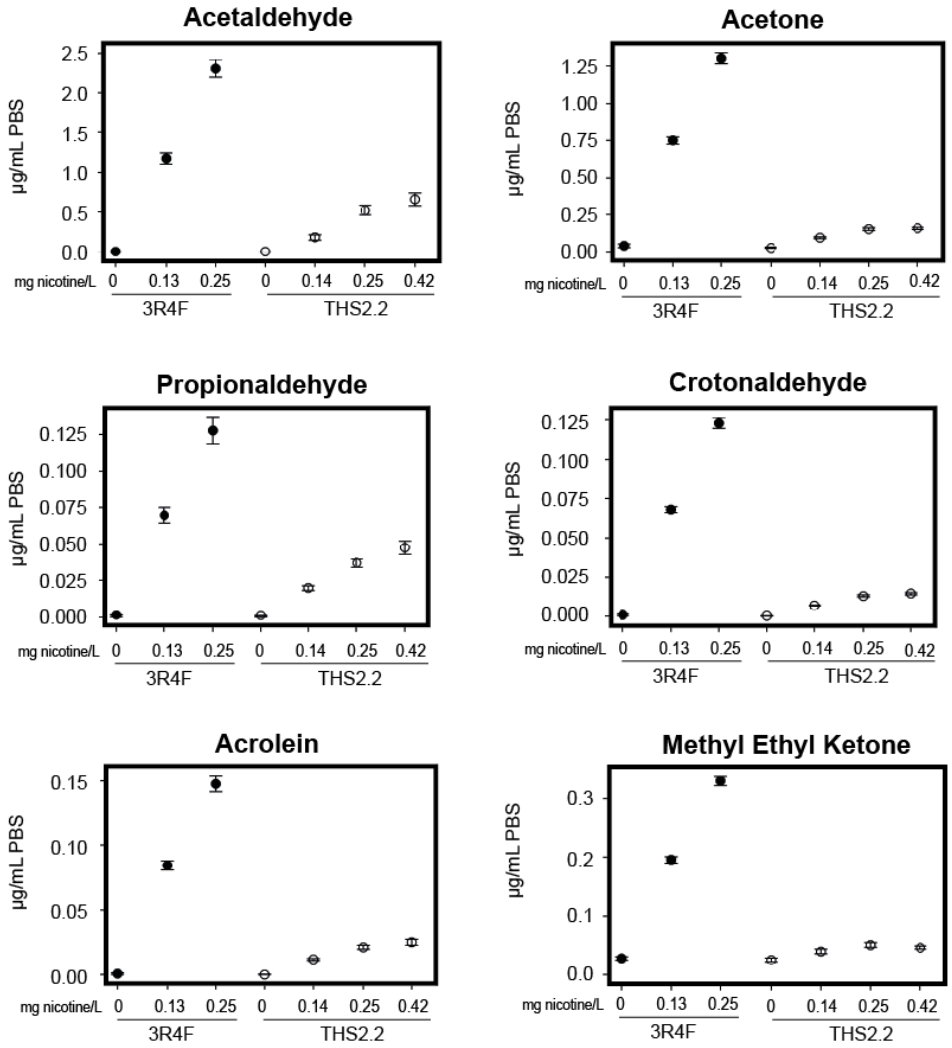
Abbreviations: CFA, Cell Fate; CST, Cell Stress; CPR, Cell Proliferation; IPN, Inflammatory Process Networks; Jak Stat, janus kinase/signal transducers and activators of transcription; Mapk, mitogen-activated protein kinases; mTor, mechanistic target of rapamycin; NFE2l2, nuclear factor, erythroid 2-like 2; PGE2, prostaglandin E2. The collection of causal biological networks used in the study was the human network suite CBN v1.3 (Boué et al., 2015).

Supplementary Table 4. KEGG pathway annotation associated with the miRNA alterations

KEGG Pathway	Cluster	Combined Score of EnrichR	miRNA Target Genes Associated with the KEGG Pathway Annotation
Insulin signaling pathway	A	4.2	PRKAA1;PRKAR1A;RPS6;PIK3R1;CALM1;CALM2;PTPRF
p53 signaling pathway	B	9.7	CCND2;APAF1;CCNE2;SESN3;CDK4;ZMAT3;CCNG2;EI24;CHEK1;ATM;THBS1
Cell cycle	B	3.6	ORC5;CCND2;CCNE2;CDK4;CHEK1;CDC27;MCM4;ATM;CDC6;MCM6;YWHAZ
Regulation of actin cytoskeleton	B	1.5	PPP1R12A;ITGB4;ARPC5;ACTB;PPP1CA;SLC9A1;TIAM1;MYH9;ITGA6;PFN1;WASF1;WASF2;VCL
Adherens junction	B	5.5	YES1;CSNK2A1;CTNNA1;PTPRJ;WASF1;WASF2;MAP3K7;ACTB;VCL
Tight junction	B	1.6	YES1;CSNK2A1;EPB41;CDK4;GNAI3;CTNNA1;MYH9;AMOTL1;ACTB;GNAI2
Gap junction	B	1.3	TUBB6;TUBB;GNAI3;LPAR1;ITPR2;GRB2;GNAI2
Phagosome	B	1.2	DYNC1H1;DYNC1LI2;TUBB6;RAB5C;TUBB;CANX;ATP6V1H;RAB5A;THBS1;ACTB
Protein processing in endoplasmic reticulum	B	9.5	SEC13;EDEM1;SSR2;EDEM2;SSR3;SEL1L;UBE4B;RAD23B;CKAP4;ERO1L;DNAJC5;LMAN2;CANX;STT3A;HYOU1;P4HB;SEC31A
Fatty acid degradation	B	1.4	HADHB;ACOX1;ECI1;ACAA1;ACAT2
Fatty acid metabolism	B	2.6	HADHB;SCD;ACOX1;FASN;ACAA1;ACAT2
Carbon metabolism	B	1.2	GLUD1;FH;GOT2;IDH3B;DLST;ALDOA;GAPDH;ACAT2
Oxytocin signaling pathway	B	1.4	RCAN1;MYL6;PPP3R1;PPP1R12A;GNAI3;ITPR2;ACTB;PPP1CA;GNAI2;CAMKK2
Vasopressin-regulated water reabsorption	B	5.8	NSF;DYNC1H1;DYNC1LI2;RAB5C;ARHGDIA;CREB3L2;RAB5A
Leukocyte transendothelial migration	B	1.0	GNAI3;CTNNA1;PTPN11;ACTB;VCL;RAPGEF3;MAPK13;GNAI2
Oocyte meiosis	C	6.2	PPP1CB;SMC1A;CALM2
Apoptosis	C	4.2	CASP7;CFLAR
TNF signaling pathway	C	4.5	CASP7;CFLAR
cGMP-PKG signaling pathway	C	3.9	PPP1CB;CALM2
cAMP signaling pathway	C	3.4	PPP1CB;CALM2
RNA degradation	C	4.8	PAN3;PABPC4L
mRNA surveillance pathway	C	4.3	PPP1CB;PABPC4L
Vascular smooth muscle contraction	C	4.2	PPP1CB;CALM2
Adrenergic signaling in cardiomyocytes	C	3.9	PPP1CB;CALM2
GnRH signaling pathway	C	5.0	MAP3K2;CALM2
Oxytocin signaling pathway	C	4.0	PPP1CB;CALM2
Insulin signaling pathway	C	3.8	PPP1CB;CALM2
Long-term potentiation	C	5.1	PPP1CB;CALM2
Dopaminergic synapse	C	4.2	PPP1CB;CALM2
Inflammatory mediator regulation of TRP channels	C	5.0	PPP1CB;CALM2
Metabolic pathways	D	1.4	GPI;B4GALT3;PANK3;SHMT2;MBOAT2;PLA2G4A;ASNS;CTPS1;ENO1;EPRS;HSD17B10;HK2;NME1;ALDH1A3;NT5E;MTHFD2;PSAT1;MAN2A1;ME1;ATP6V1B2;BCAT1;TKT;CDS2
Regulation of actin cytoskeleton	D	11.5	TIAM1;ARPC2;GNA12;PIP4K2A;MYH9;PIP4K2C;GNG12;WASF2;CRK;ACTB;CRKL;SLC9A1
Focal adhesion	D	1.2	FLNA;LAMC1;CRK;THBS1;ACTB;CRKL
Endocytosis	D	1.2	EHD1;ARF1;ARPC2;VPS37C;ARRB2;CHMP7;ARF6

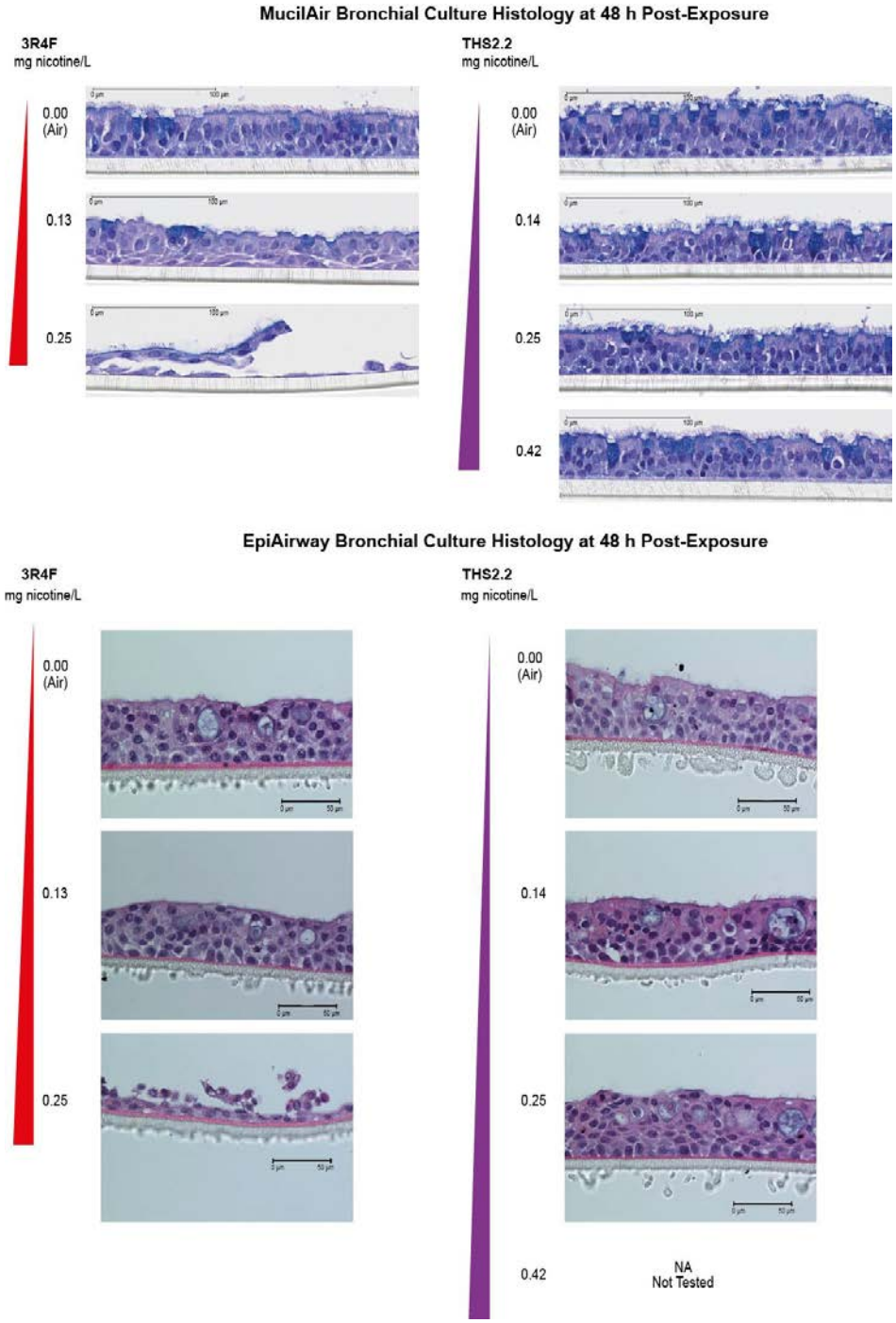
MAPK signaling pathway	D	9.5	RPS6KA3;GNA12;NF1;PLA2G4A;FLNA;ARRB2;GNG12;RASGRP1;CRK;NFKB1;CRKL;DUSP7
HIF-1 signaling pathway	D	4.7	IFNGR2;SLC2A1;ENO1;LTBR;NFKB1;HK2
Ras signaling pathway	D	3.0	TIAM1;NF1;PLA2G4A;PTPN11;GNG12;RASGRP1;NFKB1;ARF6
Phospholipase D signaling pathway	D	1.4	ARF1;GNA12;PLA2G4A;PTPN11;ARF6
Glycolysis/Gluconeogenesis	D	2.6	GPI;ALDH1A3;ENO1;HK2
Carbon metabolism	D	5.8	GPI;PSAT1;SHMT2;ME1;ENO1;TKT;HK2
Biosynthesis of amino acids	D	4.0	PSAT1;SHMT2;ENO1;BCAT1;TKT
Vasopressin-regulated water reabsorption	D	1.5	DYNC1H1;DCTN5;ARHGDIA
Fc gamma R-mediated phagocytosis	D	5.4	ARPC2;PLA2G4A;WASF2;CRK;CRKL;ARF6
Chemokine signaling pathway	D	1.5	TIAM1;ARRB2;GNG12;CRK;NFKB1;CRKL
Neurotrophin signaling pathway	D	6.0	RPS6KA3;IRAK1;ARHGDIA;PTPN11;CRK;NFKB1;CRKL
Sphingolipid metabolism	E	1.0	SMPD2;PPAP2B

1262



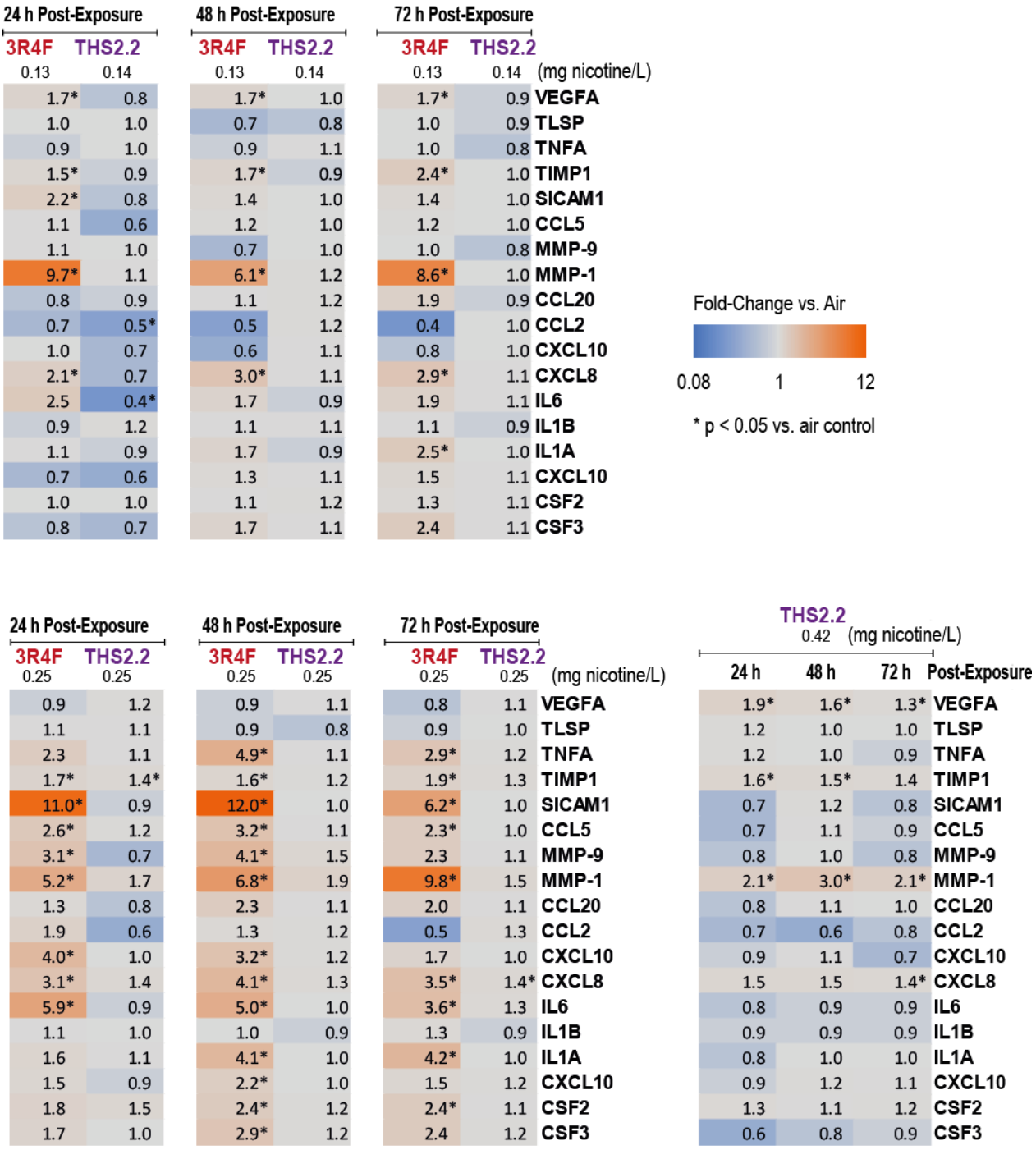
Supplementary Figure 1. Deposited concentrations of representative carbonyls in the Vitrocell® 24/48 exposure system following 28 minutes of exposure

The averaged of representative carbonyls deposited in the Base Module are reported (N = 10 samplings throughout the study period, 2014–2015). The Base Module of the Vitrocell® 24/48 exposure system was filled with PBS and exposed to the various concentrations of 3R4F smoke and THS2.2 aerosols according to the study design. Reduced concentrations of the various carbonyls were expected because THS2.2 heats tobacco without combustion, resuling in reduced formation of harmful and potentially harmful constituents (HPHC) compared with cigarette smoke (Smith, M. R., Clark, B., Lüdicke, F., et al. 2016. Evaluation of the Tobacco Heating System 2.2. Part 1: Description of the system and the scientific assessment program. Regulatory Toxicology and Pharmacology).



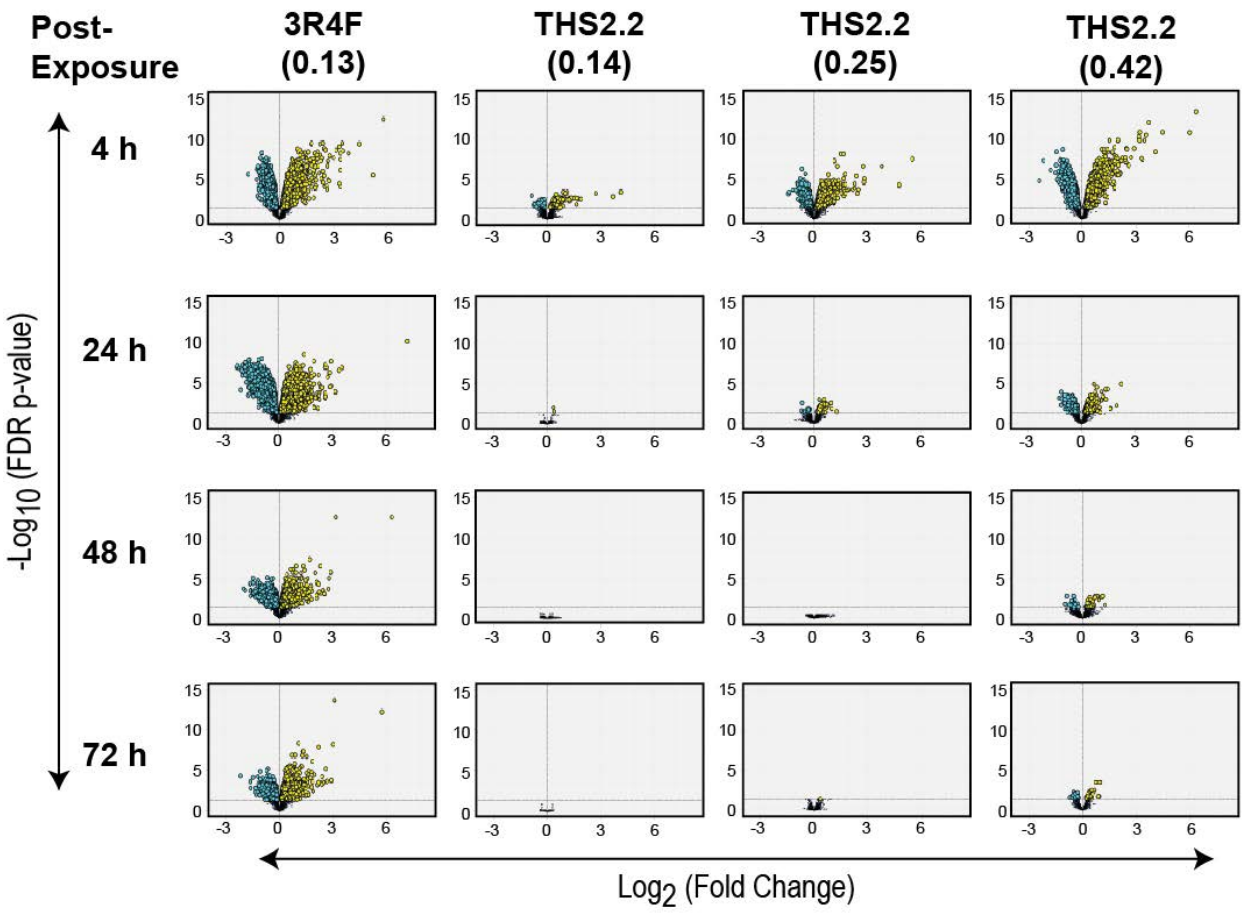
Supplementary Figure 2. Culture morphology 48 h after exposure

Representative pictures of the hematoxylin and eosin (H&E) and Alcian blue-stained culture sections at 48 h post-exposure. Representative pictures of the bronchial MucilAir™ (part of the experimental repetition 5). exposed cultures are shown in the upper panel. Representative pictures of EpiAirway™ (part of the experimental repetition 1). exposed cultures are shown in the lower panel.



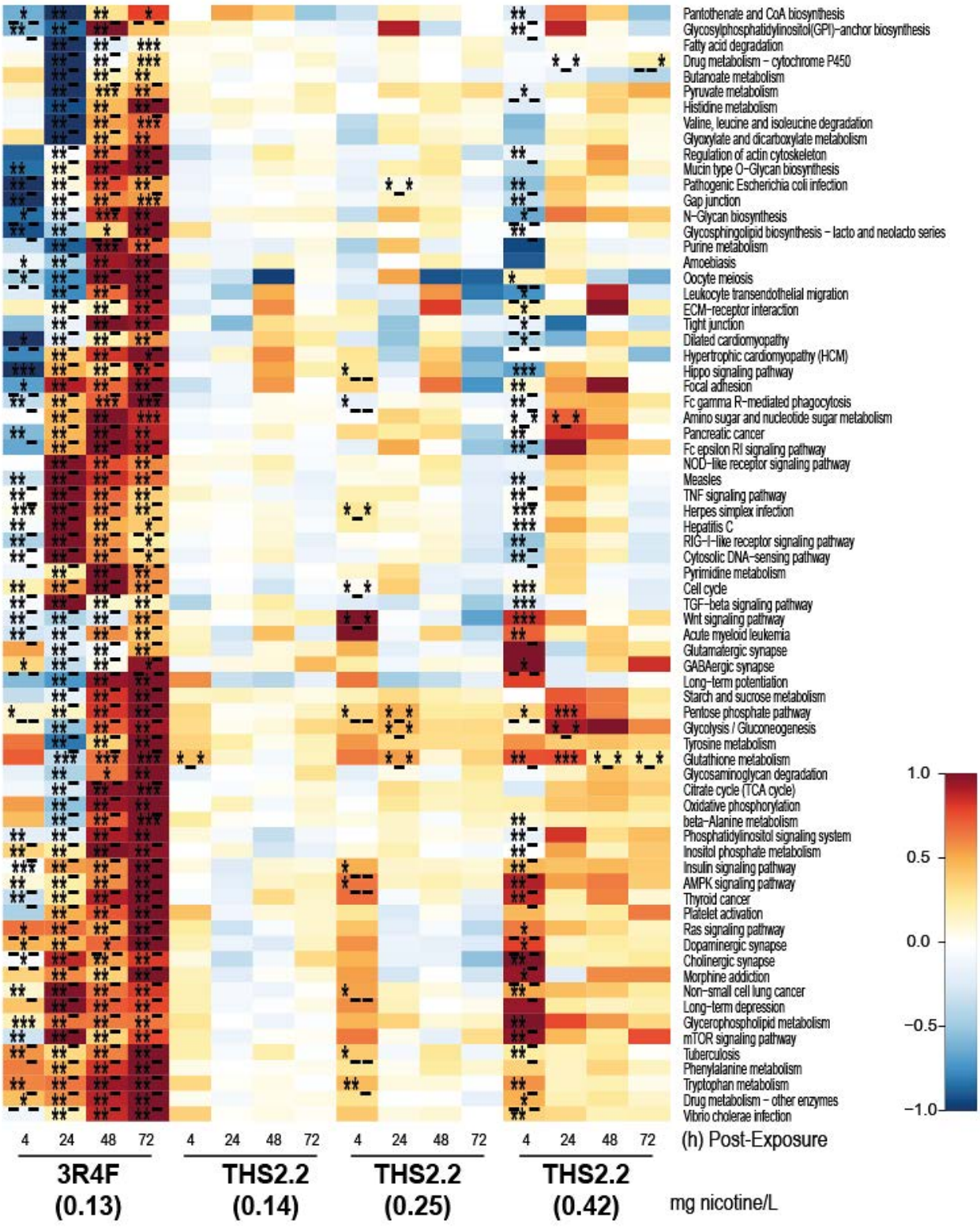
Supplementary Figure 3. Fold-changes of the mean concentrations relative to their corresponding air control.

Heatmap showing the fold-changes per mediators. Orange and blue represent the degree of increased and decreased fold-change, respectively.



Supplementary Figure 4. Exposure impact on the global transcriptome of the bronchial cultures

Volcano plots illustrate the alteration in gene expression (each dot represents a gene) for each of the exposure groups, compared with the corresponding air controls. An FDR *p*-value of 0.05 was considered as the statistically significant threshold of the gene expression alterations.



1294

1295

Figure continues

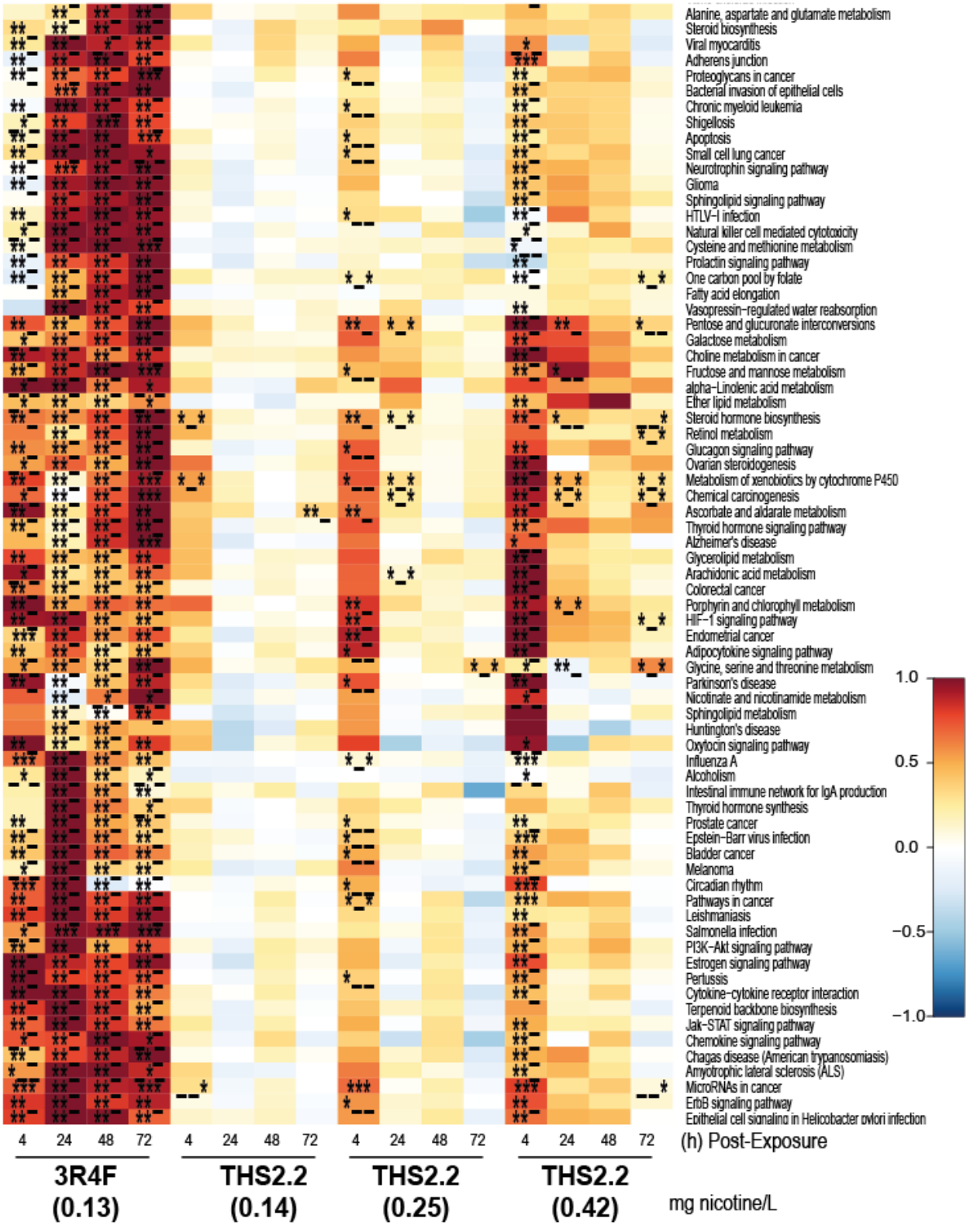
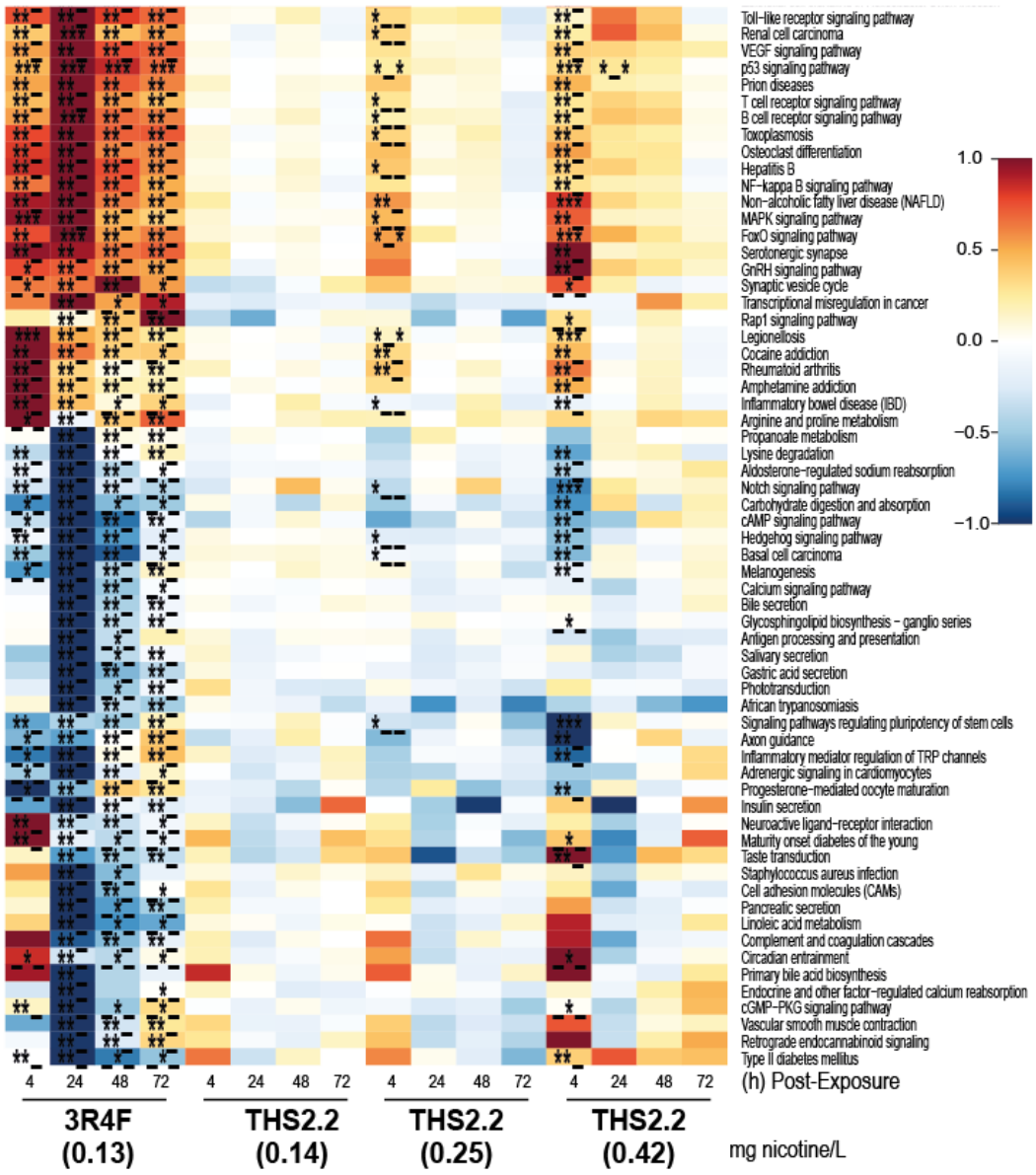
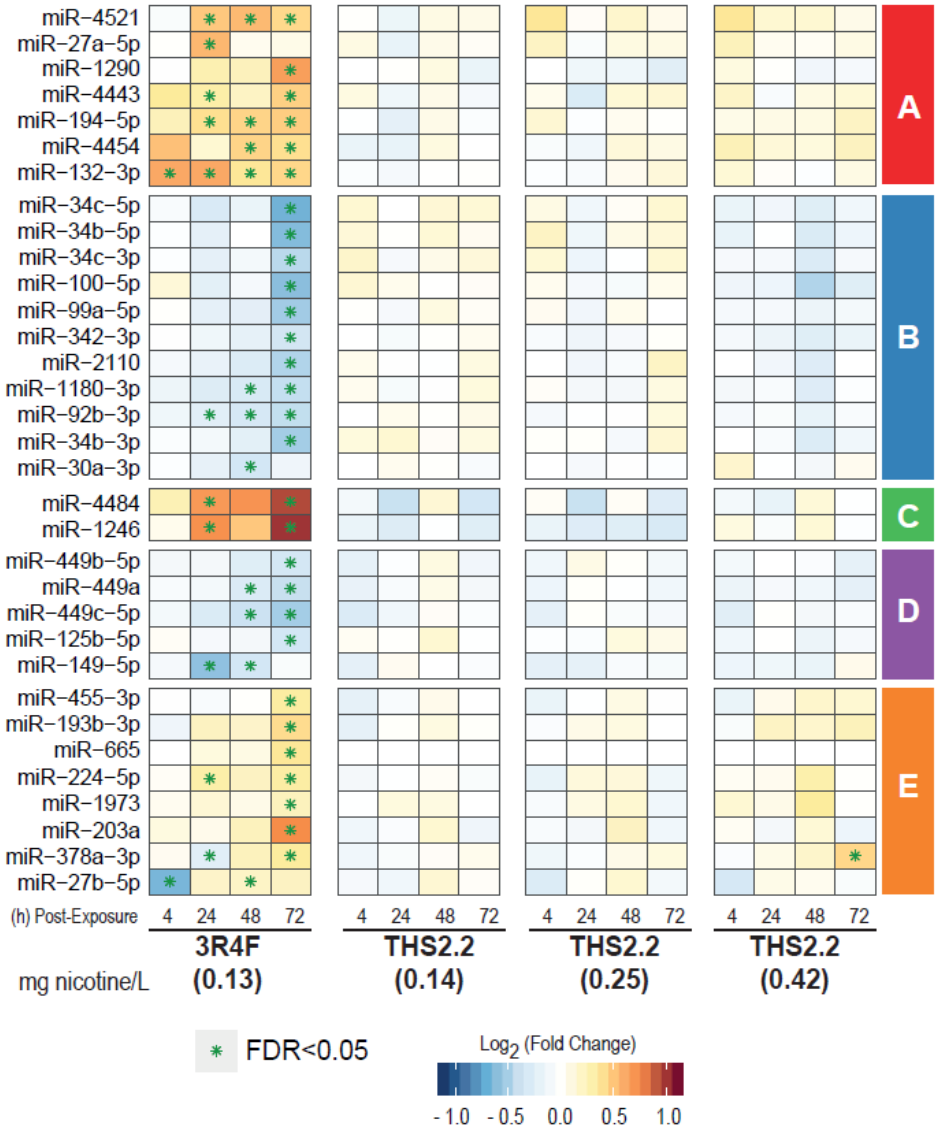


Figure continues



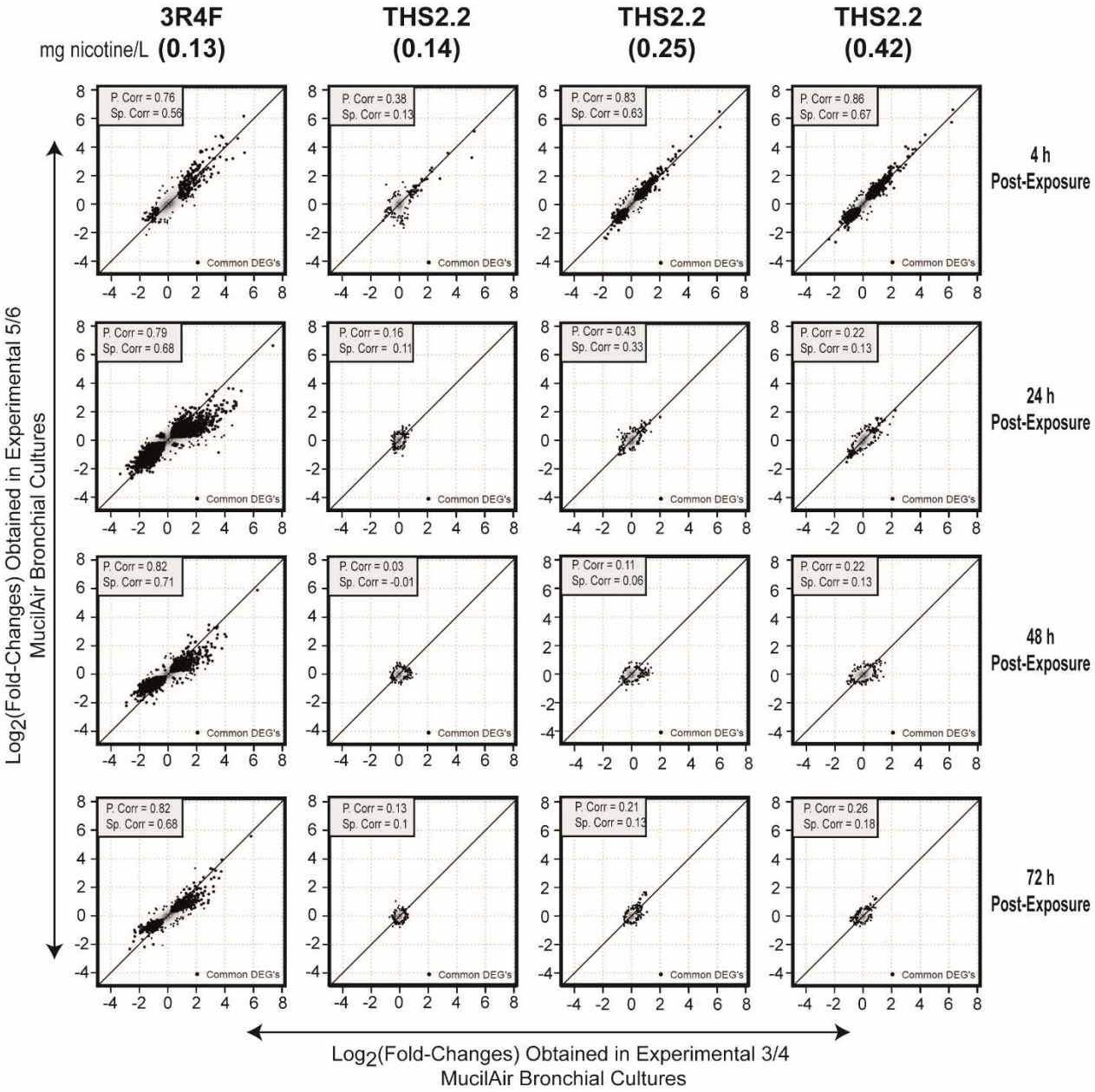
Supplementary Figure 5. Gene-set analysis showing various biological pathways enriched in the datasets

A heatmap showing selected KEGG pathways that were significantly enriched in the dataset. The color gradient represents the score enrichment: The mean of the gene score (log2(fold-change)). Three types of significance (*) are marked for each annotation as described in Supplementary Materials and Methods. The first character indicates the adjusted combined Fisher *p*-value, the second character indicates the gene-set analysis Q2 test, and the third character indicates the over-representation analysis. Non-significance is marked with the underline symbol.



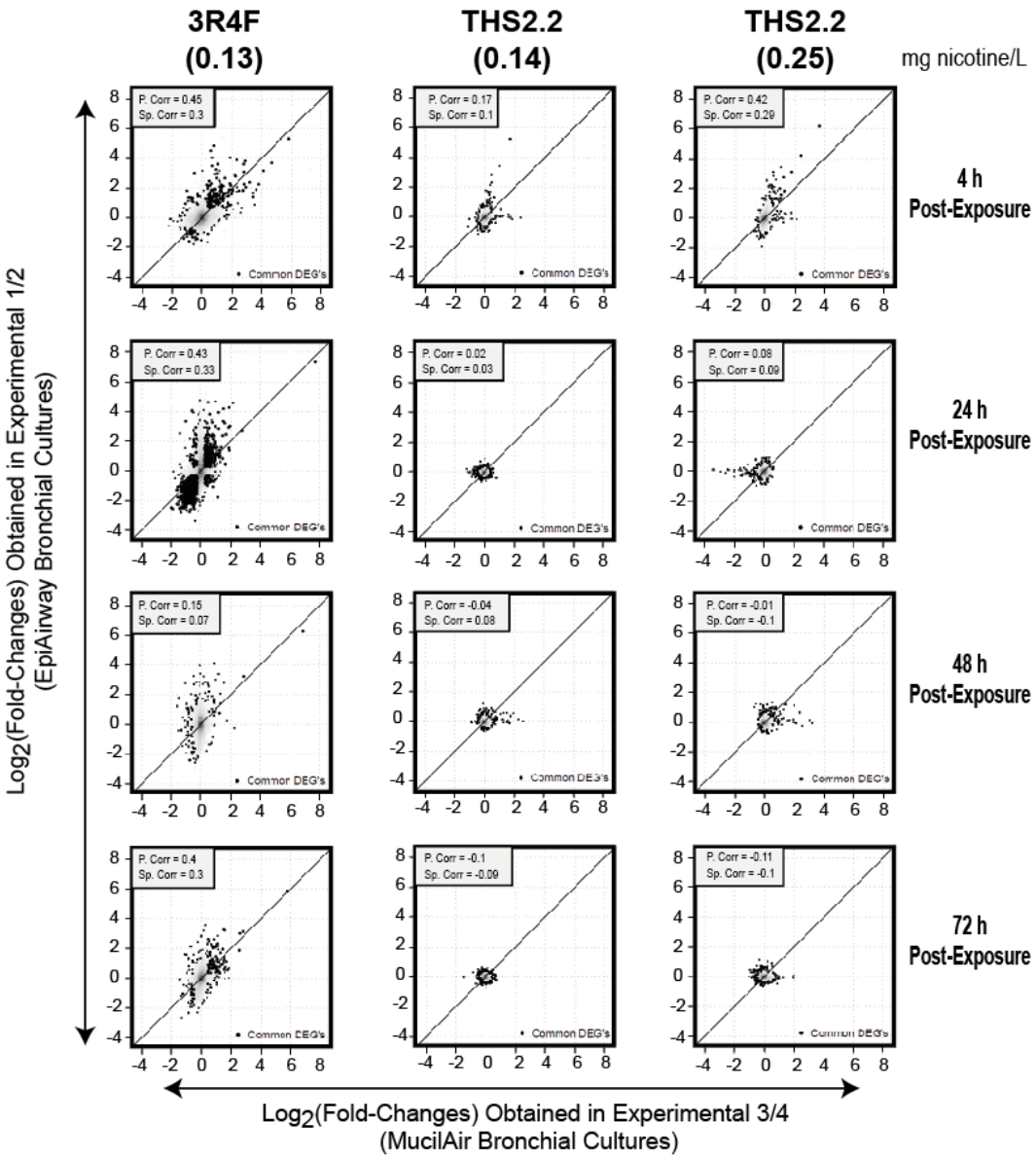
Supplementary Figure 6. Alteration of miRNAs in bronchial epithelial tissue cultures after exposure

MiRNAs are listed on the left side of the heatmap. The color gradient reflects the alterations in miRNA expression as compared with their respective air controls. For each of the clusters of miRNAs, target mRNAs were identified using DIANA-TarBase. Only the anti-correlated mRNAs present in our transcriptomic dataset were subjected to an enrichment analysis (described in the Materials and Methods). **Supplementary Table 4** lists the various KEGG pathways enriched and associated with each miRNA cluster. The collection of downregulated miRNAs within cluster B was linked to various processes regulating cell-cell communication ("adherens junction," "tight junction," "gap junction"), cell growth and death ("p53 signaling pathway," "cell cycle," "protein processing in endoplasmic reticulum"), and cellular metabolism ("fatty acid degradation," "fatty acid metabolism," "carbon metabolism"). The collection of downregulated miRNAs within cluster D was associated with cellular motility/transport ("regulation of actin cytoskeleton," "focal adhesion," "endocytosis"), cellular metabolism ("metabolic pathways," "glycolysis/gluconeogenesis," "carbon metabolism," "biosynthesis of amino acid"), and inflammatory response ("Fc gamma R-mediated phagocytosis," "chemokine signaling pathway," "neurotrophin signaling pathway"). Cluster A and cluster C were linked to calmodulin (*CALM1*, *CALM2*) genes.



Supplementary Figure 7. Correlation of gene expression fold-changes to explore the reproducibility of the experimental design

The fold-changes of gene expression in cultures post-exposure to 3R4F smoke and THS2.2 aerosol (as compared with their corresponding air controls) obtained from experimental repetitions 3 and 4 were correlated to those obtained from experimental repetitions 5 and 6. Each dot represents a gene.



Supplementary Figure 8. Correlation of the gene expression fold-changes to compare the exposure impact on two different bronchial culture models

The fold-changes of gene expression in cultures post-exposure to 3R4F smoke and THS2.2 aerosol (as compared with their corresponding air controls) from MucilAir™ bronchial cultures (*x-axis*) were correlated to those obtained from EpiAirway™ bronchial cultures (*y-axis*). Each dot represents a gene. The higher concentration of THS2.2 (0.42) was not tested in experimental repetitions 1 and 2 (in which EpiAirway bronchial cultures were used), thus correlation plots could not be generated.

Supplementary Materials and Methods

Normalization of the adenylate kinase (AK)-based cytotoxicity assay

For each experimental repetition (phase), the value of the luminescence signal was normalized using the mean of the positive control (Triton X-100-treated cultures; considered as 100% cytotoxicity) and negative control (PBS-treated or untreated cultures; considered as 0% cytotoxicity):

$$Cytotoxicity\ (\%) = \frac{AK_{Tissue} - AK_{Neg\ CTRL}}{AK_{Pos\ CTRL} - AK_{Neg\ CTRL}}\ x\ 100\%, \text{ where}$$

$$AK_{Pos\ CTRL} = \sum_{i=1}^{nbPhase} \frac{AK_{TX-100}}{nbPhase}$$

$$AK_{Neg\ CTRL} = \sum_{i=1}^{nbPhase} \frac{\sum_{j=1}^{nbCTRL^i} \frac{AK_{i,j}}{nbCTRL^i}}{nbPhase}$$

$$AK_{Tissue} = relative\ luminescence\ unit\ of\ a\ given\ sample$$

$$nbPhase = number\ of\ experimental\ phase$$

$$Neg = negative$$

$$Pos = positive$$

$$CTRL = control$$

Triton X-100 (at 1% final concentration) was added to the basolateral media of the cultures for 24 h to maximally induce cell lysis. The averages of the normalized relative luminescence unit were reported.

Gene-set Analysis

Gene-set analysis (GSA) of transcriptomics data was performed using the *Piano* package in the R statistical environment (Varemo et al., 2013). Pathway maps were obtained from the KEGG database (Kanehisa et al., 2014) and exported as R objects into the package *graphite* (Sales et al., 2012). Gene-set enrichment was assessed using over-representation analysis (ORA) and gene-set analysis. For the ORA, a one-tailed Fisher's exact test was employed. For the GSA, the fold-change was used as the gene-level statistic, the mean was used as the gene-set enrichment score, and sample permutation (Q2) was used to assess statistical significance (Ackermann and Strimmer, 2009). The two *p*-values were combined by Fisher's method to summarize the enrichment results. For each test, the *p*-value was adjusted using the Benjamini-Hochberg

procedure. Finally the two *p*-values are combined by Fisher method. The gene-set enrichment scores are the gene-set statistics mentioned before.

Normalization of the FFT Power to calculate of the power of the detected signal of cilia beating

The FFT power was normalized to the ambient noise using the following formula:

$$\frac{FFT\ Magnitude - \ Lowest\ FFT\ Magnitude^2}{Lowest\ FFT\ Magnitude}$$

$FFT =$ Fast Fourier Transformation

Acknowledgements

The authors also acknowledge Grégory Vuillaume for statistical evaluation support. We also thank the following individuals for contributing their technical expertise: Abdelkader Benyagoub, Camille Schilt and Maude Mayer (histological processing); Flavia Buchler and Maica Corciulo (support of Luminex-based measurement); and Karine Baumer, and Dariusz Peric (RNA purification); and Remi Dulize and Sophie Scheuner (microarray experiments).

References

Ackermann, M., Strimmer, K., 2009. A general modular framework for gene set enrichment analysis. BMC Bioinformatics 10, 47, doi:10.1186/1471-2105-10-47 1471-2105-10-47 [pii].

Adamson, J., Thorne, D., Dalrymple, A.*, et al.*, 2013. Assessment of cigarette smoke particle deposition within the Vitrocell(R) exposure module using quartz crystal microbalances. Chem Cent J 7, 50, doi:10.1186/1752-153X-7-50 1752-153X-7-50 [pii].

Affymetrix miRNA QCT Tool, 2011. Affymetrix miRNA QCTool: User's Guide. Available at: //media.affymetrix.com/support/downloads/manuals/mirna_qctool_user_manual.pdf.

Åstrand, A. B. M., Hemmerling, M., Root, J.*, et al.*, 2015. Linking increased airway hydration, ciliary beating, and mucociliary clearance through ENaC inhibition. American Journal of Physiology - Lung Cellular and Molecular Physiology 308, L22-L32, doi:10.1152/ajplung.00163.2014.

Aufderheide, M., Scheffler, S., Ito, S.*, et al.*, 2015. Ciliatoxicity in human primary bronchiolar epithelial cells after repeated exposure at the air-liquid interface with native mainstream smoke of K3R4F cigarettes with and without charcoal filter. Exp Toxicol Pathol 67, 407-11, doi:10.1016/j.etp.2015.04.006.

Azzopardi, D., Haswell, L. E., Foss-Smith, G.*, et al.*, 2015. Evaluation of an air–liquid interface cell culture model for studies on the inflammatory and cytotoxic responses to tobacco smoke aerosols. Toxicology in Vitro 29, 1720-1728, doi:http://dx.doi.org/10.1016/j.tiv.2015.06.016.

Benjamini, Y., Hochberg, Y., 1995. Controlling the False Discovery Rate: A Practical and Powerful Approach to Multiple Testing. J R Stat Soc Series B Stat Methodol 57, 289-300, doi:10.2307/2346101.

Berg, N., De Wever, B., Fuchs, H. W.*, et al.*, 2011. Toxicology in the 21st century--working our way towards a visionary reality. Toxicol In Vitro 25, 874-81, doi:10.1016/j.tiv.2011.02.008.

Berman, M. L., Connolly, G., Cummings, K. M.*, et al.*, 2015. Providing a Science Base for the Evaluation of Tobacco Products. Tob Regul Sci 1, 76-93, doi:10.18001/trs.1.1.8.

BeruBe, K., Aufderheide, M., Breheny, D.*, et al.*, 2009. In vitro models of inhalation toxicity and disease. The report of a FRAME workshop. Altern Lab Anim 37, 89-141.

Blaauboer, B. J., 2008. The contribution of in vitro toxicity data in hazard and risk assessment: current limitations and future perspectives. Toxicology letters 180, 81-84.

Bolstad, B. M., Irizarry, R. A., Astrand, M.*, et al.*, 2003. A comparison of normalization methods for high density oligonucleotide array data based on variance and bias. Bioinformatics 19, 185-93.

Borralho, P. M., Rodrigues, C. M. P., Steer, C. J., 2014. Mitochondrial MicroRNAs and Their Potential Role in Cell Function. Current Pathobiology Reports 2, 123-132, doi:10.1007/s40139-014-0047-x.

Boue, S., Talikka, M., Westra, J. W.*, et al.*, 2015. Causal biological network database: a comprehensive platform of causal biological network models focused on the pulmonary and vascular systems. Database (Oxford) 2015, bav030, doi:10.1093/database/bav030 bav030 [pii].

Boué, S., Talikka, M., Westra, J. W.*, et al.*, 2015. Causal biological network database: a comprehensive platform of causal biological network models focused on the pulmonary and vascular systems. Database 2015, doi:10.1093/database/bav030.

Brekman, A., Walters, M. S., Tilley, A. E.*, et al.*, 2014. FOXJ1 prevents cilia growth inhibition by cigarette smoke in human airway epithelium in vitro. Am J Respir Cell Mol Biol 51, 688-700, doi:10.1165/rcmb.2013-0363OC.

Camps, C., Saini, H. K., Mole, D. R.*, et al.*, 2014. Integrated analysis of microRNA and mRNA expression and association with HIF binding reveals the complexity of microRNA expression regulation under hypoxia. Molecular cancer 13, 1.

Carvalho, B. S., Irizarry, R. A., 2010. A framework for oligonucleotide microarray preprocessing. Bioinformatics 26, 2363-7, doi:10.1093/bioinformatics/btq431.

Cohen, N. A., Zhang, S., Sharp, D. B.*, et al.*, 2009. Cigarette smoke condensate inhibits transepithelial chloride transport and ciliary beat frequency. The Laryngoscope 119, 2269-2274.

Committee on Toxicity Testing and Assessment of Environmental Agents, National Research Council 2007. Toxicity testing in the 21st century: A vision and a strategy. In: Council, N. R., (Ed.). National Academies Press, Washington D.C.

Cormack, D. H., 2001. Essential Histology. Lippincott Williams & Wilkins.

Dai, M., Wang, P., Boyd, A. D.*, et al.*, 2005. Evolving gene/transcript definitions significantly alter the interpretation of GeneChip data. Nucleic Acids Res 33, e175, doi:10.1093/nar/gni179.

Daneshian, M., Akbarsha, M. A., Blaauboer, B.*, et al.*, 2011. A framework program for the teaching of alternative methods (replacement, reduction, refinement) to animal experimentation. ALTEX 28, 341-52.

Davis, M. A., Eldridge, S., Louden, C., 2013. Chapter 10 - Biomarkers: Discovery, Qualification and Application. In: Wallig, W. M. H. G. R. A., (Ed.), Haschek and Rousseaux's Handbook of Toxicologic Pathology (Third Edition). Academic Press, Boston, pp. 317-352.

Doke, S. K., Dhawale, S. C., 2015. Alternatives to animal testing: A review. Saudi Pharm J 23, 223-9, doi:10.1016/j.jsps.2013.11.002.

Dvorak, A., Tilley, A. E., Shaykhiev, R.*, et al.*, 2011. Do airway epithelium air-liquid cultures represent the in vivo airway epithelium transcriptome? Am J Respir Cell Mol Biol 44, 465-73, doi:10.1165/rcmb.2009-0453OC

2009-0453OC [pii].

Goldkorn, T., Filosto, S., Chung, S., 2014. Lung injury and lung cancer caused by cigarette smoke-induced oxidative stress: Molecular mechanisms and therapeutic opportunities involving the ceramide-generating machinery and epidermal growth factor receptor. Antioxid Redox Signal 21, 2149-74, doi:10.1089/ars.2013.5469.

Gonzalez-Suarez, I., Martin, F., Marescotti, D.*, et al.*, 2016. In Vitro Systems Toxicology Assessment of a Candidate Modified Risk Tobacco Product Shows Reduced Toxicity Compared to That of a Conventional Cigarette. Chem Res Toxicol 29, 3-18, doi:10.1021/acs.chemrestox.5b00321.

Health Canada, 1999. Determination of Tar, Water, Nicotine and Carbon Monoxide in Mainstream Tobacco Smoke. Health Canada Test Method T-11.

Hoeng, J., Talikka, M., Martin, F.*, et al.*, 2014. Case study: the role of mechanistic network models in systems toxicology. Drug Discov Today 19, 183-92, doi:10.1016/j.drudis.2013.07.023.

Hoeng, J., Deehan, R., Pratt, D.*, et al.*, 2012. A network-based approach to quantifying the impact of biologically active substances. Drug Discov Today 17, 413-8, doi:10.1016/j.drudis.2011.11.008.

Huber, W., Carey, V. J., Gentleman, R.*, et al.*, 2015. Orchestrating high-throughput genomic analysis with Bioconductor. Nat Methods 12, 115-21, doi:10.1038/nmeth.3252.

Institute of Medicine, 2012. Committee on Scientific Standards for Studies on Modified Risk Tobacco Products. Scientific standards for studies on modified risk tobacco products. National Academies Press.

International Organization for Standardization, 1999. ISO 3402: 1999 Tobacco and tobacco products -- Atmosphere for conditioning and testing. Available at: //iso.org/iso/home/store/catalogue_tc/catalogue_detail.htm?csnumber=28324.

Iskandar, A. R., Martin, F., Talikka, M.*, et al.*, 2013. Systems approaches evaluating the perturbation of xenobiotic metabolism in response to cigarette smoke exposure in nasal and bronchial tissues. Biomed Res Int 2013, 512086, doi:10.1155/2013/512086.

Iskandar, A. R., Xiang, Y., Frentzel, S.*, et al.*, 2015. Impact Assessment of Cigarette Smoke Exposure on Organotypic Bronchial Epithelial Tissue Cultures: A Comparison of Mono-Culture and Coculture Model Containing Fibroblasts. Toxicol Sci 147, 207-21, doi:10.1093/toxsci/kfv122.

Iskandar, A. R., Mathis, C., Martin, F.*, et al.*, 2016. 3-D Nasal Cultures: Systems Toxicological Assessment of a Candidate Modified-Risk Tobacco Product. Online First. ALTEX, doi:10.14573/altex.1605041.

Kanehisa, M., Goto, S., Sato, Y.*, et al.*, 2014. Data, information, knowledge and principle: back to metabolism in KEGG. Nucleic Acids Res 42, D199-205, doi:10.1093/nar/gkt1076.

Kauffmann, A., Gentleman, R., Huber, W., 2009. arrayQualityMetrics--a bioconductor package for quality assessment of microarray data. Bioinformatics 25, 415-6, doi:10.1093/bioinformatics/btn647.

Kentucky Tobacco Research & Development Center, 3R4F Preliminary Analysis. Available at: //ctrp.uky.edu/resources/pdf/webdocs/3R4F%20Preliminary%20Analysis.pdf.

Kozomara, A., Griffiths-Jones, S., 2013. miRBase: annotating high confidence microRNAs using deep sequencing data. Nucleic Acids Research, doi:10.1093/nar/gkt1181.

Kreindler, J. L., Jackson, A. D., Kemp, P. A.*, et al.*, 2005. Inhibition of chloride secretion in human bronchial epithelial cells by cigarette smoke extract. Am J Physiol Lung Cell Mol Physiol 288, L894-902, doi:10.1152/ajplung.00376.2004.

Kuehn, D., Majeed, S., Guedj, E.*, et al.*, 2015. Impact assessment of repeated exposure of organotypic 3D bronchial and nasal tissue culture models to whole cigarette smoke. Journal of visualized experiments: JoVE.

Lambrecht, B. N., Hammad, H., 2012. The airway epithelium in asthma. Nature medicine 18, 684-692.

Ma, Q., 2001. Induction of CYP1A1. The AhR/DRE paradigm: transcription, receptor regulation, and expanding biological roles. Curr Drug Metab 2, 149-64.

Majeed, S., Frentzel, S., Wagner, S.*, et al.*, 2014. Characterization of the Vitrocell(R) 24/48 in vitro aerosol exposure system using mainstream cigarette smoke. Chem Cent J 8, 62, doi:10.1186/s13065-014-0062-3

62 [pii].

Martin, F., Sewer, A., Talikka, M.*, et al.*, 2014. Quantification of biological network perturbations for mechanistic insight and diagnostics using two-layer causal models. BMC Bioinformatics 15, 238, doi:10.1186/1471-2105-15-238.

Marwick, J. A., Stevenson, C. S., Giddings, J.*, et al.*, 2006. Cigarette smoke disrupts VEGF165-VEGFR-2 receptor signaling complex in rat lungs and patients with COPD: morphological impact of VEGFR-2 inhibition. Am J Physiol Lung Cell Mol Physiol 290, L897-L908, doi:10.1152/ajplung.00116.2005

Mathis, C., Gebel, S., Poussin, C.*, et al.*, 2015. A systems biology approach reveals the dose- and time-dependent effect of primary human airway epithelium tissue culture after exposure to cigarette smoke in vitro. Bioinform Biol Insights 9, 19-35, doi:10.4137/BBI.S19908

bbi-9-2015-019 [pii].

Mathis, C., Poussin, C., Weisensee, D.*, et al.*, 2013. Human bronchial epithelial cells exposed in vitro to cigarette smoke at the air-liquid interface resemble bronchial epithelium from human smokers. Am J Physiol Lung Cell Mol Physiol 304, L489-503, doi:10.1152/ajplung.00181.2012

ajplung.00181.2012 [pii].

Maunders, H., Patwardhan, S., Phillips, J.*, et al.*, 2007. Human bronchial epithelial cell transcriptome: gene expression changes following acute exposure to whole cigarette smoke in vitro. Am J Physiol Lung Cell Mol Physiol 292, L1248-56, doi:00290.2006 [pii] 10.1152/ajplung.00290.2006.

McCall, M. N., Bolstad, B. M., Irizarry, R. A., 2010. Frozen robust multiarray analysis (fRMA). Biostatistics 11, 242-253, doi:10.1093/biostatistics/kxp059.

Megiorni, F., Cialfi, S., McDowell, H. P.*, et al.*, 2014. Deep Sequencing the microRNA profile in rhabdomyosarcoma reveals down-regulation of miR-378 family members. BMC Cancer 14, 1-17, doi:10.1186/1471-2407-14-880.

Mercer, B. A., Wallace, A. M., Brinckerhoff, C. E.*, et al.*, 2009. Identification of a cigarette smoke-responsive region in the distal MMP-1 promoter. Am J Respir Cell Mol Biol 40, 4-12, doi:10.1165/rcmb.2007-0310OC.

Milara, J., Armengot, M., Banuls, P.*, et al.*, 2012. Roflumilast N-oxide, a PDE4 inhibitor, improves cilia motility and ciliated human bronchial epithelial cells compromised by cigarette smoke in vitro. British journal of pharmacology 166, 2243-2262.

Musah, S., Chen, J., Hoyle, G. W., 2012. Repair of tracheal epithelium by basal cells after chlorine-induced injury. Respir Res 13, 107, doi:10.1186/1465-9921-13-107.

Nakano, M., Fukami, T., Gotoh, S.*, et al.*, 2016. RNA Editing Modulates Human Hepatic Aryl Hydrocarbon Receptor Expression by Creating MicroRNA Recognition Sequence. J Biol Chem 291, 894-903, doi:10.1074/jbc.M115.699363.

Nazarov, P. V., Reinsbach, S. E., Muller, A.*, et al.*, 2013. Interplay of microRNAs, transcription factors and target genes: linking dynamic expression changes to function. Nucleic Acids Research 41, 2817-2831, doi:10.1093/nar/gks1471.

Paur, H.-R., Cassee, F. R., Teeguarden, J.*, et al.*, 2011. In-vitro cell exposure studies for the assessment of nanoparticle toxicity in the lung--A dialog between aerosol science and biology. J Aerosol Sci 42, 668-92.

Pezzulo, A. A., Starner, T. D., Scheetz, T. E.*, et al.*, 2011. The air-liquid interface and use of primary cell cultures are important to recapitulate the transcriptional profile of in vivo airway epithelia. Am J Physiol Lung Cell Mol Physiol 300, L25-31, doi:10.1152/ajplung.00256.2010 ajplung.00256.2010 [pii].

Phillips, B., Veljkovic, E., Boué, S.*, et al.*, 2016. An 8-Month Systems Toxicology Inhalation/Cessation Study in Apoe(−/−) Mice to Investigate Cardiovascular and Respiratory Exposure Effects of a Candidate Modified Risk Tobacco Product, THS 2.2, Compared With Conventional Cigarettes. Toxicol Sci 149, 411-432, doi:10.1093/toxsci/kfv243.

Proud, D., Leigh, R., 2011. Epithelial cells and airway diseases. Immunol Rev 242, 186-204, doi:10.1111/j.1600-065X.2011.01033.x.

R Core Team, 2013. R: A language and environment for statistical computing. R Foundation for Statistical Computing, Vienna, Austria. Available at: http://www.R-project.org/.

Ritchie, M. E., Phipson, B., Wu, D.*, et al.*, 2015. limma powers differential expression analyses for RNA-sequencing and microarray studies. Nucleic Acids Research, doi:10.1093/nar/gkv007.

Roberts, J. R., Perkins, G. D., Fujisawa, T.*, et al.*, 2007. Vascular endothelial growth factor promotes physical wound repair and is anti-apoptotic in primary distal lung epithelial and A549 cells. Critical care medicine 35, 2164-2170.

Sales, G., Calura, E., Cavalieri, D.*, et al.*, 2012. graphite - a Bioconductor package to convert pathway topology to gene network. BMC Bioinformatics 13, 20, doi:10.1186/1471-2105-13-20 1471-2105-13-20 [pii].

Sauer, J. M., Kleensang, A., Peitsch, M. C.*, et al.*, 2016. Advancing Risk Assessment through the Application of Systems Toxicology. Toxicological research 32, 5.

Schlage, W. K., Bulles, H., Friedrichs, D.*, et al.*, 1998. Cytokeratin expression patterns in the rat respiratory tract as markers of epithelial differentiation in inhalation toxicology. I. Determination of normal cytokeratin expression patterns in nose, larynx, trachea, and lung. Toxicol Pathol 26, 324-43.

Schlage, W. K., Iskandar, A. R., Kostadinova, R.*, et al.*, 2014. In vitro systems toxicology approach to investigate the effects of repeated cigarette smoke exposure on human buccal and gingival organotypic epithelial tissue cultures. Toxicology mechanisms and methods 24, 470-487.

Schmid, A., Baumlin, N., Ivonnet, P.*, et al.*, 2015. Roflumilast partially reverses smoke-induced mucociliary dysfunction. Respiratory research 16, 1.

Schrottmaier, W. C., Oskolkova, O. V., Schabbauer, G.*, et al.*, 2014. MicroRNA miR-320a modulates induction of HO-1, GCLM and OKL38 by oxidized phospholipids in endothelial cells. Atherosclerosis 235, 1-8, doi:10.1016/j.atherosclerosis.2014.03.026.

Shamir, E. R., Ewald, A. J., 2014. Three-dimensional organotypic culture: experimental models of mammalian biology and disease. Nat Rev Mol Cell Biol 15, 647-664, doi:10.1038/nrm3873.

Sheldon, L. S., Cohen Hubal, E. A., 2009. Exposure as part of a systems approach for assessing risk. Environ Health Perspect 117, 119-1194, doi:10.1289/ehp.0800407.

Smith, C., Djakow, J., Free, R.*, et al.*, 2012. ciliaFA: a research tool for automated, high-throughput measurement of ciliary beat frequency using freely available software. Cilia 1, 14, doi:10.1186/2046-2530-1-14.

Smyth, G. K., 2004. Linear models and empirical bayes methods for assessing differential expression in microarray experiments. Stat Appl Genet Mol Biol 3, Article3, doi:10.2202/1544-6115.1027.

Stanley, P. J., Wilson, R., Greenstone, M. A.*, et al.*, 1986. Effect of cigarette smoking on nasal mucociliary clearance and ciliary beat frequency. Thorax 41, 519-23, doi:10.1136/thx.41.7.519.

Sturla, S. J., Boobis, A. R., FitzGerald, R. E.*, et al.*, 2014. Systems toxicology: from basic research to risk assessment. Chemical research in toxicology 27, 314-329.

Talikka, M., Kostadinova, R., Xiang, Y.*, et al.*, 2014. The response of human nasal and bronchial organotypic tissue cultures to repeated whole cigarette smoke exposure. Int J Toxicol 33, 506-17, doi:10.1177/1091581814551647.

Tang, H., Lee, M., Sharpe, O.*, et al.*, 2012. Oxidative stress-responsive microRNA-320 regulates glycolysis in diverse biological systems. FASEB J 26, 4710-21, doi:10.1096/fj.11-197467.

Thomson, T. M., Sewer, A., Martin, F.*, et al.*, 2013. Quantitative Assessment of Biological Impact Using Transcriptomic Data and Mechanistic Network Models. Toxicology and Applied Pharmacology, doi:http://dx.doi.org/10.1016/j.taap.2013.07.007.

Uraih, L. C., Maronpot, R., 1990. Normal histology of the nasal cavity and application of special techniques. Environmental health perspectives 85, 187.

Varemo, L., Nielsen, J., Nookaew, I., 2013. Enriching the gene set analysis of genome-wide data by incorporating directionality of gene expression and combining statistical hypotheses and methods. Nucleic Acids Res 41, 4378-91, doi:10.1093/nar/gkt111.

Vlachos, I. S., Paraskevopoulou, M. D., Karagkouni, D.*, et al.*, 2015. DIANA-TarBase v7. 0: indexing more than half a million experimentally supported miRNA: mRNA interactions. Nucleic acids research 43, D153-D159.

Zanetti, F., Sewer, A., Mathis, C.*, et al.*, 2016. Systems toxicology assessment of the biological impact of a candidate Modified Risk Tobacco Product on human organotypic oral epithelial cultures. Chemical Research in Toxicology.

1624

Highlights

- A systems toxicology approach was applied to comprehensively assess the biological impact of a heated tobacco aerosol and cigarette smoke
- Series of experimental repetitions were conducted to increase robustness of the assessment
- Heated tobacco aerosol elicited less biological impact than cigarette smoke at similar nicotine concentration(s)

***Conflict of Interest**

Click here to download Conflict of Interest: Article_AIskandar_TIV2016_Conflict of Interest.docx